

POST-PALEOGENE STRESS DISTRIBUTION IN THE BARTIN-ULUS-  
SAFRANBOLU BASINS, WESTERN PONTIDES, TURKEY

A THESIS SUBMITTED TO  
THE GRADUATE SCHOOL OF NATURAL AND APPLIED SCIENCES  
OF  
MIDDLE EAST TECHNICAL UNIVERSITY

BY

EMRE BENGÜ

IN PARTIAL FULFILLMENT OF THE REQUIREMENTS  
FOR  
THE DEGREE OF MASTER OF SCIENCE  
IN  
GEOLOGICAL ENGINEERING

FEBRUARY, 2017



Approval of the thesis:

**POST-PALEOGENE STRESS DISTRIBUTION IN THE BARTIN-ULUS-  
SAFRANBOLU BASINS, WESTERN PONTIDES, TURKEY**

submitted by **EMRE BENGÜ** in partial fulfillment of the requirements for the degree  
of **Master of Science in Geological Engineering Department, Middle East  
Technical University** by,

Prof. Dr. Gülbin Dural Ünver  
Dean, Graduate School of **Natural and Applied Sciences**

Prof. Dr. Erdin BOZKURT  
Head of Department, **Geological Engineering**

Prof. Dr. Bora ROJAY  
Supervisor, **Geological Engineering Dept., METU**

**Examining Committee Members:**

Prof. Dr. Erdin Bozkurt  
Geological Engineering Dept., METU

Prof. Dr. Bora ROJAY  
Geological Engineering Dept., METU

Prof. Dr. Veysel Işık  
Geological Engineering Dept., Ankara University

Assist. Prof. Dr. Erman Özsayın  
Geological Engineering Dept., Hacettepe University

Assist. Prof. Dr. Fatma TOKSOY KÖKSAL  
Geological Engineering Dept., METU

**Date:** *February 1, 2017*

**I hereby declare that all information in this document has been obtained and presented in accordance with academic rules and ethical conduct. I also declare that, as required by these rules and conduct, I have fully cited and referenced all material and results that are not original to this work.**

Name, Last Name : Emre BENGÜ

Signature :

## **ABSTRACT**

### **POST-PALEOGENE STRESS DISTRIBUTION IN THE BARTIN-ULUS-SAFRANBOLU BASINS, WESTERN PONTIDES, TURKEY**

Bengü, Emre

M.Sc., Department of Geological Engineering

Supervisor: Prof. Dr. Bora Rojay

February 2017, 104 pages

The thesis addresses the post-Paleogene tectonic evolution of the Bartın-Ulus-Safranbolu basins in Western Pontides. The study area is bounded by Black Sea from north, Sünnice Massif from west, Kargı Massif from east, and by Cretaceous ophiolitic mélanges and the North Anatolian Fault from south. These basins are separated from each other by the two main faults, namely, Bartın and Karabük faults.

Four structural domains are defined, based on lithostratigraphic differences and bounding major faults, to figure out the the structural picture.

The structural and kinematic analyses were done by means of structural elements; three hundred ninety bedding plane attitudes were analyzed with ROCKWORKS 2017™ and fourty one fault-slip lineation data were analyzed with WINTENSOR 5.8.5™ to determine paleostress directions.

For Bartın and Ulus basins general trend of beds are  $055^{\circ}\text{N}$ . However, for Safranbolu basin, general bedding trend is  $085^{\circ}\text{N}$ . The central domain (Ulus Basin) of the area bounded by Karabük and Bartın Faults is intensely folded and faulted, compared to other domains of the study area.

Paleostress analysis point out that, the studied area, which was under regionwide NW-SE compression since Late Cretaceous, was under NNW-SSE to NE-SW compression.

The structural analysis done for each domain manifests clockwise or counter clockwise rotations of  $20^{\circ}$  for the region

Keywords: Ulus Basin, Western Pontides, Karabük Fault, post-Paleogene, folding analysis, paleostress analysis.

## **ÖZ**

### **BARTIN-ULUS-SAFRANBOLU HAVZALARININ PALEOJEN SONRASI STRES DAĞILIMI, BATI PONTİDLER, TÜRKİYE**

Bengü, Emre

Y. Lisans, Jeoloji Mühendisliği Bölümü

Tez Yöneticisi: Prof. Dr. Bora Rojay

Şubat 2017, 104 sayfa

Çalışma, Batı Pontidler’de yer alan, Bartın-Ulus-Safranbolu havzalarının Paleojen sonrası tektonik evrimini ele almaktadır. Çalışma alanı kuzeyden Karadeniz, batıdan Sünnice Masifi, doğudan Kargı Masifi ve güneyden Kretase ofiyolitik melanjı ve Kuzey Anadolu Fayı ile sınırlanmaktadır. Bu havzalar birbirinden iki ana fay olan Bartın Fayı ve Karabük Fayı ile ayrılmıştır.

Yapısallığı ortaya çıkarmak amacıyla, litostratigrafik farklılıklar ve alanı sınırlayan büyük faylar göz önüne alınarak dört adet yapısal alan tanımlanmıştır.

Yapısal öğeler kullanılarak yapısal ve kinematik analizler yapılmıştır. Bu kapsamda üç yüz doksan adet tabaka doğrultu eğimleri ROCKWORKS 2017™ programı ile, kırk bir adet fay çizikleri WINTENSOR 5.8.5™ programı ile analiz edilmiş ve gerilim dağılımları ortaya konmuştur.

Bartın ve Ulus havzaları için genel tabaka yönelimleri  $055^0K$ 'dir. Safranbolu havzası içinse genel tabaka yönelimleri  $085^0K$  olarak hesaplanmıştır. Karabük Fayı ve Bartın Fayı ile sınırlanmış olan merkez alan (Ulus havzası) diğer alanlara nazaran daha yoğun bir kıvrımlanmaya ve faylanmaya maruz kalmıştır.

Geç Kretase'den beri KB-GD yönlü bölgesel bir sıkışmaya maruz kalmış olan çalışma alanında gerçekleştirilen stres dağılım analizleri sonucu sıkışma yönü KKB-GGD ve KD-GB olarak belirlenmiştir.

Her bir alan için yapılan yapısal analizler, saat yönü veya saat yönünün tersine  $20^0$ 'lik bir rotasyonu işaret etmektedir.

Anahtar Kelimeler: Ulus Havzası, Batı Pontidler, Karabük Fayı, Paleojen Sonrası, kıvrım analizi, stres dağılım analizi.



To my family...

## ACKNOWLEDGEMENTS

First of all, I would like to express my gratitude to my supervisor Prof. Dr. Bora ROJAY, for his guidance, criticism, sharing his knowledge, encouragement and most important of all, his friendly and humorous behaviours with patience throughout all the stages of this thesis.

This study is supported by Turkish Petroleum Corporation (TPAO) in the sense of their permission. Especially, I would like to thank Dr. Nazım Özgür SİPAHİOĞLU and Associate Professor Zühtü BATI from Black Sea Project for this permission and encouragement.

I would like to thank Rıza Özgür TEMEL from Black Sea Project at TP for sharing his field study knowledge, technical support and criticism about the regional geology of the Black Sea.

I would like to thank Assistant Professor Erman ÖZSAYIN for his technical support for the Win-Tensor software.

I would like to thank Derya KILIÇ DEMİRCİ, Özbil YAPAR and Seren SERT for her support for Adobe Illustrator.

I would like to thank Mahmut Olcay KORKMAZ for preparation of the topographic maps of the study area.

Finally, I would like to express my deepest gratitude to my wife, my mother, my father, my son, mother-in-law and father-in-law for their patience, unlimited support, motivation and encouragement.

## TABLE OF CONTENTS

ABSTRACT.....	v
ÖZ .....	vii
ACKNOWLEDGEMENTS .....	x
TABLE OF CONTENTS.....	xi
LIST OF TABLES .....	xv
LIST OF FIGURES .....	xvi
CHAPTERS	
1. INTRODUCTION .....	1
1.1. Purpose and Scope of the Study.....	1
1.2. Geographic Location .....	4
1.3. Method of the Study .....	5
2. REGIONAL GEOLOGY .....	7
2.1. Previous Studies .....	7
2.1.1. Amasra-Bartın Zone .....	7
2.1.2. Karabük-Safranbolu Zone .....	9
2.2. Tectonic Setting of Western Pontides, Turkey.....	12
3. STRATIGRAPHY .....	15

3.1. Pre-Jurassic Basement .....	15
3.1.1. Kartal Formation.....	16
3.1.2. Yılanlı Formation.....	16
3.1.3. Alacaagzı Formation.....	21
3.1.4. Zonguldak Formation .....	21
3.1.5. Çakraz Formation .....	22
3.1.6. Çakrazboz Formation.....	22
3.2. Upper Jurassic-Lower Cretaceous .....	23
3.2.1. İnaltı Formation .....	23
3.2.2. İncigez Formation .....	25
3.2.3. Dirgine Granite .....	25
3.2.4. Ulus Formation .....	26
3.3. Upper Cretaceous-Eocene Units.....	32
3.3.1. Bartın-Ulus Regions .....	32
3.3.1.1. Yemişliçay Group .....	32
3.3.1.1.a.Kökyol Formation.....	32
3.3.1.1.b.Unaz Formation .....	33
3.3.1.1.c.Cambu Formation .....	33
3.3.1.2. Akveren Formation .....	34
3.3.1.3. Atbaşı Formation.....	35
3.3.1.4. Kusuri Formation .....	37

3.3.2. Karabük-Safranbolu Region .....	37
3.3.2.1. Safranbolu Formation .....	37
3.3.2.2. Karabük Formation .....	38
3.3.2.3. Çerçen Formation .....	40
3.3.2.4. Soğanlı Formation.....	40
3.3.2.5. Akçapınar Formation .....	41
3.3.2.6. Yunuslar Formation .....	41
3.3.2.7. Yörük Formation.....	42
3.4. Quaternary .....	42
4. STRUCTURAL GEOLOGY .....	45
4.1. Fold Analysis.....	45
4.1.1. Attitude of Bedding Plane .....	46
4.1.2. Stereographic Analysis of Folds.....	53
4.2. Fault Analysis.....	58
4.2.1. Fault Slip Lineation Analysis .....	61
4.2.1.1. Bartın Fault .....	62
4.2.1.2. Karabük Fault .....	63
4.2.1.3. Karagöl Fault .....	64
4.2.1.4. Strike Slip Fault .....	64
4.2.1.5. Normal Fault with Strike Slip Component .....	65
4.2.1.6. Normal Fault .....	66

4.2.2. Fault Slip Lineation Analysis of the Faults in Barremian-Cenomanian Ulus Formation .....	67
4.2.2.1. Strike Slip Fault with Reverse Component.....	67
4.2.2.2. Reverse Fault.....	68
4.2.3. Post-Eocene Normal Faults .....	69
5. DISCUSSION .....	73
6. CONCLUSIONS .....	81
REFERENCES .....	83
APPENDICES .....	91

## LIST OF TABLES

### TABLES

Table A1. Bed measurements of Domain I.....	91
Table A.2. Bed measurements of Domain II.....	94
Table A.3. Bed measurements of Domain III. ....	97
Table A.4. Bed measurements of Domain IV .....	101
Table B. Fault measurements.....	103

## LIST OF FIGURES

### FIGURES

Figure 1.1. Three major tectonic belts (Taurides, Anatolides and Pontides) and tectonic setting of Turkey (modified from Ketin, 1966; Okay and Tüysüz, 1999) (NAF: North Anatolian Fault, EAF: East Anatolian Fault) .....	2
Figure 1.2. 1:500000 scaled geology map of Western Pontides (MTA, 1961). Please see the MTA geological map for more details.. ..	2
Figure 1.3. General stratigraphy of the Bartın-Ulus-Karabük-Safranbolu-Ovacık regions .....	3
Figure 1.4. Geographic setting of the study area (from Google Earth).....	4
Figure 3.1. Geological map of the study area with the structural features.....	17
Figure 3.2. Stratigraphic columnar section of the Bartın-Ulus basin (not to scale)..	19
Figure 3.3. Stratigraphic columnar section of the Karabük-Safranbolu basin (not to scale).....	20
Figure 3.4. İnaltı olistoliths within Ulus Formation near Karabük Fault in Sunduk village (NW of Safranbolu).....	24
Figure 3.5. General and close-up view of İnaltı Formation along Bartın-Amasra highway.....	24
Figure 3.6. A view of a stack turbidity channelized system in the Ulus Formation near the Dereköy village.....	28
Figure 3.7. A view of intensely deformed flysch facies of the Ulus Formation near the Dereköy village.. ..	28



Figure 3.8. Field views of boudinage structures (b) in the Ulus Formation near the Dereköy village..	29
Figure 3.9. A view from normal drag developed in Ulus Formation near the Dereköy village..	30
Figure 3.10. Field view of normal faulting forming a horst and graben structure in the Ulus Formation near the Dereköy village. ....	30
Figure 3.11. Field view of meso structures (overturned folds) indicating south to north tectonic transportation around the Dereköy village.....	31
Figure 3.12. Field view of normal fault cross-cut by the left-lateral strike slip fault with reverse components. (NW of Safranbolu along new highway)..	31
Figure 3.13. Field view of columnar jointed basalts in the Cambu Formation along Bartın-Amasra highway near the Uzunöz village..	34
Figure 3.14. A view of conformable contact between the Akveren and the Cambu Formations at the north of Bartın near the Üçkurnalı village... ..	36
Figure 3.15. Field view of Bayramoğlu lava member within the Akveren Formation in the southwest of Bartın in the Kozcağız village... ..	36
Figure 3.16. Field view of lensing out of foreset beds and lateral gradation of clastics with green mudrocks forming typical cross-beds (deltaic setting) in the Karabük Formation where the delta faces SE (northwest of Ödemiş village, SW of Karabük).....	39
Figure 3.17. Field view of southeast dipping growth faults in delta sequence of Karabük Formation in northwest of the Ödemiş village (NW of Karabük)..	39
Figure 3.18. A field view of talus deposits developed in Bartın village near Kozcağız.....	43

Figure 3.19. Field view of terrace conglomerates (Tcong) above the Karabük Formation at 400 meters altitude from sea level (which is 250 meters from the Filyos river channel) (S of Karabük village).....	43
Figure 4.1. Structural map of the study area showing general trends of bedding planes for each domains individually.....	47
Figure 4.2. NW-SE sections (A and B) showing the structural elements of the study area. ....	49
Figure 4.3. Rose diagram showing the strike of the Upper Cretaceous to Eocene beds in Domain I. ....	51
Figure 4.4. Rose diagram showing the strike of the Lower Cretaceous beds in Domain II. ....	51
Figure 4.5. Rose diagram showing the strike of the Paleogene to Plio-Quaternary beds in Domain III.....	52
Figure 4.6. Rose diagram showing the strike of the Upper Cretaceous to Eocene beds in Domain IV.. ....	52
Figure 4.7. Overturned structures in the Ulus Formation (near Dereköy village).. ....	54
Figure 4.8. Stereographic plot for the Upper Cretaceous to Eocene beds in Domain I	56
Figure 4.9. Stereographic plot for the Lower Cretaceous beds in Domain II.. ....	56
Figure 4.10. Stereographic plot for the Paleogene to Plio-Quaternary beds in Domain III.. ....	57
Figure 4.11. Stereographic plot for the Upper Cretaceous to Eocene beds in Domain IV.....	57
Figure 4.12. Paleostress analysis of the Bartın Fault. Blue arrows indicate the compression direction. $\sigma_1=18^{\circ},054^{\circ}N$ , $\sigma_2=44^{\circ},306^{\circ}N$ and $\sigma_3=41^{\circ},160^{\circ}N$ and R value is 0,50.....	62

Figure 4.13. (a) Close up view of a fault plane with moving direction, (b) Paleostress analysis of the Karabük Fault. Blue arrows indicate the compression direction.  $\sigma_1=17^\circ,129^\circ\text{N}$ ,  $\sigma_2=10^\circ,036^\circ\text{N}$  and  $\sigma_3=70^\circ,278^\circ\text{N}$  and R value is 0,86..... 63

Figure 4.14. Paleostress analysis of strike-slip faults developed during post-Eocene. Blue arrows indicate compression direction, and reds indicate extension direction.  $\sigma_1=06^\circ,066^\circ\text{N}$ ,  $\sigma_2=82^\circ,286^\circ\text{N}$  and  $\sigma_3=05^\circ,156^\circ\text{N}$  and R values is 0,54 ..... 65

Figure 4.15. a) Field view of the low angle normal fault plane ( $35^\circ$ ) cross-cutting the bedding planes and b) result of the paleostress analysis of the normal fault with strike-slip component developed during post-Late Cretaceous. Red arrow indicates extension direction.  $\sigma_1=57^\circ,257^\circ\text{N}$ ,  $\sigma_2=06^\circ,356^\circ\text{N}$  and  $\sigma_3=32^\circ,090^\circ\text{N}$  and R value is 0,58..... 66

Figure 4.16. Paleostress analysis of normal fault developed during post-Eocene. Red arrows indicate the extension directions. For this fault,  $\sigma_1=61^\circ,159^\circ\text{N}$ ,  $\sigma_2=04^\circ,256^\circ\text{N}$  and  $\sigma_3=28^\circ,348^\circ\text{N}$  orientations are calculated. R values is 0,73..... 67

Figure 4.17. Paleostress analysis of the strike-slip fault with reverse component developed during post-Barremian-Cenomanian. Blue arrows indicate the E-W compression. For this fault  $\sigma_1=15^\circ,266^\circ\text{N}$ ,  $\sigma_2=58^\circ,152^\circ\text{N}$  and  $\sigma_3=28^\circ,004^\circ\text{N}$  orientations are calculated. R value is 0,02..... 68

Figure 4.18. Paleostress analysis of reverse fault developed during post-Barremian-Cenomanian. The blue arrows show compression in WNW-ESE orientation. For this fault  $\sigma_1=08^\circ,089^\circ\text{N}$ ,  $\sigma_2=02^\circ,358^\circ\text{N}$  and  $\sigma_3=82^\circ,255^\circ\text{N}$  orientations are calculated. R value is 0.85. .... 69

Figure 4.19. Field view of normal growth faults developed in the deltaic sequences of the Lower-Middle Eocene Karabük Formation close to the Karabük Fault (SW of Karabük city).. ..... 71

Figure 4.20. Field view of normal faults developed in the Upper Paleocene-Middle Eocene Safranbolu Formation (N of Safranbolu city along Bartın highway)..... 71

Figure 4.21. Field view of two normal fault planes developed in the Lower-Middle Eocene Çerçen Formation (SW of Safranbolu city).....	72
Figure 5.1. The location of the study area respect to some major earthquakes and the seismicity of the region (Google image). The Bartın earthquake giving a solution of reverse faulting where earthquakes on NAF gives dextral strike slip faulting.. .....	75
Figure 5.2. Tectonic Model proposed for the evolution of the tectonic structures in Bartın-Ulus-Karabük-Ovacık Region.....	76
Figure 5.3. Major strike orientations in Barremian-Cenomanian sequences (a) and Upper Paleocene-Lower-Middle Eocene sequences (b) in Domain IV. ....	78

## **CHAPTER 1**

### **INTRODUCTION**

#### **1.1. Purpose and Scope of the Study**

The study area lies within an extensive deformation zone in Western Pontides (northern Anatolia) located within the Alpine-Himalayan mountain range (Figure 1.1). Major geological features in and closed the study area are; Sünnice Massif, Kargı Massif, Cretaceous ophiolitic mélangé and North Anatolian Fault Zone (Figure 1.2). Master strand of the North Anatolian Fault Zone runs through Western Pontides bounding the study area from south (Figure 1.1, Figure 1.2), which is interpreted either as a reactivated structure or a neotectonic structure, or both (partly a neotectonic structure overprinting the suture) (Şengör et al., 2005).

The studied area consists of pre-Alpine Paleozoic (Devonian-Carboniferous) units, Permo-Triassic sequences, a “syn-rift” sequence of Jurassic-Cretaceous sedimentary rocks (Oxfordian-Albian and Barremian-Cenomanian); they all are unconformably overlain by post-rift Paleogene sequences (Figure 1.3).

The rock sequences are interpreted as product of rifting on Eurasian continent that gave rise to the opening and closure of Neo-Tethys Ocean. Prior to Jurassic, Western Pontides formed as a part of Eurasian continent. Following Jurassic, Atlantic-type continental margin evolution dominated Pontides and continued its evolution until Tethys Ocean started to subduct under the Eurasian continent at the end of Early Cretaceous.

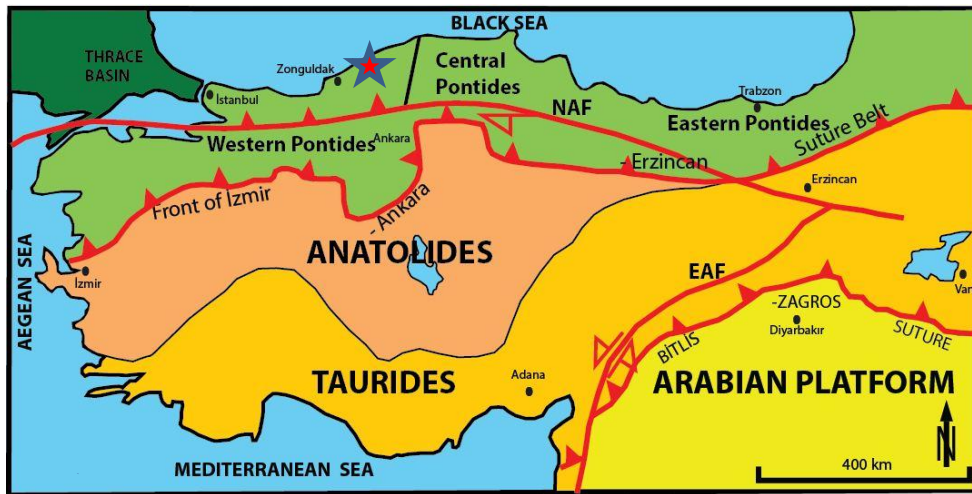


Figure 1.1. Three major tectonic belts (Taurides, Anatolides and Pontides) and tectonic setting of Turkey (modified from Ketin, 1966; Okay and Tüysüz, 1999) (NAF: North Anatolian Fault, EAF: East Anatolian Fault).

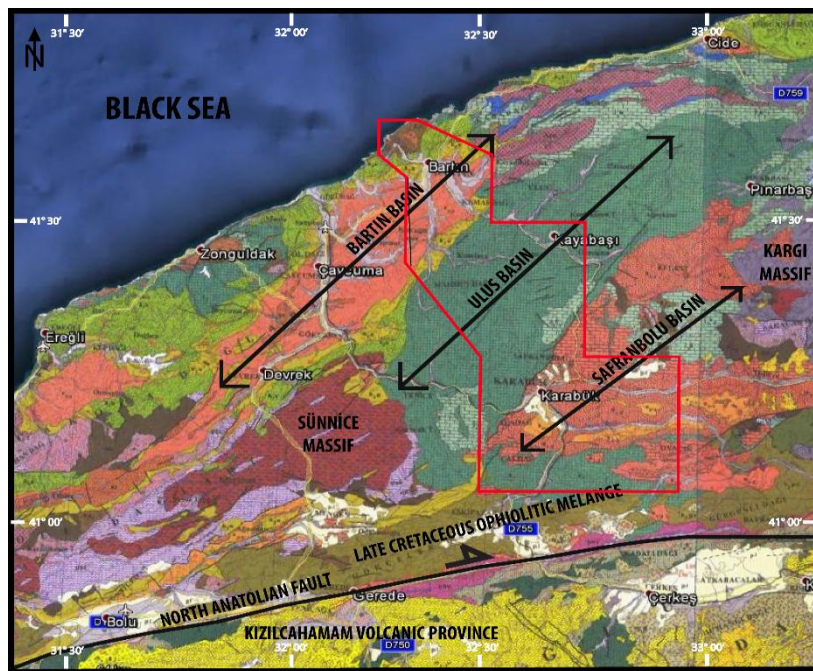


Figure 1.2. 1:500000 scaled geology map of Western Pontides (MTA, 1961). Please see the MTA geological map for more details.

<b>"Bartın-Karabük-Safranbolu-Ovacık Regions"</b>			
<b>Age</b>	<b>Northern Part (Bartın Basin)</b>	<b>Central Part (Ulus Basin)</b>	<b>Southern Part (Safranbolu Basin)</b>
<b>Eocene</b>	Lower-Middle Eocene		Lower-Middle Eocene
<b>Paleocene</b>	Maastrichtian-Paleocene	Erosion or Non-deposition or both	Late Paleocene
<b>K<sub>2</sub></b>	Santonian-Campanian		
<b>K<sub>1</sub></b>	Barremian-Cenomanian	Barremian-Cenomanian	Barremian-Cenomanian
<b>Jura-Cretaceous</b>	Oxfordian-Albian (?)	Oxfordian-Albian (?)	Oxfordian-Albian (?)
<b>Triassic</b>	Permo-Triassic		
<b>Paleozoic</b>	Devonian-Carboniferous	Devonian-Carboniferous	Devonian-Carboniferous

Figure 1.3. General stratigraphy of the Bartın-Ulus-Karabük-Safranbolu-Ovacık regions.

During Late Cretaceous, subduction complex was developed in the southern part of Western Pontides, while arc volcanism was effective in the north. Basins, Black Sea marginal back arc basin and the forearc basins, has evolved along with the island arc and Cretaceous ophiolitic mélange development. Pontide Mountains (Black Sea) were formed with the collision of southern continents and Eurasian fragments during post-Paleogene period.

The purpose of this thesis is to figure out the post-Paleogene (post-Middle Eocene-pre-Miocene) tectonics in the Western Pontides by means of; (i) bedding attitude (dip and strike) data and (ii) fault-slip data from the Bartın-Karabük-Safranbolu-Ovacık region. The most challenging part of the study is the determination of the age of deformation phases. For this purpose, the studied belt was divided into three domains to simplify tectonostratigraphy and to discuss the tectonic evolution in a rather simple

model. The domains are: northern part (Bartın basin), central part (Ulus basin) and southern part (Safranbolu basin) (Figure1.3).

## 1.2. Geographic Location

The study area is located more specifically from north by Bartın province and from south by Ovacık village. The study comprises an area of approximately 3200 km<sup>2</sup> which is covered by the Zonguldak E28-c1, E28-c2, E28-c3, E-28-c4, F28-b1, F28-b2, F28-b3, F-28-b4, F29-a1, F29a2, F29-a3, F29-a4, F29-c1, F29-c2, F29-c3, F29-c4, F29-d1, F29-d2, F29-d3, F29-d4 1/25000 topographic maps of Turkey (Figure 1.4).



Figure 1.4. Geographic setting of the study area (from Google Earth).

E-W-trending Kumluca and N-S-trending Günye Streams meet at Kozcağız village, and continue to flow as N-S-trending Bartın River. In the northern part of the study area, NE-SW-trending Gökırmak and E-W-trending Kızılırmak Streams join the N-S-trending Bartın River in Bartın village, and enters into the Black Sea. E-W-trending Araç and Soğanlı streams meet at the Karabük village, and continue to flow as NW-



SE-trending Filyos River, which also enters the Black Sea. Moreover, in the southern part of the study area, Soğanlı Stream has two branches; Boğursak Stream and Eskipazar Stream (Figure 1.4).

The highest elevation in the study is 1727 meters at the Sarıçicek Hill located within Mahmut Mountain. Demiroluk Hill (1703 meters), Örenler Hill (1654 meters) and Turnaçal Hill (1556 meters) are other important peaks in Bartın-Ulus region. Around Karabük-Safranbolu region, Çaldağ Hill is 1683 meters (Figure 1.4).

### **1.3. Methods of the Study**

Several steps were performed in during thesis study to get an idea about the tectonic evolution and regional geology of the study area. Firstly, literature survey and previous studies were studied. Stratigraphy of the region and related geological maps are revised. Stratigraphy is re-established and highly supervised to see the big picture for tectonic analysis. Moreover; unpublished Turkish Petroleum (TP) reports were taken into consideration in lithostratigraphic analysis. Then, available geological data were compiled about Bartın, Ulus, Safranbolu and Ovacık regions.

Before field works, 20 sheets of 1/25.000 scaled geological maps were compiled. While preparation of these, 1/50.000 and 1/100.000 scaled geological maps were upgraded and revised, then transferred into 1/25000 scaled maps.

Two field works were performed. First one took three weeks and the second one took a week. Two and a half week of the field work was allocated for Bartın and Ulus areas, and remaining times for Ovacık and Safranbolu areas.

Field works were performed to verify the revised geological maps, lithostratigraphy and to collect bedding and fault-slip data. In the light of existing geological maps, 2 major traverses were selected for further field works. Extreme cases were taken into consideration when deciding the location of the traverses, because they have to cross over the most of the fold axis and major faults in the study area. During this study, dip and strike data of beds were collected and contacts were checked, the dip-strike

data of the faults, slip sense on slickenlines of fault planes (pitch/rake) were measurement.

After collection of the data, verification and revision of the geological maps performed, and all structural features were analysed by WinTensor 5.8.5™, GeoRose™ and RockWorks 2017™ softwares. To draw the figures, Adobe Illustrator CS6™ was used.

At the end, structural and kinematic results of the analyses were evaluated, and structural elements -folds and faults- were interpreted by means of the calculated principal paleostress orientations. Paleostress orientations in time, post-Eocene period, are combined with the geological evolution history of the terrain.

## **CHAPTER 2**

### **REGIONAL GEOLOGY**

#### **2.1. Previous Studies**

Since 1948, many studies have been carried out in different part of the Western Pontides in the areas between the Black Sea Coast and the North Anatolian Fault. These regional studies were concentrated on two main zones; Amasra-Bartın and Karabük-Safranbolu areas.

##### **2.1.1. Amasra-Bartın Zone**

First study was carried out by Fratschner (1952) around Amasra-Bartın-Kumluca-Kurucaşile-Ulus region. According to this study, Tertiary is the youngest and Namurian is the oldest rock units in the area. Folded structures in Upper Cretaceous and Tertiary successions were explained with the vertical movement.

In Ovacuma and Eflani, oldest unit is the Paleozoic metamorphics, which are overlain by Lower Cretaceous transgressive flysch facies (Ketin, 1953). In addition to this, Lower Cretaceous succession (Barremian-Cenomanian) is unconformably overlain by Maastrichtian limestones. Flysch facies was studied by Göktunalı (1957). He concluded that intensive folded structures were mostly overturned, vertical, and show variable orientations.

Tokay (1954) identified structural features in Amasra basin, has explained these structures by gravitational sliding events during Carboniferous. However, Şahintürk and Özçelik (1983) claimed that structural features in the basin have occurred during Dogger and Cretaceous tectonics.

Gümüş (1966, 1967) stated that Upper Cretaceous units in the Amasra-Bartın region are different from those of Ulus region. However, Paleozoic and Mesozoic successions are similar.

The folds were interpreted as a result of Eocene tectonics (Gümüş, 1966) or as depositional syn-sedimentary structures (Şahintürk and Özçelik, 1983) in the Bartın region.

Around Zonguldak and Bartın regions, Paleozoic succession was folded during Hercynian and Early Cimmerian orogenesis, and then terrestrial and erosional environment were sustained. There is an angular unconformity between Jurassic transgressive sequence and the Paleozoic basement (Saner et al., 1981). The authors claimed that Lower and Upper Cretaceous deposits on the top of Upper Jurassic-Lower Cretaceous İnaltı Formation are different in the Zonguldak and Bartın regions.

Bulut and others (1982) indicated that Bartın-Amasra basin was uplifted during Early Cretaceous, and then invaded by sea during Late Cretaceous. Some of the folds were originated during Hercynian Orogenesis, and some of them during Alpine Orogenesis.

In the Amasra-Bartın region, Deveciler (1986) reported that reverse faults originated from N-S oriented compressional forces, and normal faults and landslides occurred in association with E-W oriented tensional forces.

Tüysüz and others (1997) indicated that the area was not affected by the regional deformation from Carboniferous until Early Cretaceous rifting of the Ulus Basin. According to the authors, the Ulus Basin was rifted as an extensional basin during Early Cretaceous, and maintained its position until Maastrichtian.

With the closure of Neo-Tethys Ocean in the south, the sequences were started to be contract, N-vergent thrust faults were developed, and successions were imbricated during Late Eocene-Early Miocene. Pre-Middle Eocene and Middle Eocene units exposed in the area between Amasra and Cide, were affected by compressional forces subsequent of the deposition of Campanian Cambu Formation (Sunal and Tüysüz,

2002). Sunal and Tüysüz (2002) claimed that the Upper Cretaceous units are absent to the south of thrust faults, and towards faults in Cide area, thickness of these units increases. This is the result of inversion tectonics, which means that normal faults, as a part of previous extension systems, were reactivated as thrust faults. According to their measurements and paleostress calculations, they conclude that sub-horizontal  $\sigma_1$  and  $\sigma_2$  axes orientations resulted in faults occurring in a compressive regime. They claimed that the North Anatolian Fault between the Anatolian and Eurasian plates is still active and continue to deform the Western Pontides. Therefore, Western Pontides is still under the effect of a compressional regime and uplifting along the Black Sea Mountains still continuing since the Oligocene.

Temel and others (2015) identified that the most distinctive structures of the Western Pontides in the İstanbul Zone as Paleozoic successions. These successions start with Lower Devonian marine deposits, continue with Upper Devonian-Lower Carboniferous platform carbonates, Carboniferous shallow-marine deposits, and end with Permo-Triassic deltaic-terrestrial deposits. This indicates a regression during the Paleozoic. Bartın-Ulus Basin is tectonically active along the Alpine-Himalayan zone during the Jurassic to Late Miocene time.

### **2.1.2. Karabük-Safranbolu Zone**

The first geological map at a scale of 1/100000 of the Karabük-Safranbolu region was prepared by Blumenthal (1948). Stratigraphic succession was divided into two basic units; (i) flysch facies of Tertiary which coincide with Early-Middle Eocene Karabük Formation, and (ii) limestones. Two different gray limestones, of Paleozoic and Mesozoic age, were not differentiated, and both were interpreted as Lower Cretaceous. Blumenthal (1948) proposed that metamorphic rocks in the area are pre-Paleozoic. Straight contacts in the north of Karabük and E-W-trending complex in Eskipazar are interpreted as faults.

Saner and others (1979) prepared 22 sheets of geological maps at a scale of 1/25.000 in the Karabük-Safranbolu and Ovacık regions. Based on structural analysis, the authors indicated that geological features in the study area are dominantly in E-W-

trending, and has resulted from N-S compression. In contrast to, E-W-trending Mesozoic–Tertiary structures, trend of the Paleozoic structures in NW-SE direction. The Karabük Fault was interpreted as reverse fault with uplifting northern block, and it was activated after the deposition of Paleocene-Middle Eocene limestones. The Barremian-Cenomanian Ulus Formation with Upper Jurassic İnaltı limestones was thrust over Paleocene-Middle Eocene Safranbolu Formation (Şen, 2001). The Karagöl Fault is interpreted as a reverse fault, where southern block was moving up. Age of this fault was proposed as Late Eocene or younger (Saner et al., 1979).

Güven (1977) discussed four alternating phases of sedimentation for the Eocene sequences in the Karabük area. Depositional environments are carbonate marine shelf, fluvio-deltaic, fluvial and terrestrial environments, that were started to evolve during the Late Paleocene to the Early Eocene time. Regional tectonics controlled four phases of sedimentation.

Saner and others (1979) indicated that boundary between Maastrichtian-Campanian succession and Barremian-Cenomanian Ulus Formation is conformable, and there is a paraconformity between Maastrichtian-Campanian and Paleocene-Lower Eocene Formations. Whereas, Şen (2001) suggested that contact between Maastrichtian-Campanian Formation and Barremian-Cenomanian Ulus Formations is an angular unconformity and that Maastrichtian-Campanian and Paleocene-Lower Eocene formations are conformable. Moreover, Paleocene-Lower Eocene successions are laterally and vertically transitional (Saner et al., 1979). However, Şen (2001) reported that only Paleocene-Lower Eocene formations are transitional and unconformably overlies the Paleocene-Lower Eocene Formations. Şen (2001) stated that the Karabük-Safranbolu basin has evolved above the Barremian-Cenomanian Ulus Basin during Late Cretaceous (Maastrichtian), and there is an angular relationship between these two basins.

Tokay and others (1986) discussed that Eocene sequences were intruded by same age volcanics in the west of the Karabük-Safranbolu Basin around Bolu and east of this basin around Araç-Kastamonu zone. However, no volcanic relations were in the

center of the basin. The authors agreed with Saner et al. (1979) and Blumenthal (1948) that, Eocene sequences overlay the older units (Lower Cretaceous flysch, pre-Jurassic metamorphic rocks, post-Campanian Anatolia Nappe) unconformably at the center and the eastern part of this basin. Whereas, at the western part of the basin, contacts between Eocene sequences with Paleocene units are from place to place conformable and unconformable. Due to the missing of Oligocene and Miocene succession in the basin, it is difficult to explain post-Lutetian geological evolution of the Karabük-Safranbolu region (Tokay et al., 1986). However, the authors sure that the basin has experienced two uplifting during Late Paleocene-Pleistocene and Late Quaternary times. The unconformable boundaries between northward dipping overturned beds of Lower Lutetian deposits and Lower Cretaceous flysch were interpreted as Karagöl Fault (Erten and Özcan, 1997). Moreover, south dipping shear fracture was named as Değirmenci Fault near the contact between Lower Cretaceous flysch and Lower Lutetian sequences (Tokay et al., 1986). Southern block of this fault has downthrown about 30-40 meters. The Eocene beds were overturned as a result of compressional forces. The age of the fault is Late Paleocene-Pleistocene or younger (Tokay et al., 1986). On the other hand, Değirmenci fault formed after Karabük Fault evolution (Saner et al., 1979).

The rock units in the Karabük region are classified into six formations and four members (Güven, 1977; Koçyiğit, 1987). According to Koçyiğit (1987), southwest of the basin is narrow, northwest of the basin is wide and current shape was originated at the end of Late Lutetian. Northwestern part of the Karabük-Safranbolu Basin is characterized by a thrust fault at southeast, and continues with overturned folding and normal stratigraphy with angular unconformity towards to northwest. Moreover, NNW-SSE horizontal compression force was continued and more effective in the southwestern part of the region than the northeastern part (Koçyiğit, 1987). Yergök and others (1987) said that N-S or NE-SW-trending compressional forces in Karabük region, interpreted from the E-W-trending structures. The authors added that these forces were originated from Alpine Orogenesis, and normal faults were generally active during Early Cretaceous.

Erten and Özcan (1997) agreed with Saner and others (1979) about the trends of Mesozoic-Tertiary and Paleozoic structures. The Paleocene-Middle Miocene Safranbolu Formation are transgressive above Upper Cretaceous, and there is an angular unconformity in between. The Karagöl Fault is an E-W-trending reverse fault with a length of about 50 km (Erten and Özcan, 1997). However, Aydın and others (2001) interpreted this as a strike-slip fault. They claimed that the fault firstly had a dip slip component and then gained a strike-slip component during Late Miocene. Aydın and others (2001) also added that the fault forms an inactive arm of the North Anatolian Fault, because the Gökçesu thrust fault is the probably the western continuation of Karagöl Fault. Overturned syncline was the result of Karagöl Fault (Erten and Özcan, 1997). Age of the Karagöl Fault is Late Eocene or younger. Aydın and others (2001) interpreted the Karabük Fault as NE-SW-trending reverse dip slip fault with a length of 60 km. It is claimed that throw of the fault has to be more than 1000 meters (Erten and Özcan, 1997).

## **2.2. Tectonic Setting of Western Pontides, Turkey**

Turkey can be basically divided into three major tectonic belts as Taurides, Anatolides and Pontides (Ketin, 1966). Anatolides, is made up of metamorphic massifs and core complexes, which are the Kırşehir Block and Menderes Massif (Şengör and Yılmaz, 1981). Southern part of these massifs is called Taurides and northern part, Pontides (Ketin, 1966).

The Pontides record evidence of Alpine and Cimmerides orogenic events in Tethyside collage (Şengör et al., 1984). Tethyan evolution of Turkey can be divided into two phases that are overlapping in time; Paleotethys and Neotethys (Şengör and Yılmaz, 1981). The Cimmerian orogeny was occurred with the elimination of Paleotethys, and part of the Cimmerian continent constitutes the basement of Pontides. Neotethys evolved with the diminishing of the Paleotethys Ocean. The Cimmerian continent and the Scythian platform of Laurasia were collided in the north. The ocean totally was consumed during Dogger. Neotethys continued to evolve until Late Cretaceous. During Late Cretaceous, Neotethys was started to subduct



beneath the Eurasia. Pontides and Tauride-Anatolide Platform collided during closure of the Neotethys in post- Middle Miocene. Finally, today's mountains have started to elevate since Late Miocene.

Pontides has three tectono-stratigraphically distinctive regions. The Eastern Pontides, the Central Pontides and the Western Pontides, which are amalgamated to form Pontides (Figure 1.1). The Eastern Pontides consist of a curvilinear tectonic entity, which is Cretaceous-Paleocene magmatic belt, the fore arc and related basins, belt of metamorphic massifs and an ophiolitic belt. The Central Pontides are a tectonic knot and formed by the juxtaposition of the Eastern and Western Pontides. The Central Pontides, which is a NE-SW -trending tectonic entity, is composed of the Araç-Daday shear zone (Deveciler et al., 1989; Şengün, 1993), the Kastamonu-Boyabat Basin fill (continuous succession from Upper Cretaceous to Oligocene), the Kargı Massif and an ophiolite belt. The Western Pontides is made up of four different tectonic zones as the Istranca Massif, the İstanbul-Zonguldak Zone, the Armutlu-Almacık Zone and the Sakarya Continent (Okay and Tüysüz, 1999). These four tectonic entities are differentiated from each other with different geological successions, and are separated from each other with tectonic structures.

The study area is located within İstanbul-Zonguldak zone (İstanbul Nappe: Şengör et al., 1984) in the northeastern part of the Western Pontides. Stratigraphic section of the zone starts with high-grade metamorphic rocks at the base. The Precambrian basement rocks are exposed in the Sünnice Massif and in Safranbolu village (Yılmaz and Tüysüz, 1984). In the Zonguldak and Amasra regions, Paleozoic shallow-marine carbonate and terrestrial successions overlies the Precambrian metamorphic rocks. Triassic red fluvial and eolian deposits are exposed in Amasra and Cide, while Triassic marine succession, in the Kocaeli Peninsula. After the deposition of Oxfordian-Barremian platform carbonates, two large basins (Zonguldak and Ulus Basins) were rifted. Carbonate and clastic rocks were deposited in the Zonguldak Basin, while the turbiditic facies deposited in the Ulus Basin during Late Barremian–Cenomanian (Derman 1990). Turonian-Campanian magmatic-arc volcanism has highly affected the whole Turonian-Santonian succession in the Western Pontides.

After the arc volcanism in the Late Santonian, the basin was suddenly subsided, and widespread pelagic carbonates were deposited. Then, in the northern part of the Pontides, Maastrichtian deep marine calciturbidites were deposited. Upper Cretaceous-Eocene successions transgressively cover all Paleozoic and Triassic units (Temel et al., 2015).

## CHAPTER 3

### STRATIGRAPHY

Stratigraphy of the study area constructed on three successions; pre-Jurassic units, Upper Jurassic-Lower Cretaceous units, and Upper Cretaceous-Eocene units (Figure 1.3, Figure 3.1). Pre-Jurassic units show some differences between the Bartın-Ulus and the Karabük-Safranbolu regions, but in both regions, they are considered to form the basement. The Upper Jurassic- Lower Cretaceous successions are same in both regions. Upper Cretaceous-Eocene units in both two basins are however, totally different from each other. Moreover, effects of the Upper Cretaceous volcanism are not recorded in the Karabük-Safranbolu region.

#### 3.1. Pre-Jurassic Basement

The Pre-Jurassic units are mainly composed of six formations with ages ranging from Early Devonian to Triassic. These formations are; Early Devonian Kartal Formation, Late Devonian-Early Carboniferous (Upper Visean) Yılanlı Formation, Late Visean-Late Namurian-Westphalian Alacaağız Formation, Westphalian Zonguldak Formation, Triassic Çakraz Formation and Late Triassic Çakraboş Formation.

Some formations are exposed in the study area, and some do not. In this study, these formations are mapped as one unit (Figure 3.1). They are shown as a single unit in stratigraphic columnar sections of the Bartın-Ulus Basin (Figure 3.2) and the Karabük-Safranbolu Basin (Figure 3.3).

### **3.1.1. Kartal Formation**

The formation was firstly identified by Haas (1968) as Kartal layers, and then named as Kartal Formation by Kaya (1973) (Işıker et al., 2004). It crops out in the northwest of the Karabük Fault with a very limited exposure in the study area.

Lower contact of the Kartal Formation is conformable with the Lower Devonian units whereas, upper contact is unconformable with the Upper Devonian-Lower Carboniferous Yılanlı Formation in the Zonguldak region (Şahintürk and Özçelik, 1983; Derman and Özçelik, 1993). Maximum thickness attained in the İnkumu region is 200 meters. The Kartal Formation consists of black and greyish black color shale, dark colored limestone, dolomitic limestone and nodular fossiliferous limestone (Şahintürk and Özçelik, 1983).

Age of this formation is Early Devonian (Şahintürk and Özçelik, 1983) and was deposited in a shallow-marine environment (Temel et al., 2015).

### **3.1.2. Yılanlı Formation**

Yılanlı Formation was named by Saner and others (1979). The formation is mapped in the north of the Bartın region and northwest of the Karabük Fault in the study area.

Yılanlı Formation has conformable upper contact with the Upper Viséan-Westphalian Alacaagzı Formation (Şahintürk and Özçelik, 1983). It is covered unconformably by Upper Jurassic İnaltı Formation in the Karabük region (Saner et al., 1979). Bottom contact of this formation is unconformable with Lower Devonian Kartal Formation (Şahintürk and Özçelik, 1983; Derman and Özçelik, 1993; Saner et al., 1979). Maximum thickness is about 1200 meters around İnkumu Village (Şahintürk and Özçelik, 1983). Yılanlı Formation starts with alternation of shale, siltstone and nodular limestone. Towards top, it is represented by thin to medium bedded, light gray to black color of mudstone, wackestone, locally siltstone and boundstone alternation. At the most upper part, dolomitization increases, and dolomitic limestones reported. The transitional zone with Upper Viséan-Westphalian Alacaagzı Formation contains widespread chert nodules (Temel et al., 2015).







AGE		FORMATION	THICKNESS (m)	LITHOLOGY	DESCRIPTION	
TERTIARY	Plio- Quaternary				Gaverl, sand, mud	
	EOCENE	KUSURİ	2000		Sandstone-shale alternation	
						Siltstone-shale alternation
	PALEOCENE	ATBAŞI	250		Carbonaceous marl	
LATE CRETACEOUS	MAASTRICHTIAN	<div>BAYRAMOĞLU LAVA MEMBER</div> AKVEREN	500		<div>Basaltic lava</div> Clayey limestone with marl	
	CAMPANIAN	YEMİŞLİÇAY GROUP	CANBU	1000		Basaltic lava
			UNAZ	120		Clayey pelagic limestone
	SANTONIAN		KÖKYOL	500		Pelagic limestone
	CENOMANIAN					
	EARLY CRETACEOUS	ALBIAN	ULUS	3000		Sandstone-siltstone-shale alternations with İnalı olistoliths and clastics
APTIAN						
BARREMIAN		<div>AHMETUSTA MEMBER</div> İNCİGEZ	50		Pebbly sandstone	
HAUTERIVIAN		İNALTI	1200			
BERRIASIAN						
LATE JURASSIC	TITHONIAN	BASEMENT	> 4000		Platform carbonates	
KIMMERIDGIAN						
OXFORDIAN						
Pre-JURASSIC	DEVONIAN - CARBONIFEROUS				Çakrazboz Fm. Alacaağzı Fm. Çakraz Fm. Yılanlı Fm. Zonguldak Fm. Kartal Fm.	

Figure 3.2. Stratigraphic columnar section of the Bartın-Ulus Basin (not to scale).

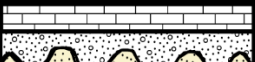

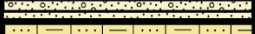


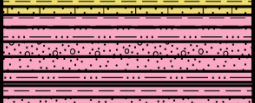
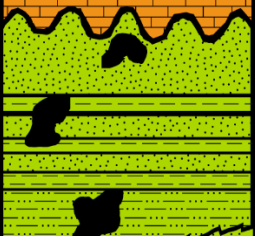
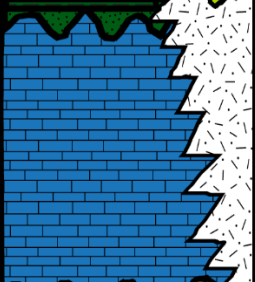
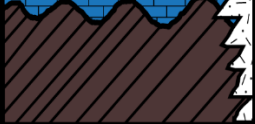
AGE		FORMATION	THICKNESS (m)	LITHOLOGY	DESCRIPTION		
TERTIARY	Plio-Quaternary	YÖRÜK	100		Conglomerate and limestone		
	EOCENE	YUNUSLAR	150	    	KÖSELER MEMBER	40	Ripple and cross bedded sandstone and conglomerate
		AKÇAPINAR	200		Sandstone and marl		
		SOĞANLI	150		Clayey limestone with siltstone and sandstone alternation		
		ÇERÇEN	450		Sandy limestone interbedded with mudstone		
		KARABÜK	2000		Conglomerate-sandstone - siltstone-mudstone alternation		
		SAFRANBOLU	700		Sandstone interbedded with siltstone-mudstone, cross bedded sandstone		
	PALEOCENE				Limestone interbedded with clayey limestone		
	EARLY-LATE CRETACEOUS	CENOMANIAN	ULUS	3000		Sandstone-siltstone-shale alternations with İnaltı olistoliths and clastics	
		ALBIAN					
APTIAN							
BARREMIAN		AHMETUSTA MEMBER	50	Pebbly sandstone			
		İNCİGEZ	60	Sandstone with mudstone			
HAUTERIVIAN		İNALTI	1200		Platform carbonates		
BERRIASIAN							
TITHONIAN							
KIMMERIDGIAN							
LATE JURASSIC	OXFORDIAN						
Pre-JURASSIC	DEVONIAN - CARBONIFEROUS	BASEMENT	> 4000		Çakrazboz Fm. Alacaağzı Fm. Çakraz Fm. Yılanlı Fm. Zonguldak Fm. Kartal Fm.		
		Dirgine Granite		Granite			

Figure 3.3. Stratigraphic columnar section of the Karabük-Safranbolu Basin (not to scale).



The age of the formation is Late Devonian-Early Carboniferous (Upper Visean) (Saner et al., 1979) and it was deposited in a shallow-marine environment in reefal facies (Şahintürk and Özçelik, 1983).

### **3.1.3. Alacaağzı Formation**

It is named as Alacaağzı layers and Alacaağzı Formation (Kerey et al., 1986). Its widespread exposures are around the Bartın-Süzükdere region and the Gavurpınar village.

Lower contact with Upper Devonian-Lower Carboniferous Yılanlı Formation is conformable. Upper contact is conformable with Westphalian Zonguldak Formation (Şahintürk and Özçelik, 1983). In the Bartın region, its thickness reaches 400 meters (Şahintürk and Özçelik, 1983). At the bottom, the formation is composed of mudstone and wackestone with brachiopoda and trilobite fossils. These layers are followed by coarsening upward succession of dark mudstone and sandy siltstone sequence (Kerey et al., 1986).

The age of the formation is Late Visean-Late Namurian (Şahintürk and Özçelik, 1983; Kerey et al., 1986) and Namurian-Westphalian (Derman and Özçelik, 1993). Depositional setting is a delta front, delta plain and flood plain (Temel et al., 2015).

### **3.1.4. Zonguldak Formation**

Zonguldak Formation is named by Kerey (1982). Type locality is in the Zonguldak-Kozlu mining sections and it is widely exposed along the Zonguldak-Amasra villages.

The formation is conformable with Upper Visean-Westphalian Alacaağzı Formation at the bottom, whereas Permian-Triassic Çakraz Formation overlies it with an angular unconformity. Thickness of the formation is about 400 meters in the Amasra-Bartın regions, and maximum thickness up to 700 meters is attained in the Zonguldak region. Zonguldak formation is made up of alternation of conglomerate, sandstone, siltstone and mudstone with coal seams intercalations. Conglomerates are composed of well-rounded quartzite, magmatic and metamorphic grains (Temel et al., 2015).

Zonguldak Formation is at Westphalian age and it is correlated with the Kozlu and Karadon Formations (Şahintürk and Özçelik, 1983). Zonguldak Formation was deposited in meandering river, flood plain, and lacustrine environments with thick and widespread coal deposits (Temel et al., 2015).

### **3.1.5. Çakraz Formation**

It is named as Çakraz sandstone (Akyol et al., 1974), then as a Çakraz Formation (Aydın et al., 1986; Akman, 1992; Alişan and Derman, 1995).

There is an unconformity between Çakraz Formation and older units. Çakraz Formation is overlain conformably by Upper Triassic Çakrazboz Formation and unconformably by Jurassic units (Temel et al., 2015). Thickness of the formation is around 1200 meters near the Çakraz region (Akyol et al., 1974). Dominant lithology is dark and reddish color sandstone and mudstone. Towards upper parts of succession, grain size decreases whereas alternation of sandstone, siltstone and mudstone increases.

There is no direct evidence of age due to the lack of fossil content. According to the stratigraphic position, the formation is in Triassic age (Akman, 1992; Tüysüz et al. 1997) or Permian to Triassic age (Akyol et al. 1974). Çakraz Formation was deposited in a fluvial environment (braided fluvial to meandering river, and flood plain) to terrestrial environment under wind-blown regime (Temel et al., 2015).

### **3.1.6. Çakrazboz Formation**

It is named as a Çakrazboz Formation and type locality and type section are reported as Çakrazboz village on the Çakraz-Amasra highway (Akman, 1992).

Çakrazboz Formation, which has a transitional contact with Triassic Çakraz Formation at the base, has an unconformable relationship with younger units at the top (Işıker et al., 2004). In the field, pinkish, greenish and grayish mottled color is used as a distinguishing marker of the formation. Thickness of the formation is around 350 meters (Akman, 1992). Çakrazboz Formation consists of fine-grained clastics and carbonates. Dominant lithology is homogenous alternation of marl-

siltstone and this alternation is in place replaced by siltstone, sandstone and limestone sequences (Temel et al., 2015).

The age of the formation is Late Triassic according to palynological data (Rutherford et al., 1992; Alişan and Derman, 1995). Çakrazboz Formation was deposited in lacustrine and freshwater environment (Temel et al., 2015).

### **3.2. Upper Jurassic-Lower Cretaceous Units**

In both Bartın-Ulus and Karabük-Safranbolu regions, Upper Jurassic and Lower Cretaceous cropped out (Figure 3.1). The succession starts with syn-rift Upper Jurassic carbonates and ended with Lower Cretaceous clastic and detrital carbonate rocks (Figure 3.2 and Figure 3.3).

#### **3.2.1. İnaltı Formation**

It is named as İnaltı Formation by Ketin and Gümüş (1963). Type locality is İnaltı village (S of Sinop-Ayancık) (Ketin and Gümüş, 1963). In the study area, the formation is exposed at very few locations as olistoliths (Figure 3.1, Figure 3.4, Figure 3.5).

It has an unconformable contact with pre-Jurassic basement and is unconformably overlain by Lower Cretaceous units. Thickness of the formation is about 150-1200 meters (Derman and Sayılı, 1995).

The succession starts with transgressive very shallow-marine clastics (Tüysüz et al., 1997) and continues with the fossiliferous micritic limestone. The formation shows shallow-marine to reefal environment to shelf carbonate facies (Temel et al., 2015). The İnaltı Formation is a platform carbonate, deposited on passive continental margin.

The formation is divided into members due to the intraformational unconformities (Akman, 1992; Tüysüz et al., 1997). The succession below the unconformity is Oxfordian-Berriasian in age, and above the unconformity is Barremian-Albian in age. Age of İnaltı Formation is accepted as Late Jurassic-Early Cretaceous in this study.

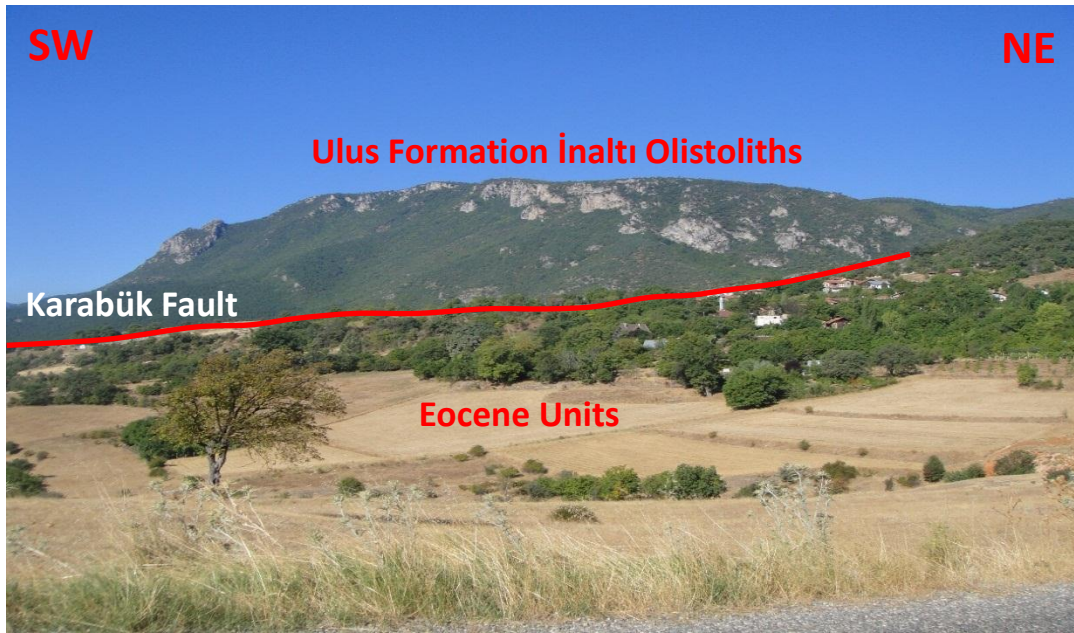


Figure 3.4. İnaltı olistoliths within Ulus Formation near Karabük Fault in Sunduk village (NW of Safranbolu).



Figure 3.5. General and close-up view of İnaltı Formation along Bartın-Amasra highway.

### **3.2.2. İncigez Formation**

The formation is named as Indjues-Schicht (Arni, 1931), İncüvez layers (Altınlı, 1951), İncigez clastic member (Saner et al., 1980; Yergök et al., 1987) and finally İncigez Formation (Derman, 1990). The formation is exposed in Karadağ Hill at northwest of Karabük Fault in the study area (Figure 3.1).

The İncigez Formation lies conformably above the Berriasian limestones where the upper contact is an unconformity (Tokay, 1952; Saner et al., 1980; Yergök et al., 1987). However, Derman (1990) indicated that the İncigez Formation have unconformable contact with Oxfordian-Berriasian and Barremian-Aptian limestones. Maximum thickness of the formation reaches up to 60 meters (Saner et al., 1980). The İncigez Formation is composed of sandstones, mudstones, sandy limestones and limestones (Saner et al., 1980; Yergök et al., 1987). Sandstones are mostly brownish, gray, well sorted, and made up of limestone, granite, quartzite, serpentine fragments. Mudstones are mostly in red color and contain carbonate nodules, bioturbation traces coal fragments (Saner et al., 1980). Limestones are beige in color, medium-thick bedded to lens shaped and contains abundant macrofossil (Temel et al., 2015).

The age of the formation is Aptian (Arni, 1931; Altınlı, 1951) or Early Barremian-Early Aptian (Yergök et al., 1987) or Early Aptian (Tokay, 1952) or Hauterivian (Siyako et al., 1980). Depositional environments of this formation are reported as lagoon, river and flood plain (Saner et al., 1980).

To sum up, Upper Jurassic and Lower Cretaceous sequences were mapped as the İnaltı Unit in this study, and age is accepted as Oxfordian-Barremian with an unconformable upper, lower contacts and with an intraformational unconformity (Figure 3.2 and Figure 3.3).

### **3.2.3. Dirgine Granite**

It is named as Dirgine granite (Aydın et al., 1987; Cerit, 1990) and as Bolu granitoids (Ustaömer, 1996). Sünnice massif, bounding the Ulus Basin from south, consists of Paleo-Tethys ophiolites (Yiğitbaş and Elmas, 1997). These ophiolites and their cover

units (Basement and Upper Jurassic) were intruded by the Dirgine Granite (Yergök et al 1987; Yiğitbaş and Elmas, 1997). The granite is exposed at the northern part of the Bartın region and the eastern part of Karabük region in the study area (Figure 3.3).

Paleozoic Yılanlı Formation and Upper Jurassic-Lower Cretaceous İnaltı limestones were cross-cut by this intrusion. Furthermore, recrystallization of the İnaltı limestone can be seen at the contact of intrusion. The Dirgine Granite consists of granites, granodiorites, tonalites, quartz rich granodiorites and quartz monzonites (Yiğitbaş and Elmas, 1997). The granite is I-type granite.

The age is Carboniferous or Late Jurassic (Aydın et al., 1987; Yergök et al 1987; Yiğitbaş and Elmas 1997) or Lower Paleozoic (Ordovician) (Cerit, 1990) or older than Early Ordovician (Bolu granitoids) (Ustaömer, 1996). However, age of the granite is accepted as post-Oxfordian-Barremian as it intrudes into the İnaltı limestone and overlain by the Barremian-Cenomanian Ulus Formation.

#### **3.2.4. Ulus Formation**

Ulus Formation is named by Akyol and others (1974). Type locality of the formation is in the Ulus region, and type section is at Ovacuma Village (Saner et al., 1979). This formation is bounded by Sünnice Massif in the west, Azdavay region in the east. It is cropped out largely between Bartın and Karabük Faults in the study area (Figure 3.1).

Ulus Formation unconformably overlies Upper Jurassic-Lower Cretaceous İnaltı Formation and overlain by Paleocene units with angular unconformities (Şahintürk and Özçelik, 1983). Exact thickness is unknown but thickness may reach up to 3000 meters in the Ulus Basin (Saner et al., 1979). Base of the Ulus Formation starts with submarine fan deposit, and grades into turbiditic facies towards top. Submarine fan deposit, defined as Barremian Ahmetusta Member (Saner et al., 1979), is composed of pebbly sandstone, sandstone, siltstone up to 50 meters thick. Grains are very angular, poorly sorted and well cemented (Saner et al., 1979). The submarine fan sequence continues with alternation of shale-siltstone and sandstone. In the Karabük region, Ulus Formation is defined as calcareous sandstone, which are high jointed,

joints are filled with calcite, and flute cast, groove cast, horizontal burrows are common. Dominant lithology of the Ulus Formation is deep marine turbidities with sandstone-shale alternation. Therefore, Ulus Formation forms a good example of stack turbidity channelized system (Figure 3.6). Moreover, olistoliths of İnaltı Formation are common in Ulus Formation. This flysch facies is highly deformed in the region (Figure 3.7).

Because of intense deformation of the Ulus Formation in the Bartın region, many structural features were formed. The structural features like; shear zones/fractures (Figure 3.7), boudinage structures (Figure 3.8), normal drag folds related to normal faulting (Figure 3.9), horst and graben structures (Figure 3.10) and asymmetrical to overturned folds with a vergence of south to north (Figure 3.11), are extensively observed.

According to the structural features, i) there is a northward tectonic transportation in the region (Figure 3.11) and ii) normal faults are cross-cut by reverse and strike slip faults (Figure 3. 12).

The formation dated by its stratigraphic position because of poor fossil content. Valanginian (?) to Campanian age was given to the formation (Saner et al., 1979; Saner et al., 1980; Aydın et al., 1986; Yergök et al., 1987). However, Turkish Stratigraphic Committee (Işıker et al., 2004) proposed the age of Barremian to Cenomanian and this age interval is accepted in the thesis. The horst and graben system was formed during the rifting phase in extensional regime on Jurassic-Cretaceous carbonate platform (Temel et al., 2015). Ulus Formation is probably equivalent to Tasmaca, Sapça and Velibey Formations in the Zonguldak region, and to Çağlayan Formation in the Sinop region (Saner et al., 1980).





Figure 3.6. A view of a stack turbidity channelized system in the Ulus Formation near the Dereköy village.

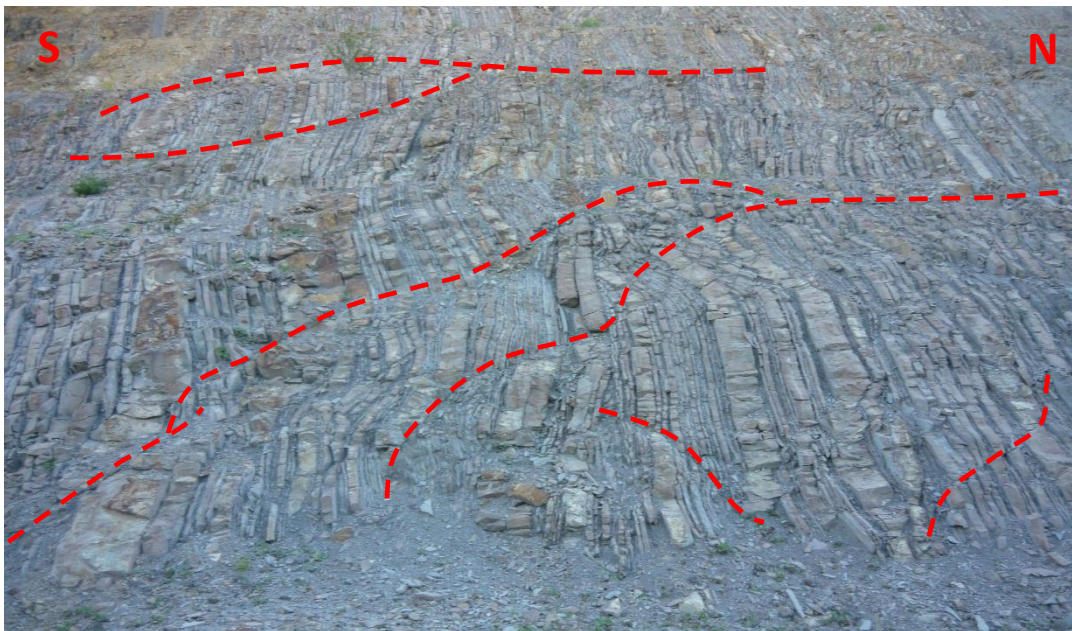


Figure 3.7. A view of intensely deformed flysch facies of the Ulus Formation near the Dereköy village.





Figure 3.8. Field views of boudinage structures (b) in the Ulus Formation near the Dereköy village.





Figure 3.9. A view from normal drag developed in Ulus Formation near the Dereköy village.

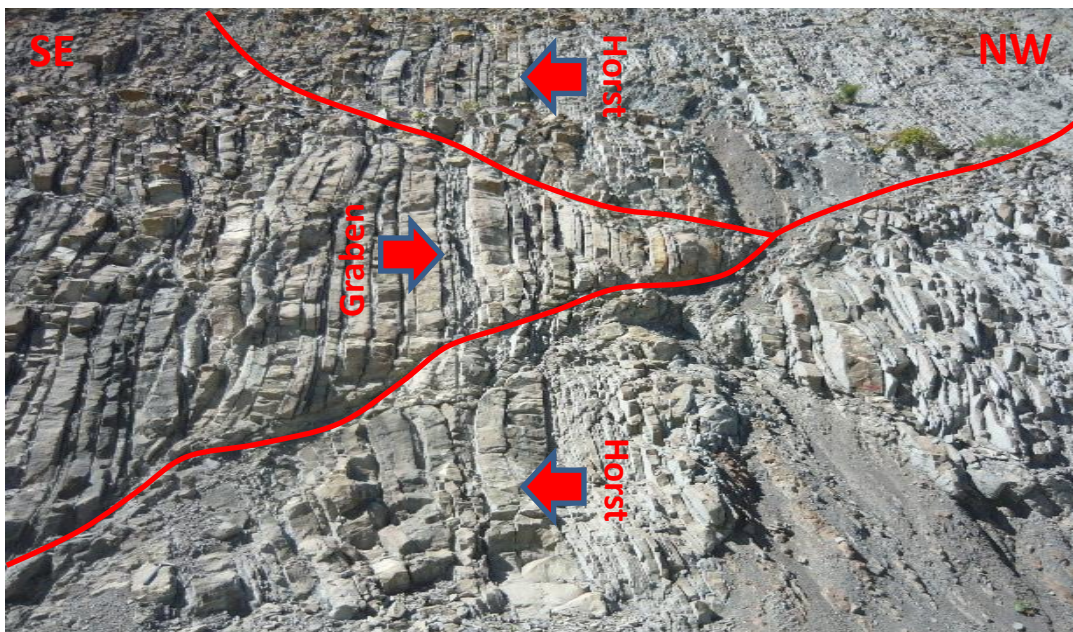


Figure 3.10. Field view of normal faulting forming a horst and graben structure in the Ulus Formation near the Dereköy village.



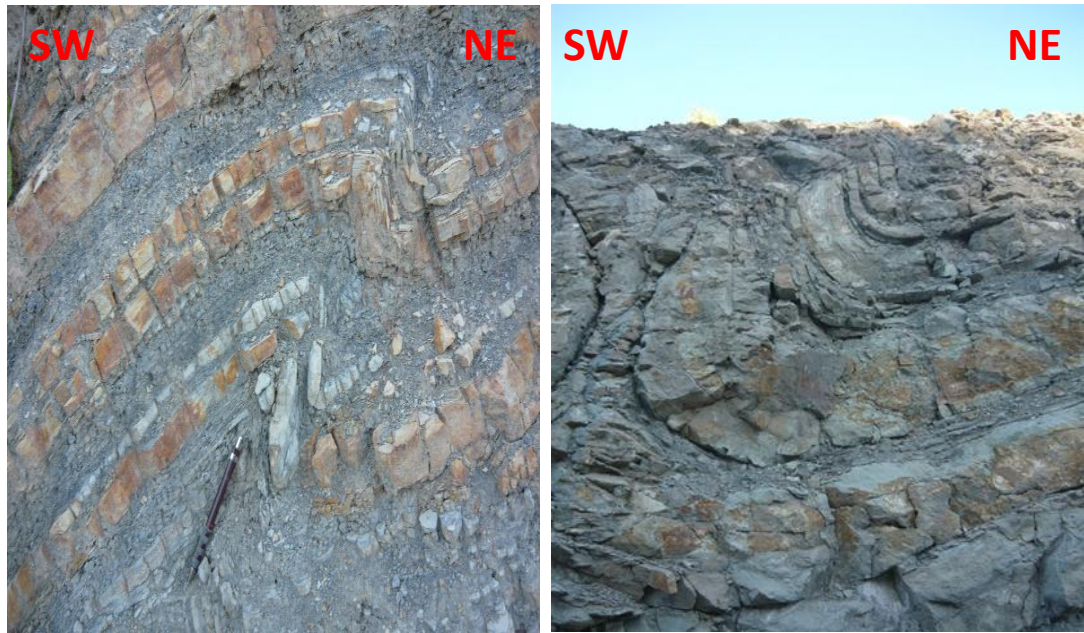


Figure 3.11. Field view of meso structures (overturned folds) indicating south to north tectonic transportation around the Dereköy village.

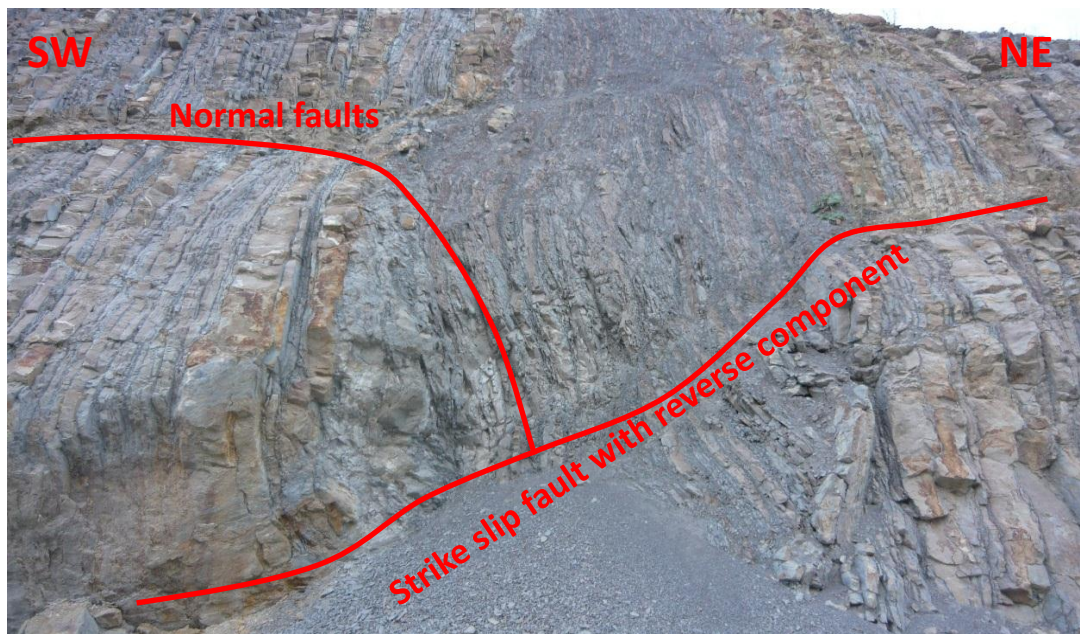


Figure 3.12. Field view of normal fault cross-cut by the left-lateral strike slip fault with reverse components. (NW of Safranbolu along new highway).

### **3.3. Upper Cretaceous – Eocene Units**

Upper Cretaceous-Eocene successions are different in Bartın-Ulus (Figure 3.2) and the Karabük-Safranbolu (Figure 3.3) regions. Therefore, two different depositional settings are set forward and used in tectonic interpretations.

#### **3.3.1. Bartın-Ulus Region**

##### **3.3.1.1. Yemişliçay Group**

It is composed of Late Cretaceous arc volcanism products (volcanic and volcanogenic succession) was defined as Yemişliçay Formation (Ketin and Gümüş, 1963) and then, the formation is upgraded to group stage (Kaya et al., 1982/1983). In the Zonguldak region, Yemişliçay group starts with Turonian Kapanboğazı Formation at the base in Karabük area, and continues with Turonian-Coniacian Dereköy and Yenice Formations. In the Bartın region, the group starts with Santonian Kökyol Formation at the base, and continues with Upper Santonian-Lower Campanian Unaz and Campanian Cambu Formations. In this study, Kökyol Formation, Unaz Formation and Cambu Formation were mapped together as Yemişliçay Group (Figure 3.1).

##### **3.3.1.1.a. Kökyol Formation**

The formation is named as Kökyol Formation by Şahintürk and Özçelik (1983). Type section is in İnpiri village (Akman, 1992). Kökyol Formation is exposed at the northern part of Bartın in the study area.

Kökyol Formation unconformably overlies the Lower Cretaceous units and conformably overlain by Upper Santonian-Lower Campanian Unaz Formation. The measured thickness range between 100-500 meters (Şahintürk and Özçelik, 1983). Formation is composed mainly of pelagic limestone.

The age of the formation is Cenomanian (Şahintürk and Özçelik, 1983). However, according to stratigraphic position, based on the underlying Cenomanian units and overlying Upper Santonian-Lower Campanian units, the age is Santonian (Akman,

1992; Tüysüz et al., 1997). This formation was deposited in intra-shelf environment (Şahintürk and Özçelik, 1983).

#### **3.3.1.1.b. Unaz Formation**

Akyol and others (1974) identified the clayey limestones as Unaz member. Tüysüz and others (1997) and Akman (2002) defined it as a formation. Type section is in the Unaz Village (Akman, 1992). It is exposed in the north of Bartın in the study area.

The formation is gradational with underlying Santonian Kökyol Formation, and overlying Campanian Cambu Formation. The thickness of the formation is about 120 meters (Yergök et al., 1987) and 377 meters (Akman, 1992/2002). This formation refers to micritic limestones (Işiker et al., 2004; Turkish Stratigraphic Committee). The formation is composed of reddish, pinkish, and creamy color clayey pelagic limestones.

For the Unaz Formation, Campanian-Early Maastrichtian (Şahintürk and Özçelik, 1983; Akman, 2002), Early Campanian (Kaya et al., 1982/1983), Turonian-Campanian (Yergök et al., 1987), Campanian (Özçelik and Çaptuğ, 1990), and Late Santonian-Early Campanian (Tüysüz et al., 1997) ages are proposed. According to its stratigraphic position and foraminifer content, the age accepted as Late Santonian-Early Campanian. The formation was deposited in a deep marine environment accompanying a suddenly subsiding basin.

#### **3.3.1.1.c. Cambu Formation**

Tokay (1954) named this unit initially as Kazpınar Formation, then it is defined as a volcanic belt, extending to the Black Sea coast and named as Cambu Formation (Akyol and others 1974; Tüysüz et al., 1997). Type locality is around Bartın-Amasra, Çakraz-Kurucaşile-Cide highway and in Cambu village.

The formation has a conformable contact with underlying Upper Santonian-Lower Campanian Unaz Formation and overlying Maastrichtian-Lower Paleocene Akveren Formation. Thickness is more than 1000 meters (Temel et al., 2015). Columnar joints and pillow lavas are the characteristic features exposed to the north of Bartın (Figure

3.13). Cambu Formation consists of basaltic to basaltic andesites. lava, pyroclastic, volcanogenic sequence, and has dark green, dark grey, brown color.

The age of the formation, based on the age of underlying and overlying formations, assigned a Campanian (Tüysüz et al., 1997).



Figure 3.13. Field view of columnar jointed basalts in the Cambu Formation along Bartın-Amasra highway near the Uzunöz village.

#### **3.3.1.2. Akveren Formation**

Akveren layers name was first used by Gayle (1959) for clayey limestones exposed in the south of Ayancık Village. Later, Ketin and Gümüş (1963) revised this name as a Akveren Formation. Type locality is in Doğaşı and Kayadibiçavuş villages (Akman, 1992), where type section is in the Aksöke village (Gedik and Korkmaz, 1984). This formation extends along the north of Bartın Fault in a NE-SW direction along the Gökırmak river (Figure 3.1).

Akveren Formation has gradational contacts with the overlaying Upper Paleocene-Early Eocene Atbaşı Formation and underlying Campanian Cambu Formation

(Temel et al., 2015) (Figure 3.14). The thickness is about 390 to 593 meters (Akyol et al., 1974; Akman, 1992). Akveren Formation consists of clayey limestone, calcareous mudstone, calciturbidite-calcarenite-marl alternation and massive bioclastic limestones. Volcanic rocks named as Çangaza volcanic unit (Yergök and others 1987). Because of its stratigraphic position, it can be correlated with Çömlekçi andesite and Bayramoğlu lava member (Saner et al., 1981). This lava is composed of basaltic pillow lavas (Saner et al., 1981). Thickness of the basalt member is approximately 10-100 meters in the area (Akbaş et al., 2002). Lava member trends in NE-SW direction and major exposures are observed along the Bayramoğlu village to the Tütüncüoğlu village (Figure 3.15).

Maastrichtian (Ketin and Gümüş, 1963), Maastrichtian-Paleocene (Gedik and Korkmaz, 1984), Campanian-Paleocene (Akman, 1992), and Campanian-Late Maastrichtian (Tüysüz et al., 1997) ages were obtained for the Akveren Formation. Maastrichtian age is accepted for the lava member (Akbaş et al., 2002). In this study, Maastrichtian-Lower Paleocene age is accepted. Depositional environment of Akveren Formation is deep marine (Temel et al., 2015) with reefal shallow-marine depositional environments (Akbaş et al., 2002).

### **3.3.1.3. Atbaşı Formation**

The name is given by Ketin and Gümüş (1963). Type locality is in the Gerze-Tangal village. The formation is exposed in the northern part of study area. It can easily be distinguished in the field with its reddish color. The Atbaşı Formation has an angular unconformity with the overlying siliciclastics of Lower-Middle Eocene Kusuri Formation and conformable contact with the underlying Maastrichtian-Lower Paleocene Akveren Formation (Şahintürk and Özçelik, 1983). Thickness of the formation is 260 meters (Akyol et al., 1974) and 537 meters (Gedik and Korkmaz, 1984). Dominant lithology is pinkish to reddish, thin to medium bedded marl and carbonaceous mudstone.



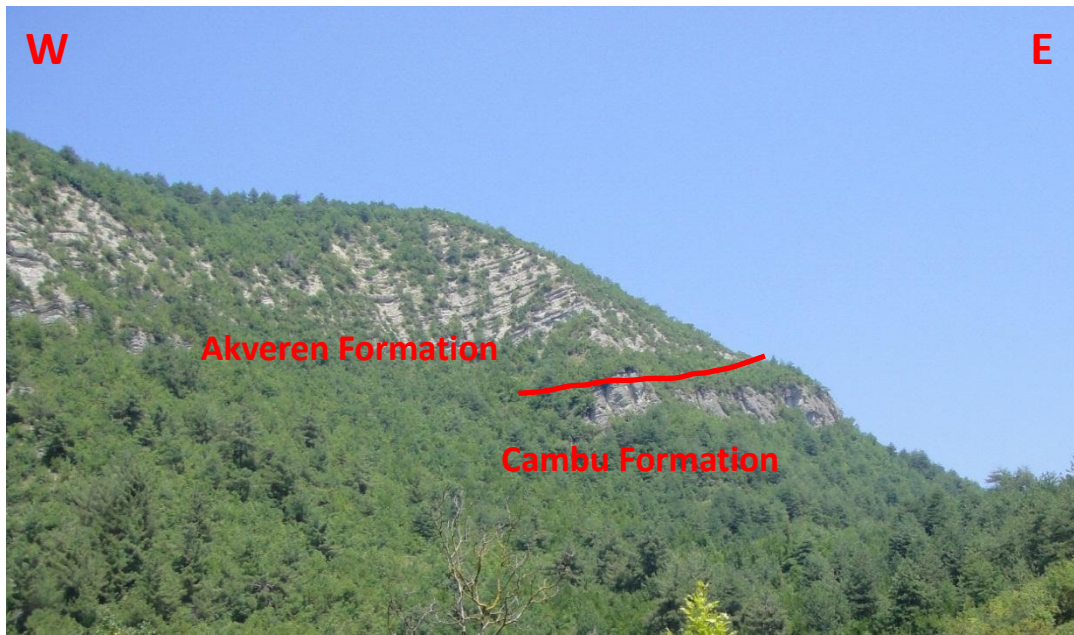


Figure 3.14. A view of conformable contact between the Akveren and the Cambu Formations at the north of Bartın near the Üçkurnalı village.

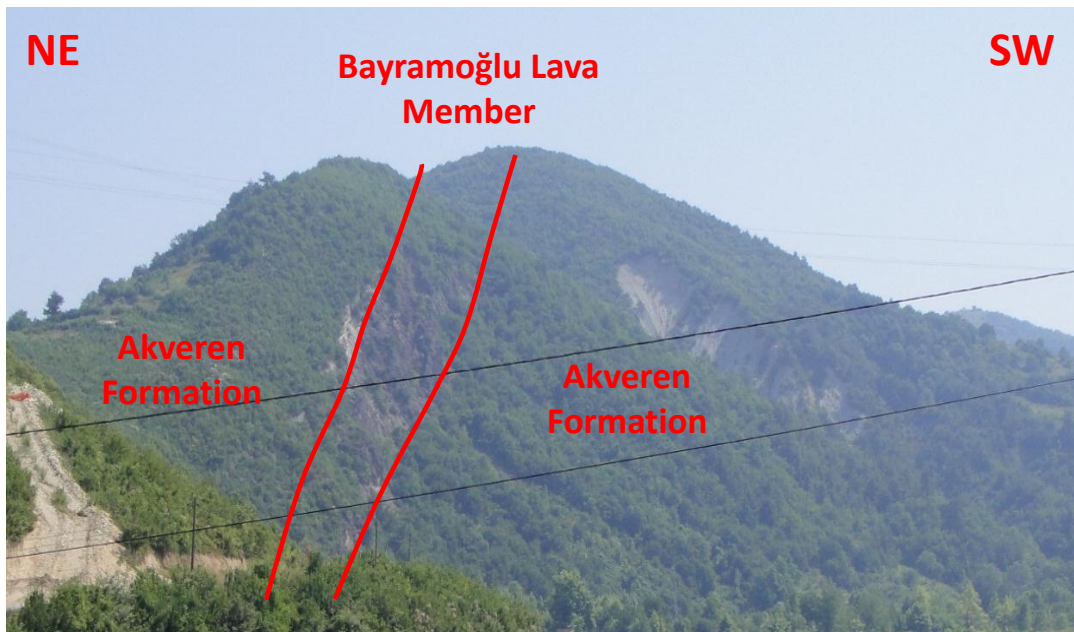


Figure 3.15. Field view of Bayramoğlu lava member within the Akveren Formation in the southwest of Bartın in the Kozcağız village.



The age of the formation is assigned as Paleocene-Early Eocene (Ketin and Gümüş, 1963), Paleocene (Akyol et al., 1974; Tüysüz et al., 1997) and Early Eocene (Gedik and Korkmaz, 1984). In this study, age of the formation is accepted as Paleocene-Early Eocene. The formation was deposited in a deep marine environment.

Akveren and Atbaşı Formations are mapped as a single unit in the study (Figure 3.1)

#### **3.3.1.4. Kusuri Formation**

The name was given by Ketin and Gümüş (1963). Type section is around Karapınar village in Sinop (Gedik and Korkmaz, 1984).

Kusuri Formation has an angular unconformity with the underlying Paleocene-Lower Eocene Atbaşı Formation. Thickness is more than 2000 meters (Şahintürk and Özçelik, 1983). The formation is represented by turbiditic sandstone-shale alternation. Lower part of this succession starts with the alternation of thin bedded siltstone-marl with grain size decreasing upward and continues with sandstone-shale alternation. Convolute and parallel laminations are observed in fine grained layers (Tüysüz et al., 1997).

This formation is the youngest unit in the Bartın region. According to fossil content, Ketin and Gümüş (1963) and Tüysüz et al. (1997) assigned an age of Early-Middle Eocene, but Akyol et al. (1974) assigned Early Eocene age. The formation was deposited in a deep marine environment, with shallow-marine depositional settings (Temel et al., 2015).

#### **3.3.2. Karabük – Safranbolu Region**

##### **3.3.2.1. Safranbolu Formation**

Fossiliferous limestones with high terrigenous influx were named by Güven (1977) as Safranbolu Formation. In the study area, Safranbolu Formation is exposed in Bartın-Safranbolu highway at the junction of Bartın-Eflani highway junction.

Safranbolu Formation overlies Barremian-Cenomanian Ulus Formation with an angular unconformity. Upper boundary is conformable and transitional with Lower-

Middle Eocene Karabük Formation. Thickness ranges from 100 meters to 700 meters and increases towards the eastern part of the basin. The formation is composed of white and creamy-white nodular limestone and clayey limestone with *Alveolina* fossils (Saner et al., 1979).

The age of the formation is Late Paleocene-Middle Eocene (Saner et al., 1979; Yergök et al., 1987). Safranbolu Formation was deposited during transgression of Tertiary Sea where limestones were precipitated in an alkaline environment (Saner et al., 1979).

### **3.3.2.2. Karabük Formation**

The Karabük Formation name was given by Güven (1977), it is then divided into two formations by Saner and others (1979) as Karabük and Çerçen Formation. This study choose the use of latest nomenclature. Type section is in Karıt village (Güven, 1977) and in the Bıçaklı village (Saner et al., 1979; Yergök et al., 1987).

The Karabük Formation has conformable contacts with underlying Upper Paleocene-Middle Eocene Safranbolu Formation, with overlying Lower-Middle Eocene Çerçen Formation (Saner et al., 1979). Maximum thickness reaches up to 2000 meters in the Eflani village. General thickness however ranges from 350 meters to 400 meters in the Karabük area. Major components of the Karabük Formation are the alternation of mudstone, siltstone and sandstone. The formation start with mudstone at the bottom, and continues with mudstone-sandstone alternation where sandstone content increases towards the top. The upper part is composed of mostly thick bedded, coarse grained sandstone. *Alveolina*, bryozoa, nummulites and plant fragments are common (Saner et al., 1979).

The Karabük Formation is of Early-Middle Eocene in age (Saner et al., 1979). The formation which was deposited in a shallowing alluvial-delta environment (Figure 3.16) with a coarsening-upward succession evolved under extensional regime manifested by growth normal faults (Figure 3. 17).

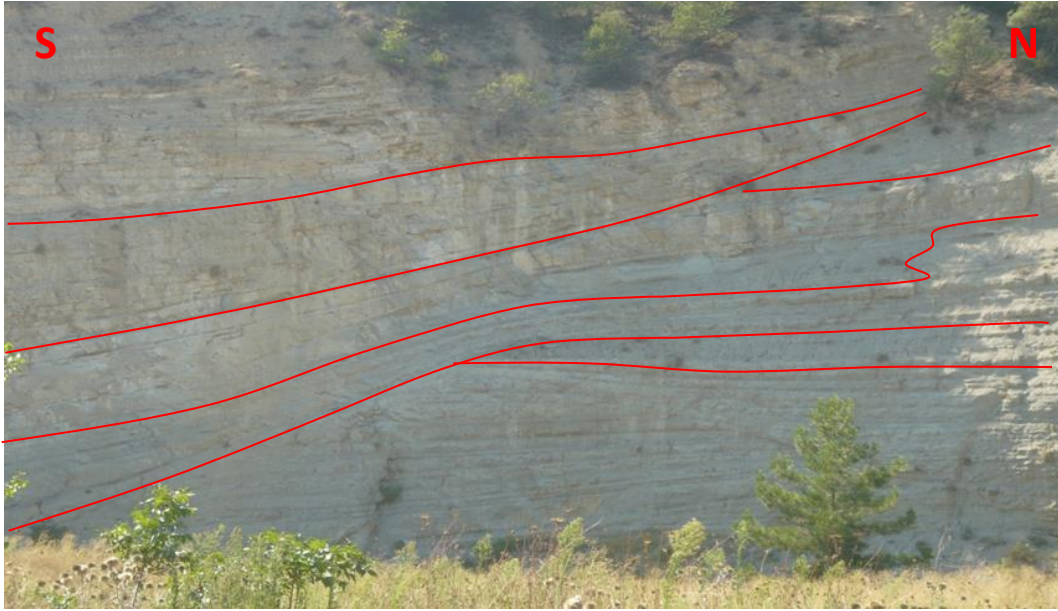


Figure 3.16. Field view of lensing out of foreset beds and lateral gradation of clastics with green mudrocks forming typical cross-beds (deltaic setting) in the Karabük Formation where the delta faces SE (northwest of Ödemiş village, SW of Karabük).

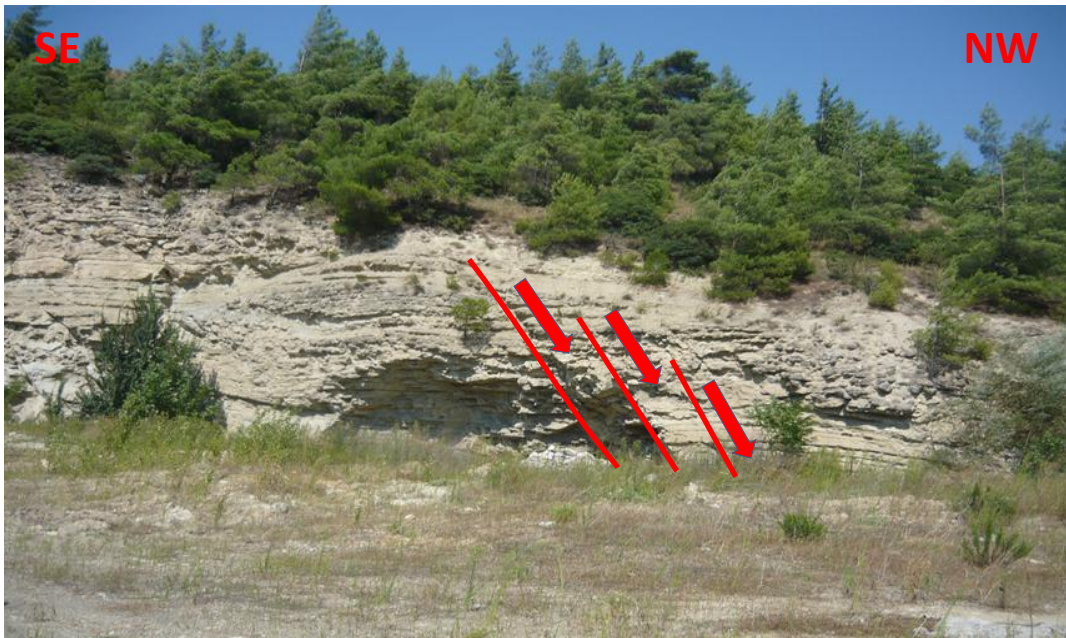


Figure 3.17. Field view of southeast dipping growth faults in delta sequence of Karabük Formation in northwest of the Ödemiş village (NW of Karabük).

### **3.3.2.3. Çerçen Formation**

Terrestrial deposits above the Karabük Formation was defined as Çerçen Formation in the south of the Araç Stream (Saner et al., 1979). Type locality is in the Cumayanı village at about 15 km away from Karabük (Yergök et al., 1987).

Çerçen Formation displays conformable contact relationships with the underlying Lower-Middle Eocene Karabük Formation and overlying Lower-Middle Eocene Soğanlı Formation. Its thickness is approximately 450 meters (Saner et al., 1979). The Formation consists of conglomerates, alternation of sandstone-siltstone-claystone and mudstone. Polygenic conglomerates and sandstones with fragments derived from limestone, granite, ophiolite, radiolarite and quartzite common. Clastic rocks are poorly sorted and weakly cemented. The formation is represented by a fining-upward sequences (Timur, 2002). Beds are horizontal, but gets steeper near the Karagöl Fault.

The Early-Middle Eocene age is assigned according to stratigraphic position. The formation was deposited in a terrestrial environment (Saner et al., 1979).

### **3.3.2.4. Soğanlı Formation**

The Soğanlı Formation was first defined by Güven (1977). It is divided into Akyar and Çakmak members. Then, Saner and others (1979) named the Akyar Member as Soğanlı Formation and Çakmak Member as Akçapınar Formation. In this study, Soğanlı and Akçapınar names are preferred. Type section is in the Soğanlı river (Güven, 1977) and type locality is along the Boyalı (Güven, 1977) and Akçapınar villages (Yergök et al., 1987). The formation is exposed in a E-W belt in the area between the Araç and Soğanlı streams.

The Soğanlı Formation has conformable boundary with underlying Lower-Middle Eocene Çerçen and overlying Lower-Middle Eocene Akçapınar Formations (Saner et al., 1979). Average thickness of the formation is about 150 meters (Timur, 2002). The Soğanlı Formation is represented by thin bedded limestones where sandy at base

(Güven, 1977). The sand content and thickness of beds increase towards top. Beds are interbedded with marls.

Depending on benthic foraminifers and stratigraphic position, Early-Middle Eocene age is assigned (Saner et al., 1979). The formation was deposited in a back reef, shallow-marine and shore of shallow-marine environments (Saner et al., 1979).

#### **3.3.2.5. Akçapınar Formation**

The Akçapınar Formation was first named by Saner and others (1979). Like Soğanlı Formation, it is exposed in the area between the Araç and Soğanlı streams.

The Akçapınar Formation displays conformable contact relationship with underlying Lower-Middle Eocene Soğanlı Formation, and overlying Lower-Middle Eocene Yunuslar Formation (Saner et al., 1979). Its thickness ranges between 110 meters to 190 meters, and gets thinner eastwards (Işıker et al., 2004). Dominant lithology is clayey limestone with minor dolomitic limestone, siltstone, mudstone and marl alternation. The formation can easily be distinguished from other carbonates with silica layers, nodules and interbedded gypsum layers.

Age of the formation is accepted as Early-Middle Eocene, according to its stratigraphic position (Saner et al., 1979). Depositional environment was interpreted as lagoon to tidal flat (Timur, 2002).

#### **3.3.2.6. Yunuslar Formation**

The youngest unit of the Eocene succession is named by Güven (1977) as Boyalı Formation. Later, Saner and others (1979) reevaluated the formation, and divided it into two units; lower most unit as Köşeler Member and rest of Eocene units as Yunuslar Formation. Type section of the Yunuslar Formation is in the Boyalı Village (Saner et al., 1979), whereas type locality is in the Yunuslar Village (Yergök et al., 1987).

The boundary between the Köşeler Member and the Yunuslar Formation is transitional. Köşeler Member and Lower-Middle Miocene Akçapınar Formation has

conformable contact. The Yunuslar Formation is unconformably overlain by Plio-Quaternary units. The formation has a thickness of 150 meters. Köşeler Member has a thickness of about 40 meters; it starts with alternation of marl-sandstone, which grades into sandstone towards to top. The Yunuslar Formation is made up of reddish sandstones, conglomerates and mudstones. Ripple marks and cross-parallel lamination are common.

According to its stratigraphic position, age of the formation is accepted as Early-Middle Eocene (Saner et al., 1979). Depositional setting is in a terrestrial regime (fluvial channels and flood plain) (Timur, 2002).

In this study, Çerçen Formation, Soğanlı Formation, Akçapınar Formation, Köşeler Member and Yunuslar Formation are mapped as a single unit (Figure 3.1).

#### **3.3.2.7. Yörük Formation**

In the Karabük-Safranbolu region, Plio-Quaternary successions was named as Yörük Formation (Saner et al., 1979); it is exposed in the area between the south of Karabük and north of the Araç Stream (Figure 3.1). Type section is in the Yörük village.

Yörük Formation unconformably overlies all of older units. Due to the Quaternary erosion at the top, original thickness cannot be detected. Therefore, maximum thickness is measured as approximately 100 meters. It is composed of small gastropoda bearing lacustrine limestones and mottled conglomerates.

Plio-Quaternary Yörük Formation was deposited in a lacustrine environment (Saner et al., 1979).

#### **3.4. Quaternary**

In the Bartın-Amasra region, Quaternary deposits are mostly made up of unconsolidated sand, gravel and mud, deposited in river channel and flood plains. Quaternary is represented by alluvial, talus (Figure 3.18) and terrace conglomerates (Figure 3.19). Terrace conglomerates situated at 400 meters elevations (250 meters above the Filyos River bed).





Figure 3.18. A field view of talus deposits developed in Bartın village near Kozcağız.

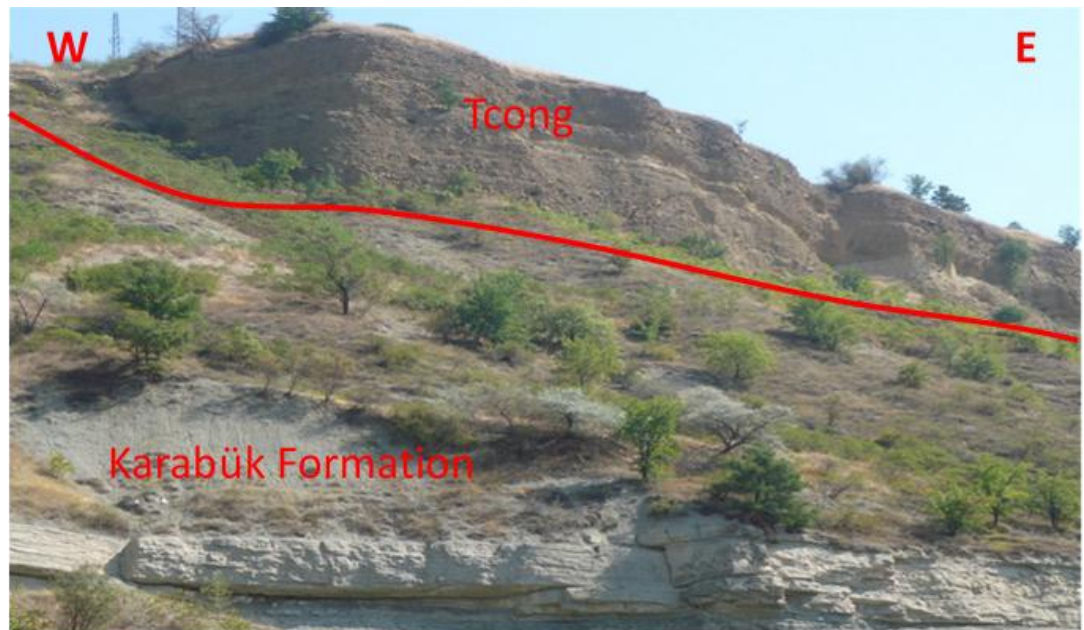


Figure 3.19. Field view of terrace conglomerates (Tcong) above the Karabük Formation at 400 meters altitude from sea level (which is 250 meters from the Filyos river channel) (S of Karabük village).





## **CHAPTER 4**

### **STRUCTURAL GEOLOGY**

The main subject of this chapter is to describe the geological structures in the study area, and present the results of the structural analyses. Two types of structural data were collected: (i) dip and strike of bedding planes, and (ii) dip and strike of the fault planes with slip-lineation (rake/pitch) data.

Three hundred ninety dip and strike measurements from bedding plane and forty-eight dip and strike of faults with fault-slip lineation measurements were collected. Three major faults with many minor faults and folds were identified from four major domains (Figure 4.1). Two NE-SW-trending traverse performed in the area and cross-sections are prepared (Figure 4.2).

Four structural domains are defined; (i) northern domain bounded by Black Sea in northwest and Bartın Fault in the southeast, (ii) central domain bounded by Bartın Fault in the northwest and the Karabük Fault in southeast, (iii) eastern domain bounded by the Karabük Fault in the northwest and the Karagöl Fault in the south, and (iv) southern domain bounded by the Karagöl Fault from north (Figure 4.1).

#### **4.1. Fold Analysis**

For the fold analysis, three hundred ninety dip dip and strike measurements from bedding plane were carried out in the field from different stratigraphic levels (Figure 4.1, Appendix A).

Rose diagrams (obtained from GeoRose™ software) and stereonet diagrams (obtained from Rockworks 2017™ software) were used for the analyses of bedding plane.

#### **4.1.1. Attitude of Bedding Planes**

Since the study area cross-cut by continuous long faults and different rock packages, analyses were made for four domains, based on the major bounding faults in the study area, namely, Bartın, Karabük and Karagöl faults (Figure 4.1).

The rose diagram of the Domain I, where Upper Cretaceous to Eocene rocks are exposed, shows that majority of the strike measurements are in a range of 40°-50° N trends. 50°-60° N range concentration is higher than 30°-40° N, so that average strike of the beds is 050° N (Figure 4.3). Dip of the beds are in a range of 10°-60° with NW and SE dip directions. Generally, dip amount increases southeastwards towards the Bartın Fault.

The rose diagram of the Domain II, where Lower Cretaceous Ulus Formation is exposed, shows wide range of distribution of bedding strikes. Majority of the strikes are in a range of 50°-60° N direction. However, 30°-40° N and 60°-70° N measurements are also dominant. Therefore; average trend of the strikes is 055° N for the Domain II (Figure 4.4). Dip of the beds ranges of 17°-79° with NW and SE dip directions.

The rose diagram of the Domain III, where Paleogene rocks are exposed, shows 70°-80° N, 80°-90° N and 90°-100° N strike distribution of the beds. For this domain, 085° N is the average strike of the beds (Figure 4.5). Dips ranges between 04° and 88° with N and S dip directions. There are overturned beds near the Karabük Fault contact and Karagöl Fault contact (Figure 4.1.)

The rose diagram of the Domain IV, where Lower Cretaceous to Eocene rocks are exposed, shows 70°-80° N and 80°-90° N strike distribution of the beds. 080° N is the general trend of the strike in this domain (Figure 4.6). Dip of the beds ranges between 12° and 80° with N and S dip direction.

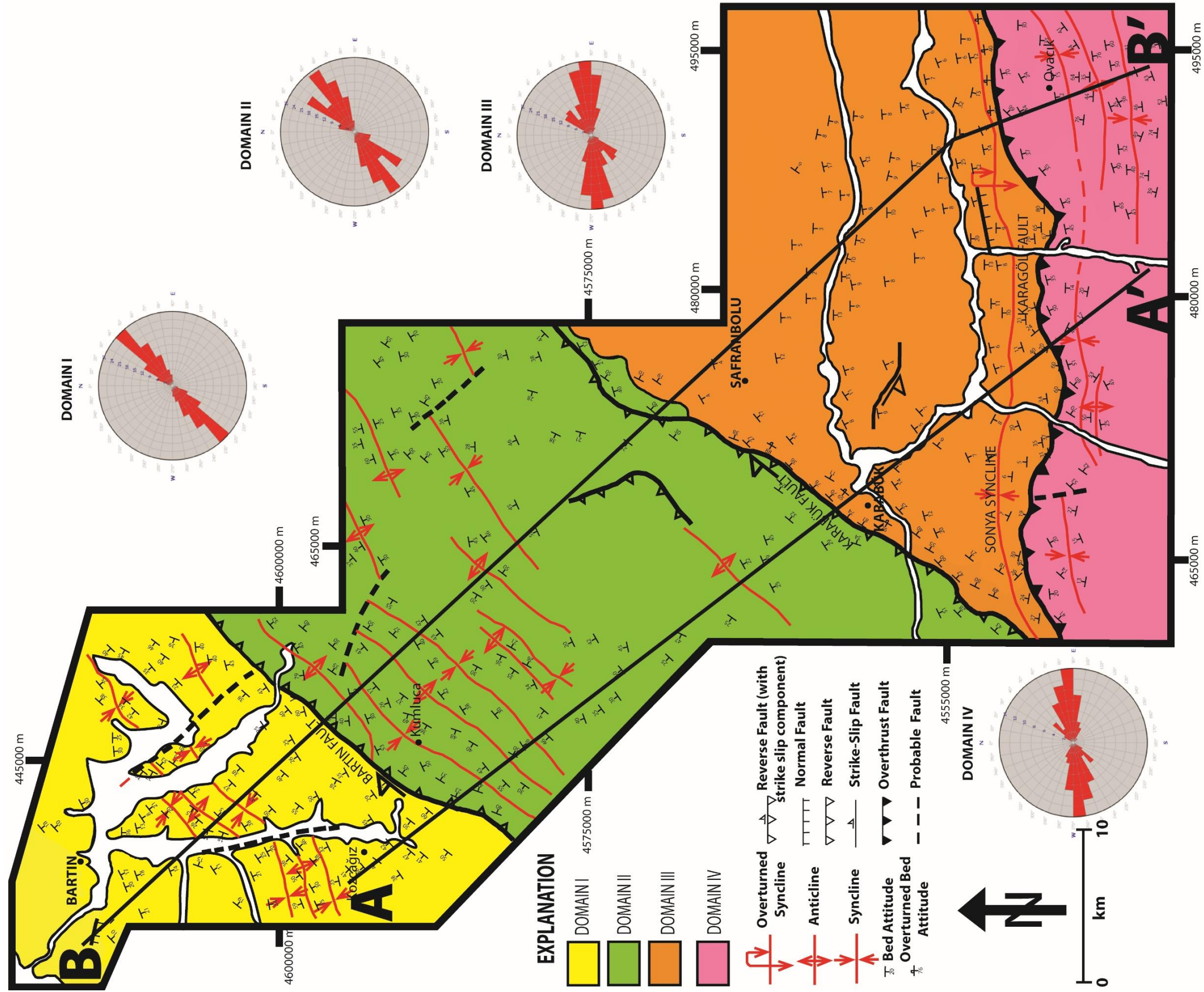


Figure 4.1. Structural map of the study area showing general trends of bedding planes for each domains individually



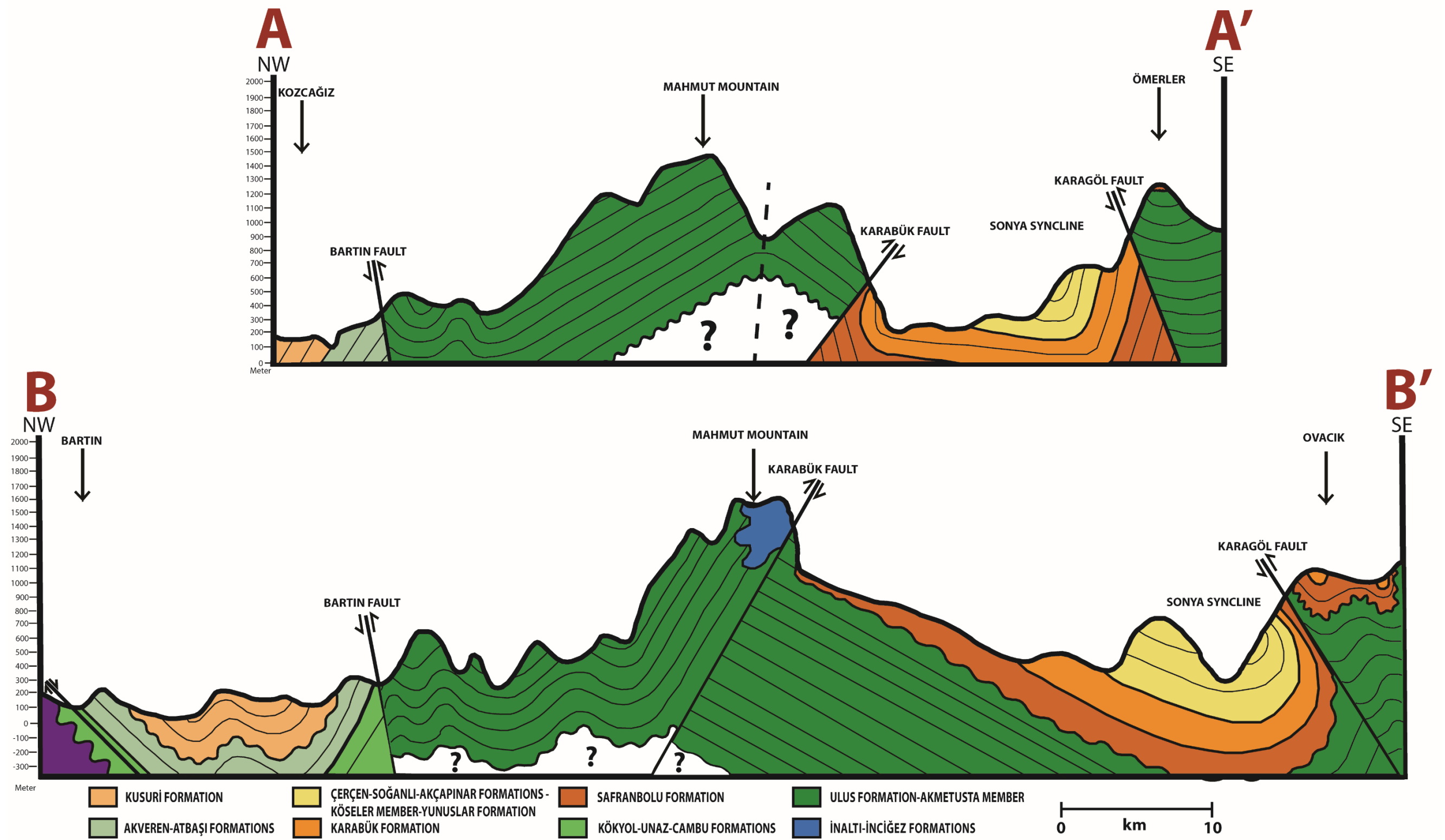


Figure 4.2. NW-SE sections (A and B) showing the structural elements of the study area.





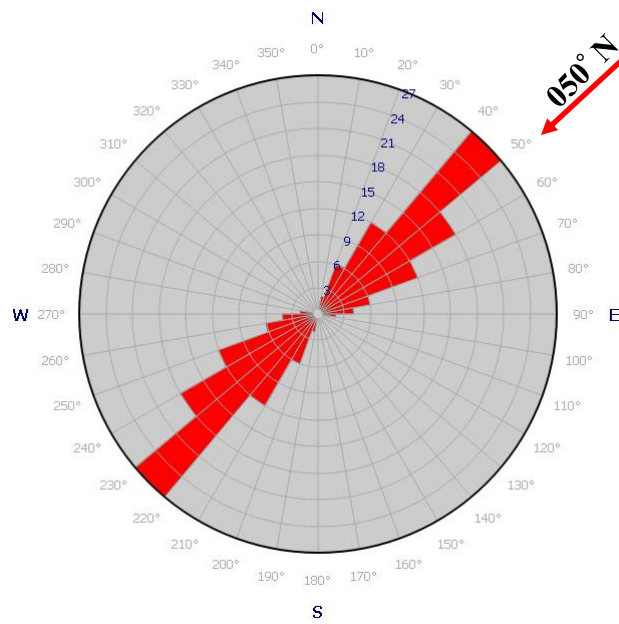


Figure 4.3. Rose diagram showing the strike of the Upper Cretaceous to Eocene beds in Domain I.

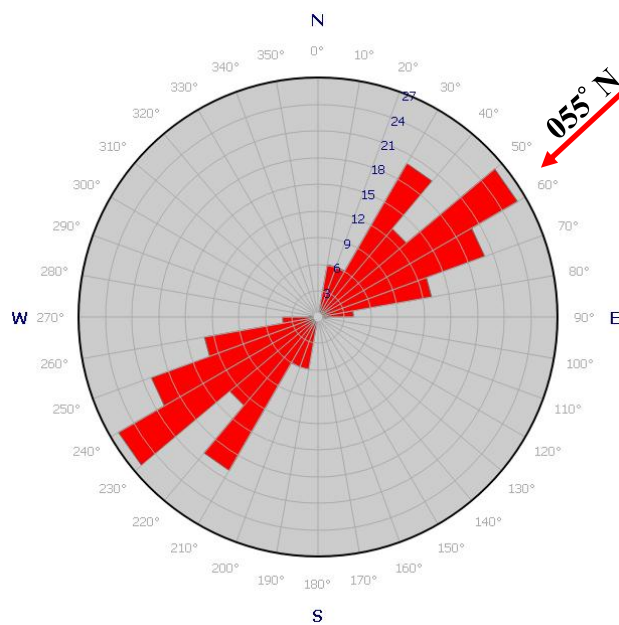


Figure 4.4. Rose diagram showing the strike of the Lower Cretaceous beds in Domain II.

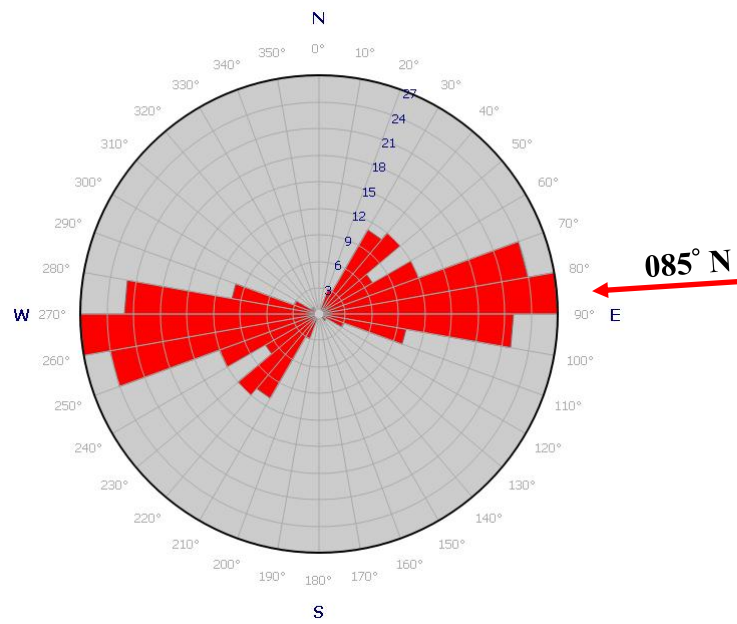


Figure 4.5. Rose diagram showing the strike of the Paleogene to Plio-Quaternary beds in Domain III.

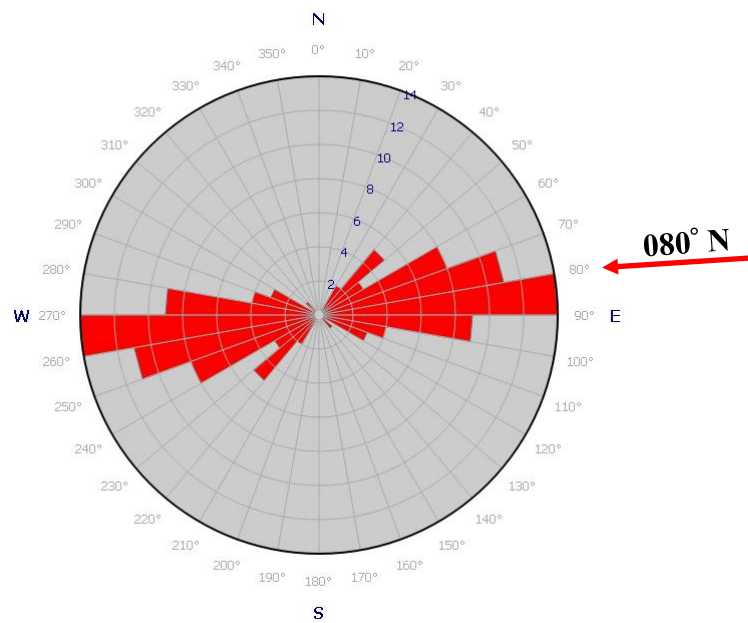


Figure 4.6. Rose diagram showing the strike of the Upper Cretaceous to Eocene beds in Domain IV.



#### 4.1.2. Stereographic Analysis of Folds

Stereographic analysis of fold is widely used for large-scale folds or for not very well exposed folds. There are two main diagrams for this analysis, one is beta ( $\beta$ ) diagram and the other one is pi ( $\pi$ ) diagram.

Beta ( $\beta$ ) diagram is a simple method and used for finding the orientation of the cylindrical fold axis. For this purpose, limbs of the folds projected on the stereonet and if the fold is cylindrical, all limbs intersect at a common point, which is called a  $\beta$  axis. This  $\beta$  axis is parallel to the fold axis. However, generally folds are not perfectly cylindrical, so that fold limbs not perfectly intersect in one point, and if plotted folds have different folding histories, then different  $\beta$  axis will appear (Stephen et al., 2007).

Pi ( $\pi$ ) diagram method, which was firstly recommended by Ramsay (1967), is a widely used mathematical technique for fold analysis. This method bear; conversion of bedding plane data to pole attitudes, computation of the mean pole vector of fold limbs, getting the best fit  $\pi$ -circle, finding the fold geometric properties and determining the fold cylindricity. Methodology is plotting of the S-poles, which is perpendicular to bedding plane by using an equal area projection on stereonet. After plotting the S-poles, one should count the concentration of the poles, and then apply the counteracting to these counted poles. Finally, this counteracting diagram gives a geometric view of fold axis, fold symmetry and attitude of axial plane (Nabeel, 2006).

If all S-poles of bedding planes of the fold fall on the  $\pi$ -circle, then this fold is perfectly cylindrical. On the other hand, if the S-poles disperse around the  $\pi$ -circle, then fold is non-cylindrical. Fold axis overlap with the  $\pi$ -axis, which is perpendicular to  $\pi$ -circle on stereonet. Generally, S-poles are not perfectly fit on the  $\pi$ -circle, so that  $\pm 2$  degrees measurement error has to be taken into consideration (Ramsay, 1967). Then, Ramsay and Huber (1987) reclassified the folds as perfectly cylindrical if all S-poles on the  $\pi$ -circle, cylindrical if 90% of the S-poles between  $-10/+10$  degrees near  $\pi$ -circle, sub-cylindrical if 90% of the S-poles between  $-20/+20$  near  $\pi$ -circle and non-cylindrical if more than 10% of the S-poles  $\pm 20$  degree out of  $\pi$ -circle.

Fold symmetry depends on the length of the fold limbs on a stereonet. Generally, folds have no equal length limbs on both sides. If the limbs of the fold have equal length on both side of the fold axis, then this fold is symmetric fold. However, if the limbs are unequal in length, then fold is asymmetric.

In this study, the folds of an intensely deformed region (Figure 4.7) are analyzed according to their cylindricity and symmetry by using the stereonet projection techniques.



Figure 4.7. Overturned structures in the Ulus Formation (near Dereköy village).

Stereographic plots utilizing the dip and strike measurements give us the folding pattern of the domains.

The result of stereographic diagrams for Domain I are consistent with NE-trending asymmetrical fold whose northwest dipping limbs are steeper than the southeastern dipping limb (Figure 4.8).

For the Domain II, stereographic diagrams show that NE-trending symmetrical folds (Figure 4.9). However, the field observations clearly manifest that this domain is

intensely deformed as mentioned in above lines, northern limbs are much steeper than the southern ones. Some of the northern limbs of folds are overturned (Figure 4. 7)

For the Domain III, stereographic diagrams are interpreted as homocline with south dipping axial plane (Figure 4.10). However, on the geological map, a continuous fold-extending parallel to the Karagöl Fault, in this domain indicates a E-W-trending overturned syncline (Figure 4.1). This is not manifested on stereonet plots (Figure 4.10).

For the Domain IV, stereographic diagram show that almost E-W -trending asymmetrical fold with steeper northern limb then southern limb (Figure 4.11).

According to cylindricity, all of the folds in each domain are non-cylindrical. Because, all S-poles are not on the same  $\pi$ -circle, and also they are located more than -20/+20 degrees away from the  $\pi$ -circle.

The folds are mainly compression resulted folds evidenced by their tight structures, overturned beds, associated intense strike slip to reverse to overthrust faulting in each domain. From this point of view, for domain I and II post-Eocene applied compressional stress orientation is NW-SE direction (140°N). For domains III and IV post-Eocene applied compressional stress orientation is WNW-ESE direction (170°N). Therefore, there is considerable amount of angular difference (30°) between the domains I to II (almost 050°N) and domains III to IV (almost 080°N).

The fold axis drawn on stereographic plots well-conformable with the rose diagram analysis done for the dominant orientation of strikes of beds for each domain. The same angular shift is observed on rose diagrams for post-Eocene period deformation which is around 30° (Figure 4.3, Figure 4.4, Figure 4.5 and Figure 4.6).

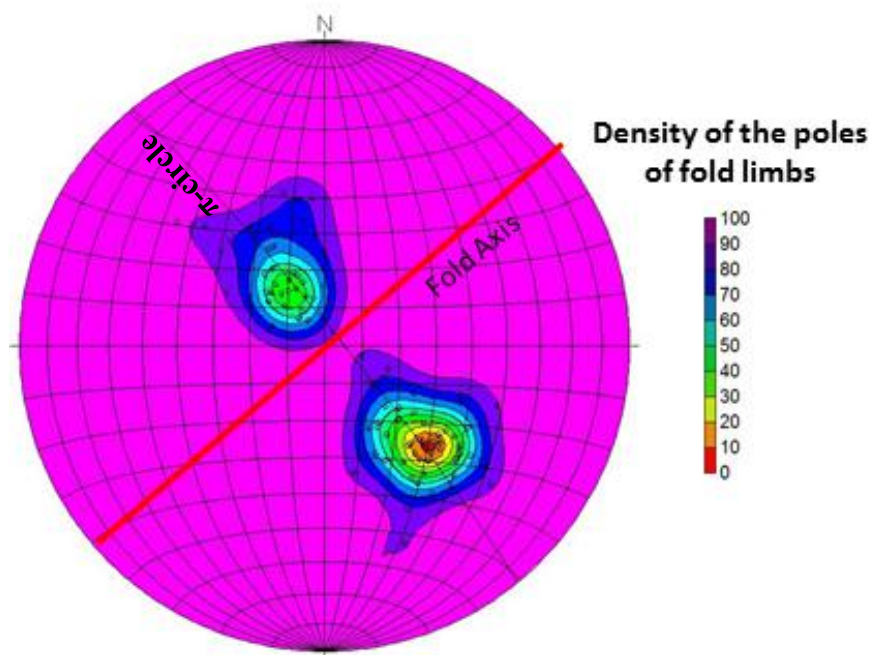


Figure 4.8. Stereographic plot for the Upper Cretaceous to Eocene beds in Domain I.

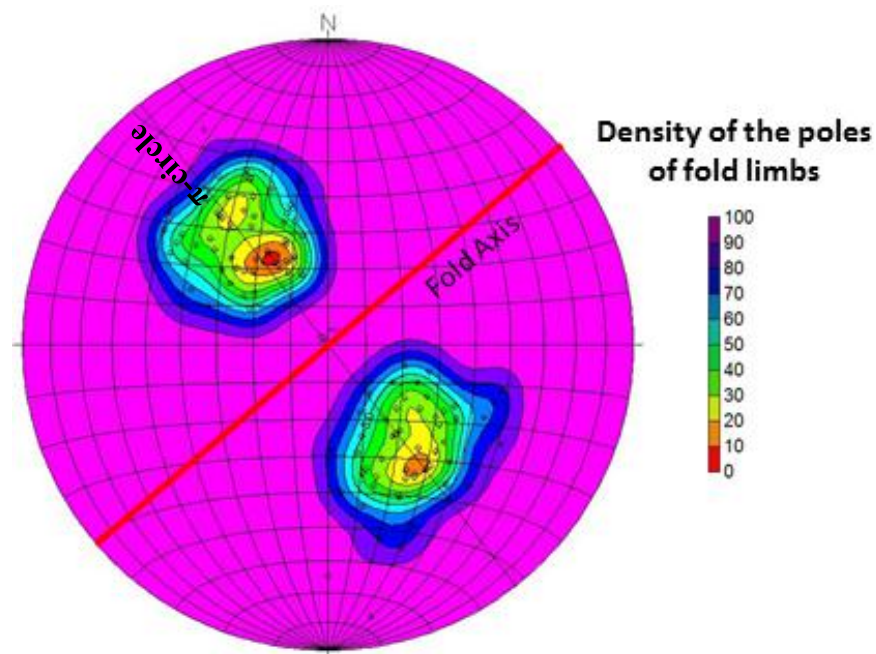


Figure 4.9. Stereographic plot for the Lower Cretaceous beds in Domain II.

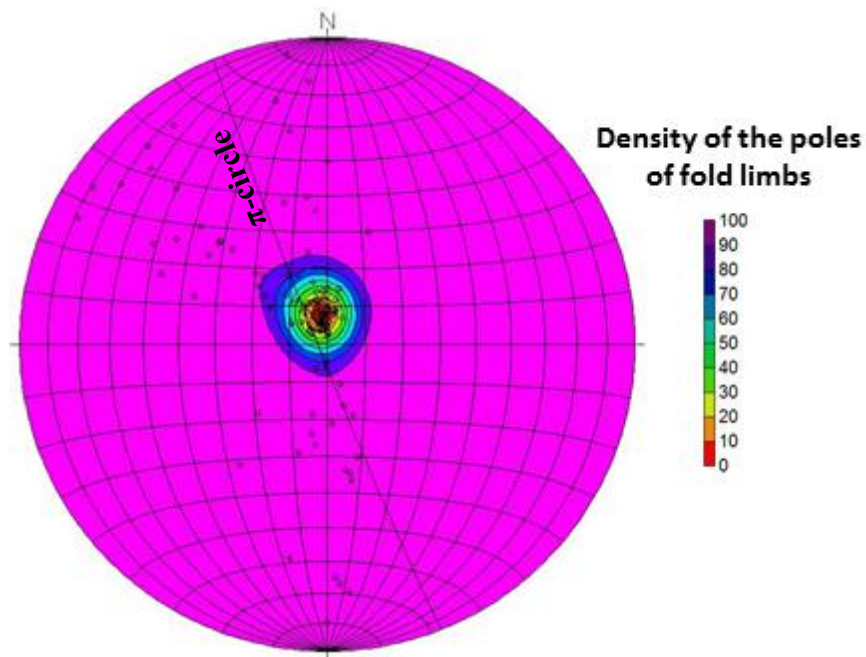


Figure 4.10. Stereographic plot for the Paleogene to Plio-Quaternary beds in Domain III.

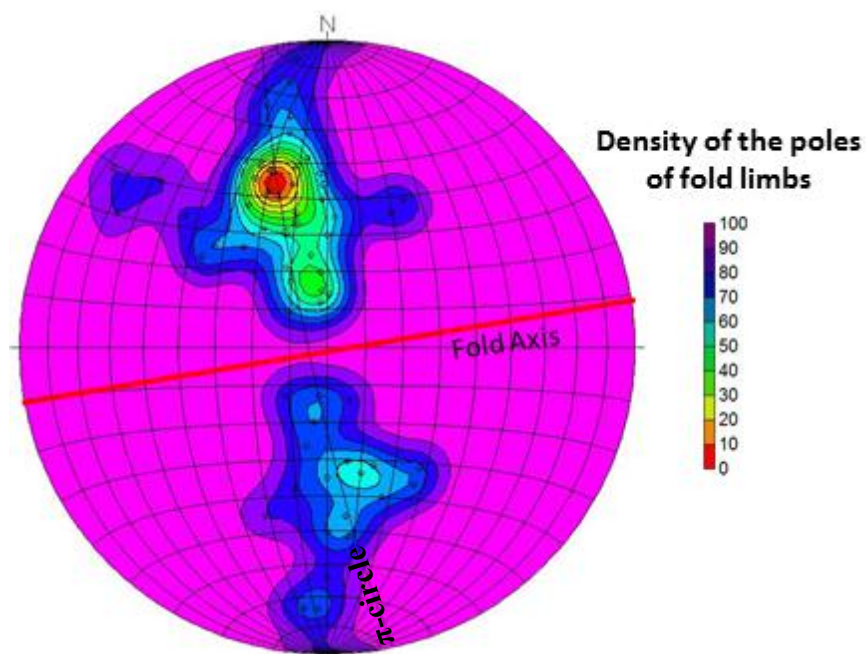


Figure 4.11. Stereographic plot for the Upper Cretaceous to Eocene beds in Domain IV.

## 4.2. Fault Analysis

Paleostress analysis is used to determine the stress tensor compatible with pre-existing geological structure. Several techniques can be used for estimating stress tensor and fault family (dip direction and dip amount of fault, pitch (rake) of slickenside), which is the widely used for this purpose (Schimmrich, 1991). Fault-slip data, which are collected from the field, is used to calculate the principle stress orientations and relative stress magnitudes in the fault family techniques. Slip directions can be obtained from slickenlines (fibrous lineations) and frictional grooves in the field (Fleuty, 1974; Doblas, 1998). Paleostress analysis studies have been grouped in two categories (Allmendinger et al., 1989). First one is a graphical method (Aleksandrowski, 1985; Krantz, 1988). This method is only used when the special conditions achieved. For example; M-Plane Method used by Aleksandrowski (1985), depend on the two of principal stress magnitudes which are equal under uniaxial stress condition in plain view. Also, the Odd Axis Method, which is used by Krantz (1988), is valid when the two pairs of conjugate faults sets developed in triaxial strain condition. Therefore, numerical technique is widely used in the paleostress analysis (Carey and Brunier, 1974; Angelier, 1979, 1984, 1989; Etchecopar et al., 1981).

There are two main assumptions in numerical technique:

- Slip on the fault plane occurs in the direction of maximum resolved shear stress and is accepted as parallel to the slickenline direction. This means that free slip of the fault plain might be ceased by some heterogeneities and relation with other faults are unimportant (Allmendinger et al., 1989).
- The slip direction on the fault plane is assumed to have occurred in the uniform stress field. This implies that faults were slipped with only one tectonic event, and there was no post-slip deformation of the region to change the fault orientations (Will and Powell, 1991).

In order to determine the stress tensor with the help of slip direction along a fault plane, some hypothesis has to be generated about the failure mechanisms (Schimmrich, 1991).

Coulomb's failure criterion was used by Anderson (1951) in order to find the orientation of principal stress axes. According to Anderson fault classification theory says that principal stress ( $\sigma_1, \sigma_2, \sigma_3$ ) has to be perpendicular to the surface of the Earth and there is no shearing stress on the surface of the Earth. Anderson assumption continues to constitute the basis of dynamic analysis. Three different classes of faults were explained by this theory. In normal fault,  $\sigma_1$  is vertical and  $\sigma_2$ - $\sigma_3$  is horizontal with a  $60^\circ$  dipping fault plane. In strike-slip faults,  $\sigma_2$  is vertical and  $\sigma_1$ - $\sigma_3$  is horizontal with vertical fault plane. In reverse fault,  $\sigma_3$  is vertical and  $\sigma_1$ - $\sigma_2$  is horizontal with  $30^\circ$  dipping fault plane.

It is easy to interpret conjugate system of pure normal, pure reverse and pure strike-slip faults, but to show the geometric properties of oblique-slip conjugate faults are difficult. Geometries are mostly independent of orientation, and because of this, some requirements have to be satisfied in order to identify these systems (Angelier, 1994). There has to be two faults, and intersection direction of these two faults is perpendicular to slickenside lineations. Moreover; these two fault-slips must be in reverse sense, and shortening direction is at the acute angle between these two faults. Also, the angle between faults remains same while faulting occurs. When these requirements sustained, paleostress axes can be interpreted as below;

- The acute angle between faults is bisected by the  $\sigma_1$  axis
- The intersection direction of faults corresponds to the  $\sigma_2$  axis
- Obtuse angle between faults is bisected by the  $\sigma_3$  axis

However, it should be kept in mind that these are the average orientations because of the uncertainties and natural irregularities (Angelier, 1994).



Other important steps in paleostress analysis are; slip on fault plane occurs along the same direction with the greatest shear stress, blocks are rigid, faults are planar, no block rotations occur along fault plane, and the stress is uniform (Pascal et al., 2002).

Slip direction also depend on shear stress direction and so the shape of stress ellipsoid. Shape of stress ellipsoid and principal paleostress magnitudes can be determined from a number, which is obtained from the stress ratio formula:  $R(\phi) = (\sigma_2 - \sigma_3) / (\sigma_1 - \sigma_3)$ . R values range between 0 and 1 and there is no negative value because of  $\sigma_1 > \sigma_2 > \sigma_3$ . When  $\sigma_1 > \sigma_2 = \sigma_3$ , R-values equal to 0 and this shows the prolate uniaxial compressional ellipsoid. When  $\sigma_1 = \sigma_2 > \sigma_3$ , R-values equal to 1 and this shows the oblate uniaxial extensional ellipsoid. If  $0 < R < 1$ , this indicate that triaxial ellipsoid. Wallace and Bott hypothesis indicate that slip direction parallel to the maximum shear stress, but in two extreme cases ( $R=1$ ,  $R=0$ ) above slip direction intersect the sphere in great circle while the principal stress axis perpendicular to the fault plane. Moreover, in the last case ( $0 < R < 1$ ), intermediate orientations can be seen in slip directions. Reliability of R-values in conjugate fault system is very low. Because, intermediate stress direction and fault intersection are parallel to each other in conjugate fault system, so that chancing of R values do not affect this fault system (Angelier, 1994).

Firstly, graphical methods were used, and then numerical methods were developed base on the graphical methods. These methods are based on the inversion techniques and mainly depend on the idea of maximum resolved shear stress and the slip direction is parallel to each other (Wallace, 1951; Bott, 1959) and Coulomb failure criterion of Anderson (1951).

Direct Inversion Method's target is to find the three principal stresses and stress ratio. Least mean-square angular deviation between the slickenlines and the maximum shear stress direction is the main procedure of this method. Under deformation phase, stress field was accepted as homogenous; also the result can be controlled with histogram, best-fit tensor position and angular deviation value.



Stress tensor results obtained from graphical and numerical methods are very similar. However, in order to get close values of stress tensor with different methods, dataset has to be abundant and good. Moreover, results obtained from R ratio are scattered when applied to a large scale regional analysis. If regional orientation of paleostress is more important than magnitudes of stress in the study, graphical methods give the better result than numerical methods. Consequently; if the stress axis, and compressional and extensional sectors is important in the study, graphical methods give the reliable solution, but if the numerical parameters of stress is needed, numerical methods give more reliable solutions (Ciancaleoni, 2005).

In this study, the kinematic of the faults in Bartın-Ulus-Safranbolu region was identified with the help of paleostress inversion method. The main concern of the study is to find the direction of paleostress. The reliability of results of the analysis were based on (i) the orientation of  $\sigma_1$  and  $\sigma_3$  axes, and (ii) the ratio between the principal axes (R). When the ratio is less than 0.4, but over 0.2, the  $\sigma_1$  axis is clear and the quality of the result was accepted good. However, when the ratio exceeded 0.7, the orientation of  $\sigma_3$  axis was clear. Field observations are used as cross-checks for the interpretations done by inversion methods.

Totally fifteen different faults were identified with forty-eight slip lineation and only forty-one of them could be analyzed with WinTensor 5.8.5<sup>TM</sup> freeware to obtain the principal stress directions and type of the faults (Appendix B). This part divided into three main subsets; (i) fault-slip lineation analysis with enough slip data, (ii) fault-slip lineation analysis of the faults in Ulus Formation, (iii) fault-slip lineation analysis of post-Eocene normal faults without enough slip data to use in numerical analysis.

#### **4.2.1. Fault-slip Lineation Analysis**

In that frame, five different faults were identified and classified according to fault mechanism, which were occurred in different time domains and on different formations. Three major faults, namely, Bartın, Karabük and Karagöl Faults are important element in structural analysis. However, no fault-slip lineation data was measured along the Karagöl Fault.

#### 4.2.1.1. Bartın Fault

The Bartın Fault is a strike-slip fault with reverse character along a length of about 25 kms (Figure 4.1). General trend of the fault is NE-SW with a NW-dipping fault plane (Figure 4.12).

This fault was occurred between the Barremian-Cenomanian Ulus Formation and Maastrichtian-Lower Paleocene Akveren Formation. The fault activated during post-Paleocene.

Four slip lineation data was collected, and analyzed with the freeware program (Appendix B). In the analysis, Angelier's optimization was not applied because of the "dispersion of plane too small" error. This means that all data belong to the same family, no conjugate fault data is present. Therefore, simple graphical method was used. According to this analysis, maximum stress axis ( $\sigma_1$ ) is on circle and compressional stress is in NE-SW direction. Moreover, minimum stress ( $\sigma_3$ ) is between the center and circle (Figure 4.12). This relationship between  $\sigma_1$  and  $\sigma_3$  indicates almost a strike-slip fault with oblique-slip component. According to field observations, fault is a dextral strike-slip fault with reverse component.

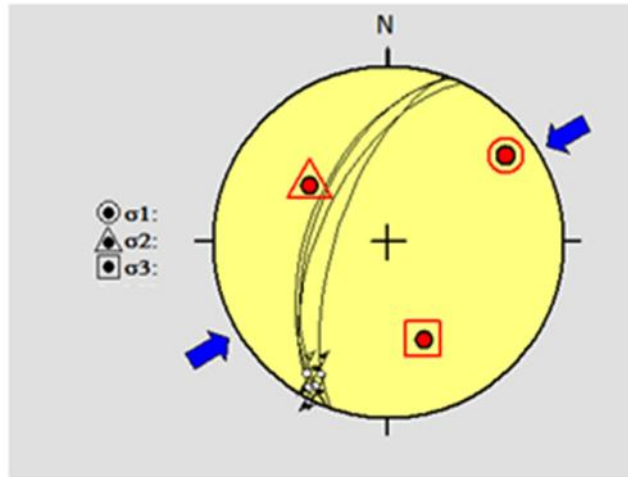


Figure 4.12. Paleostress analysis of the Bartın Fault. Blue arrows indicate the compression direction.  $\sigma_1=18^{\circ},054^{\circ}\text{N}$ ,  $\sigma_2=44^{\circ},306^{\circ}\text{N}$  and  $\sigma_3=41^{\circ},160^{\circ}\text{N}$  and R value is 0,50.

#### 4.2.1.2. Karabük Fault

The Karabük Fault is a reverse fault with a length more than 40 km in the study area (Figure 4.1). General trend of the fault is NNE-SSW direction with SE to NE dipping fault planes (Figure 4.13).

The Barremian-Cenomanian Ulus Formation thrusts onto Upper Paleocene-Middle Eocene Safranbolu Formation and Barremian-Cenomanian Ulus Formation. Near the fault plane, beds of the Paleogene Safranbolu Formation are overturned and/or vertical. The fault activated during post-Eocene.

Seven slip lineation data were collected and analyzed (Appendix B). In the analysis, Angelier's optimization was applied, and one slip data was neglected because of the high misfit error. The analysis shows that principal stress axis ( $\sigma_1$ ) and medium stress axis ( $\sigma_2$ ) are radial. Minimum stress ( $\sigma_3$ ) is almost at the center of the circle. The compressional stress ( $\sigma_1$ ) is in NNW-SSE direction (Figure 4.13). The relationship between  $\sigma_1$  and  $\sigma_3$  shows a reverse faulting. However, both SE and NW dipping fault planes may indicate a reverse faulting with a minor strike-slip component (Figure 4.13a).

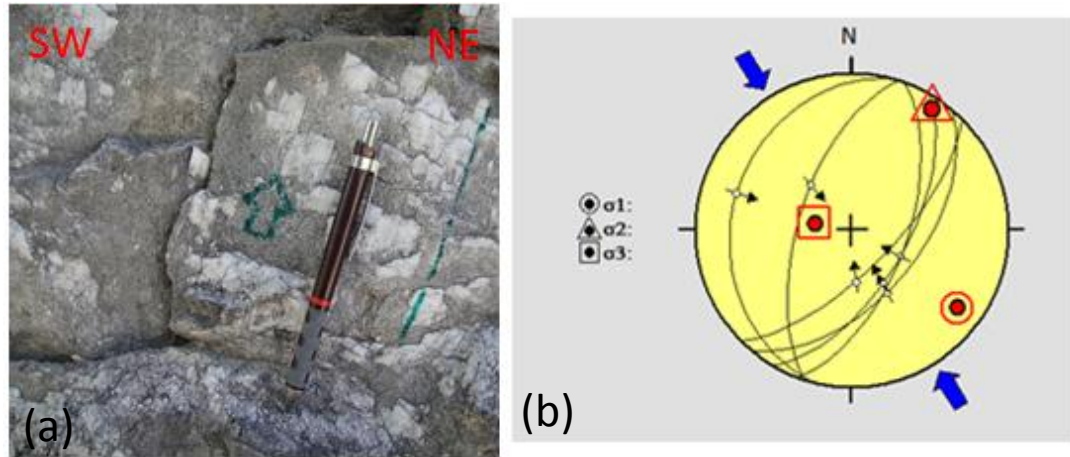


Figure 4.13. (a) Close up view of a fault plane with moving direction, (b) Paleostress analysis of the Karabük Fault. Blue arrows indicate the compression direction.  $\sigma_1=17^\circ, 129^\circ\text{N}$ ,  $\sigma_2=10^\circ, 036^\circ\text{N}$  and  $\sigma_3=70^\circ, 278^\circ\text{N}$  and R value is 0,86.

#### **4.2.1.3. Karagöl Fault**

The Karagöl fault is a thrust fault well-manifested with intense deformation-fracturing and folding- along the fault line. Another important observation is the overturned and steeply dipping Eocene beds below the fault line (Figure 4.1).

Along this fault –which extends more than 400 kms- the Barremian-Cenomanian Ulus Formation is thrust onto the Paleogene sequences. The fault plane dips towards south where southern block is uplifted relative to northern block. The faulted contact is making a V-shape on map pointing a plane dipping south (Figure 4.1). Along the fault, aligned springs, landslides and some sag ponds are recorded. It is very clear that fault activated during post-Eocene, but, the presence of geomorphological structures, the fault might re-activated or activated during Quaternary. No slip data collected along the fault.

#### **4.2.1.4. Strike-slip Fault**

There is a strike-slip fault at the southwestern part of the Karabük Fault with a length of more than 10 kms (Figure 4.1). General trend of the fault is nearly E-W direction with N and S dipping steep fault plane (Figure 4. 14).

This fault occur in Lower-Middle Eocene Soğanlı Formation; and it deform the debris deposit, thus it is Plio-Quaternary. The fault activated during Quaternary.

Four slip lineation data was analyzed with the freeware program (Appendix B). In this analysis, Angelier optimization could not be applied because of the high errors. Therefore, simple graphical method was used. This analysis shows that maximum stress ( $\sigma_1$ ) is on circle. Compressional stress applied in NE-SW direction (Figure 4.14). The minimum stress ( $\sigma_3$ ) is on circle. The relationship between  $\sigma_1$  and  $\sigma_3$  indicates a transtensional stress regime. The fault is a sinistral strike-slip fault (Figure 4.14).

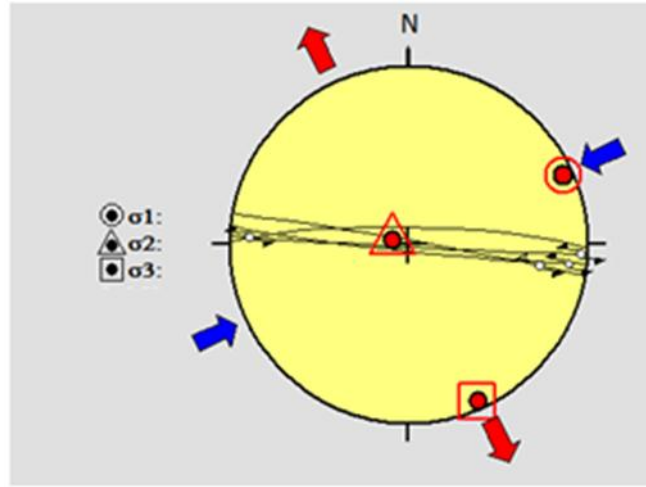


Figure 4.14. Paleostress analysis of strike-slip faults developed during post-Eocene. Blue arrows indicate compression direction, and reds indicate extension direction.  $\sigma_1=06^\circ,066^\circ\text{N}$ ,  $\sigma_2=82^\circ,286^\circ\text{N}$  and  $\sigma_3=05^\circ,156^\circ\text{N}$  and R values is 0,54.

#### 4.2.1.5. Normal Fault with Strike-slip Component

There is a normal fault with a minor strike-slip component to the north of Bartın extending for more than 1 km (Figure 4.1). General trend of the fault is NNW-SSE with a SW dipping low angle fault plane; (Figure 4.15).

The fault lineation data were collected on the Late Santonian-Early Campanian Unaz Formation. The fault probably activated during post-Late Santonian-Early Campanian.

Four slip lineation data was analyzed with the freeware program (Appendix B). Three of four measurements are normal faults and the forth is a left-lateral strike-slip fault with normal component ( $N48^\circ\text{E}/35^\circ\text{NW}/14^\circ\text{W}$ ). In this analysis, Angelier's optimization was applied and none of the slip data was neglected because of very minor misfit errors. This analysis shows that maximum stress ( $\sigma_1$ ) is almost at the center and minimum stress ( $\sigma_3$ ) is close to the circle. There is a small shift of ( $\sigma_1$ ) from the center. Intermediate stress axis ( $\sigma_2$ ) is on circle. (Figure 4.11). The

relationship between  $\sigma_1$ - $\sigma_3$  and attitude of the stresses indicate that the fault is a normal fault with a strike-slip component developed under E-W extension.

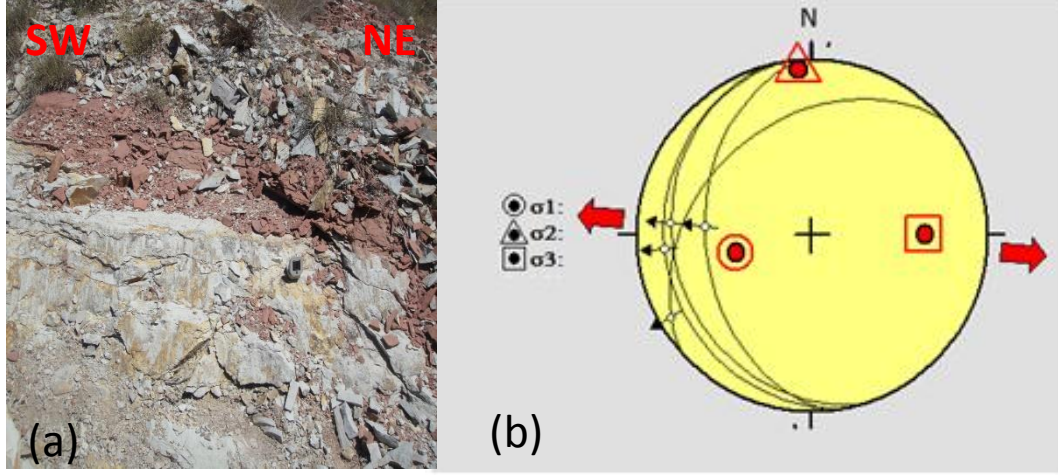


Figure 4.15. a) Field view of the low angle normal fault plane ( $35^\circ$ ) cross-cutting the bedding planes and b) result of the paleostress analysis of the normal fault with strike-slip component developed during post-Late Cretaceous. Red arrow indicates extension direction.  $\sigma_1=57^\circ, 257^\circ\text{N}$ ,  $\sigma_2=06^\circ, 356^\circ\text{N}$  and  $\sigma_3=32^\circ, 090^\circ\text{N}$  and R value is 0,58.

#### 4.2.1.6. Normal Fault

In the southern part of the Karagöl Fault, there is normal fault with a length of 5 km in the study area (Figure 4.1). General trend of the fault is in ENE-WSW with SE and SW dipping fault planes (Figure 4.16).

The fault cross-cut the Lower-Middle Eocene Soğanlı Formation. The fault is activated during post-Eocene.

Eight slip lineation data with conjugates were analyzed with the freeware program. The measurements with rake with  $83^\circ\text{S}$  and rake with  $81^\circ\text{NE}$  are the ridal conjugate measurements (Appendix B). Maximum stress axis ( $\sigma_1$ ) is close to center, where

minimum stress ( $\sigma_3$ ) close to the circle (Figure 4.16). The kinematic analysis and field observations manifest a normal fault developed under almost N-S extension.

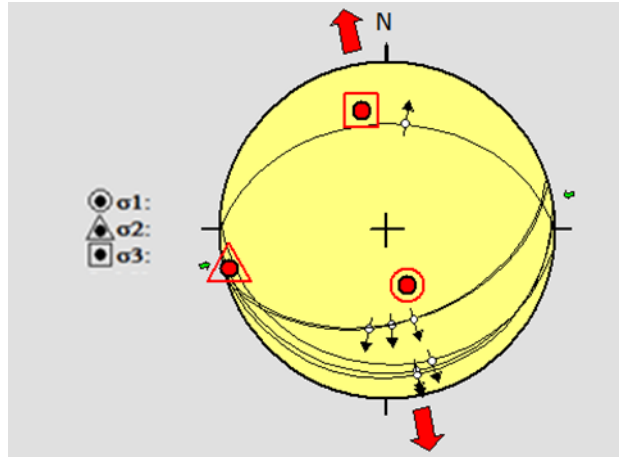


Figure 4.16. Paleostress analysis of normal fault developed during post-Eocene. Red arrows indicate the extension directions. For this fault,  $\sigma_1=61^\circ, 159^\circ\text{N}$ ,  $\sigma_2=04^\circ, 256^\circ\text{N}$  and  $\sigma_3=28^\circ, 348^\circ\text{N}$  orientations are calculated. R values is 0,73.

#### 4.2.2. Fault-slip Lineation Analysis of the Faults in the Barremian-Cenomanian Ulus Formation

There are several well-developed faults in Barremian-Cenomanian Ulus Formation. However, the possible age of the faults was not well-fixed.

##### 4.2.2.1. Strike-slip Fault with Reverse Component

The fault is NW-SE trending fault with a SW-NE dipping fault planes (Figure 4.17). The fault developed in the Barremian-Cenomanian Ulus Formation. Normal faults are cross-cut by the left-lateral reverse fault. This shows that strike-slip faulting clearly developed after the normal faulting during post-pre Miocene time (Figure 4.16).

Six slip lineation data was collected and analyzed with the freeware program (Appendix B). In this analysis, Angelier's optimization was applied and none of the slip data was neglected because of very minor misfit errors. The analysis show that



maximum stress axis ( $\sigma_1$ ) is on circle, minimum stress ( $\sigma_3$ ) close to the circle, and intermediate stress ( $\sigma_2$ ) is close to the center of the circle (Figure 4.17). Compressional stress is nearly in E-W direction with transtensional stress operating nearly in N-S direction. The relationship between  $\sigma_1$  and  $\sigma_3$  indicates a strike-slip faulting with normal and reverse oblique slip components. According to the field observations, this fault is sinistral strike-slip fault with reverse components.

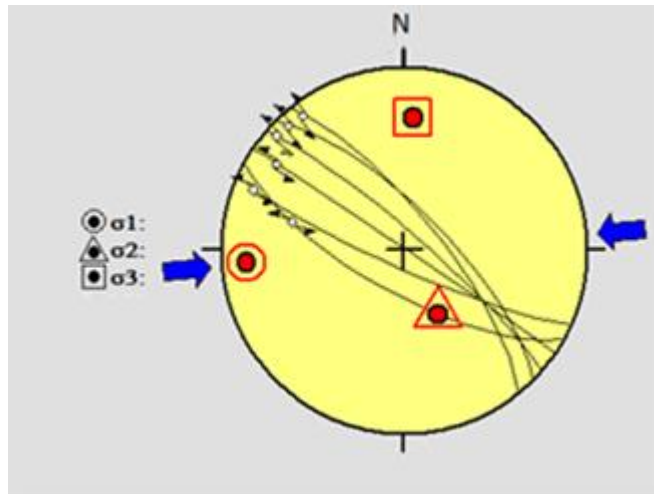


Figure 4.17. Paleostress analysis of the strike-slip fault with reverse component developed during post-Barremian-Cenomanian. Blue arrows indicate the E-W compression. For this fault  $\sigma_1=15^\circ, 266^\circ\text{N}$ ,  $\sigma_2=58^\circ, 152^\circ\text{N}$  and  $\sigma_3=28^\circ, 004^\circ\text{N}$  orientations are calculated. R value is 0,02.

#### 4.2.2.2. Reverse Fault

General trend of the fault is ENE-WSW with SE and SW dipping fault planes (Figure 4.18).

This fault deformed the Barremian-Cenomanian Ulus Formation. Totally twelve slip lineation data were collected (Appendix B).

These slip lineation data were analyzed with the freeware program. In the analysis, Angelier's optimization was applied and three slip data out of twelve were neglected

because of the high misfit errors. The analysis shows that principal stress axis ( $\sigma_1$ ) and medium stress ( $\sigma_2$ ) are on circle, minimum stress ( $\sigma_3$ ) is at the center. The relationship between  $\sigma_1$  and  $\sigma_3$  shows a reverse faulting under compressional stress in WNW-ESE direction. (Figure 4.18).

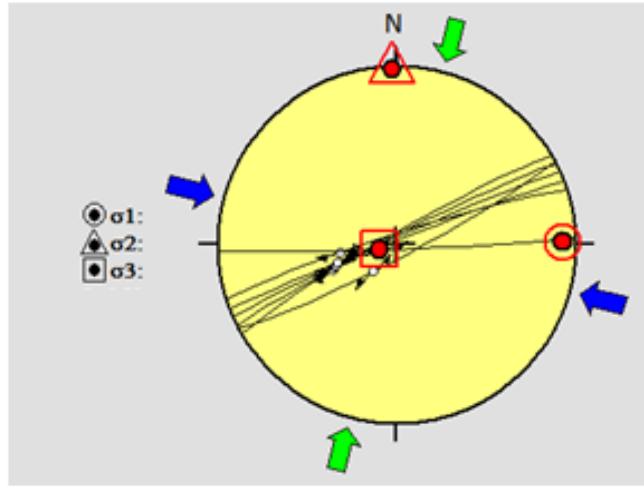


Figure 4.18. Paleostress analysis of reverse fault developed during post-Barremian-Cenomanian. The blue arrows show compression in WNW-ESE orientation. For this fault  $\sigma_1=08^{\circ},089^{\circ}\text{N}$ ,  $\sigma_2=02^{\circ},358^{\circ}\text{N}$  and  $\sigma_3=82^{\circ},255^{\circ}\text{N}$  orientations are calculated. R value is 0.85.

#### 4.2.3. Post-Eocene Normal Faults

In the study area, 8 normal faults in post-Eocene units were identified. Because of the limited ( $< 4$ ) or lack of slip-lineation data, paleostress analysis could not be applied.

The first set of normal faults in the Lower-Middle Eocene Karabük Formation have attitude of NE-SW ( $\text{N}47^{\circ}\text{E}$ ) with a  $45^{\circ}$  SE dipping plane. In that area, there are 6 similar fault planes with the same attitude. These normal faults probably occurred when the Eocene basin was developed. Therefore, the beds in hanging blocks are thicker than the beds on footwall blocks. These accommodation faults are interpreted as a normal growth faults (Figure 4.19).

The second set of normal faults present in the Upper Paleocene-Middle Eocene Safranbolu Formation with attitudes in NNW-SSE direction ( $N14^{\circ}W$ ) with a  $73^{\circ}$  SW dipping plane where southern blocks are downthrown. In that area, there are two similar faults with the same attitude. These normal faults occurred under the post-Eocene extensional tectonics (Figure 4.20).

The third set of normal faults are developed in the Barremian-Cenomanian Ulus Formation, and attitude of the fault is NNE-SSW ( $N17^{\circ}E$ ) with a  $56^{\circ}$  SE dipping plane. This normal fault is turned through counterclockwise direction.

The fourth set of normal faults also occur in the Upper Paleocene-Middle Eocene Safranbolu Formation, and attitude of the fault planes are NNE-SSW ( $N29^{\circ}E$ ) with  $89^{\circ}$  NW dipping plane; rake of slickenlines is  $89^{\circ}$  NE. In this fault, northern block is the downthrown block.

The fifth set of normal faults deformed the Lower-Middle Eocene Çerçen Formation with two displacement surfaces. Fault plane attitude of first displacement surfaces NNW-SSE trend ( $N28^{\circ}W$ ) with a  $57^{\circ}$  SW dipping plane. The second one is an almost E-W structure ( $N87^{\circ}E$ ) with a  $55^{\circ}$  S dipping plane; where rake is  $87^{\circ}$  SE. These faults control debris accumulation. This indicate that there is an extensional regime during Plio-Quaternary or post-Quaternary which might be operating in NNW-SSE orientation (Figure 4.21).

The sixth set of normal faults was occurred in Lower-Middle Eocene Yunuslar Formation. Fault plane attitudes are ENE-WSW ( $N60^{\circ}E$ ) with a  $55^{\circ}$  NW dipping plane and one is ENE-WSW ( $N57^{\circ}E$ ) with a  $61^{\circ}$  NW dipping plane and rake amount of  $81^{\circ}$  NE . The northern block is downthrown.

The seventh set of normal fault deformed the Lower-Middle Eocene Yunuslar Formation. The attitude of the fault plane is ENE-WSW trend ( $N70^{\circ}E$ ) with a  $21^{\circ}$  NW dipping plane where northern block is downthrown.



Figure 4.19. Field view of normal growth faults developed in the deltaic sequences of the Lower-Middle Eocene Karabük Formation close to the Karabük Fault (SW of Karabük city).



Figure 4.20. Field view of normal faults developed in the Upper Paleocene-Middle Eocene Safranbolu Formation (N of Safranbolu city along Bartın highway).





Figure 4.21. Field view of two normal fault planes developed in the Lower-Middle Eocene Çerçen Formation (SW of Safranbolu city).

The eighth set of normal faults affected the Lower-Middle Eocene Akçapınar Formation. The attitude of the fault plane is NNE-SSW trend ( $N15^{\circ}E$ ) with a  $66^{\circ}$  NW dipping plane. The northern block is downthrown.

To sum up on post-Eocene faulting; It is the time which NW-SE Eocene extension continues until the strike-slip faulting that starts to operate during Plio-Quaternary. The normal growth faults developed during the deposition the Lower-Middle Eocene Karabük Formation under NW-SE extension. And followed by NW-SE to N-S multi extensional deformation until Plio-Quaternary strike-slip faulting.

## **CHAPTER 5**

### **DISCUSSION**

The closure of Paleo-Tethys followed by another ocean, named Neo-Tethys. Newly created basin evolved by the rifting on Cimmerian continent during Liassic to platform carbonate evolution during Dogger to Malm period (Şengör and Yılmaz 1981). During Upper Jurassic-Lower Cretaceous, the deepening gave rise to the evolution of oceanic basin with flysch sequences and newly created oceanic crust. The Cenomanian-Barremian Ulus basin which is the site of flysch deposition with turbidities, slump structures and olistoliths was evolved during this time. Active depositional sites turned into site of active continental margin by the northward subduction of southern continents beneath Eurasian continent during post-Turonian (Şengör and Yılmaz 1981; Yılmaz et al., 1997).

Black Sea Basin is an oceanic basin rifted as a back-arc basin on northward subducting northern Neotethyan oceanic plate during post-Turonian (Görür, 1988; Yılmaz et al., 1997; Sunal and Tüysüz, 2002). To the south, various Upper Cretaceous to Paleogene extensional basins rifted on top of southward-accreted tectonic slices and mélanges under N-S compressional system between Black Sea Basin in north and northward subducting plate in south. Closure of the northern Tethys ended with the collision of Eurasia plate and southern continents along Pontides during Miocene (Şengör and Yılmaz, 1981). The collision resulted in imbrication of various tectonic blocks, thickening of uppermost crust as a result of accretion, evolution of fold and

thrust belts and closure of the foreland to piggy-back basins since Eocene (Saner et al., 1979; Yılmaz et al 1997; Sunal and Tüysüz, 2002).

The Cenomanian-Barremian age Ulus basin, once the site of deposition, is intensely deformed and uplifted, and became site of erosion. The uplifted terrain became the source for Paleogene basins, Bartın and Safranbolu basins. Based on post-Early Cretaceous stratigraphical differences among the Bartın, Ulus and Safranbolu basins, their evolution can be explained by inversion tectonics took place during post-Early Cretaceous and end of Paleogene period. The evolution of the Ulus basin continued until the end of Cenomanian. Then extension in basin under region wide contraction ended at the end of Cenomanian and was followed by fully compressional regime. The Ulus Basin was uplifted under E-W to NE-SW compression where no Paleogene deposition take place in the Ulus Basin. After Paleocene transgression, volcanic activity ended in the Bartın region and sedimentation was started in Bartın and Safranbolu basins while the Ulus Basin was still in a non-depositional stage during the Paleocene-Eocene.

Continuing uplift of the basin along the Bartın and the Karabük faults under NE-SW to NW-SE compression, continued during post-evolution of the Bartın and Safranbolu basins, which is post-Middle Eocene. Both Bartın and Karabük faults are thrusts onto Paleogene sequences.

Under region wide N-S compression, Paleocene-Eocene basins evolved under NW-SE extension as manifested by normal growth faults. Later the basins folded having almost NE-SW to ENE-WSW trends under region wide compressional system. Knowing that the master strand of the North Anatolian Fault as a scar (suture line) exit since Late Cretaceous (Yiğitbaş and Elmas, 1997; Şengör et al., 2005), the region wide possible principal stress orientation might be NNW-SSE direction.

The activity of Karabük Fault continued and a fault to the south –Karagöl Thrust- is evolved or re-activated under the northward push of the Cretaceous ophiolitic mélanges. Cenomanian-Barremian and Paleogene sequences overthrusts onto which the Eocene sequences along the Karagöl Thrust, under NNW-SSE orientation



compressional stresses during post-Eocene period. There are records of normal faulting under NNW-SSE extension in the study area, however, there are no records of post-Eocene normal faulting in the region. This phenomenon possibly linked with the accommodation faults related with thickening under region wide NNW-SSE contraction.

The Plio-Quaternary period is fully evolved in strike slip deformation as manifested with faults evolved in the study area under NE-SW compressional tectonics. However, the earthquakes happened in the region (eg. Abant and Kurşunlu earthquakes along NAF and Bartın earthquakes in Black Sea (Figure 5.1) under region wide principal compressional NNW-SSE orientation, have no conformity with the calculated stress orientation (Alptekin et al., 1986; Barka, 1992). In general, Black Sea region is regarded as neotectonically weakly active region which is not experiencing important internal deformation (Figure 5.1) (Şengör et al., 2005). Therefore, 1968 Bartın earthquake (Ms. 6.8) is one of the controversial issues in understanding the deformation mechanism in Western Pontides.

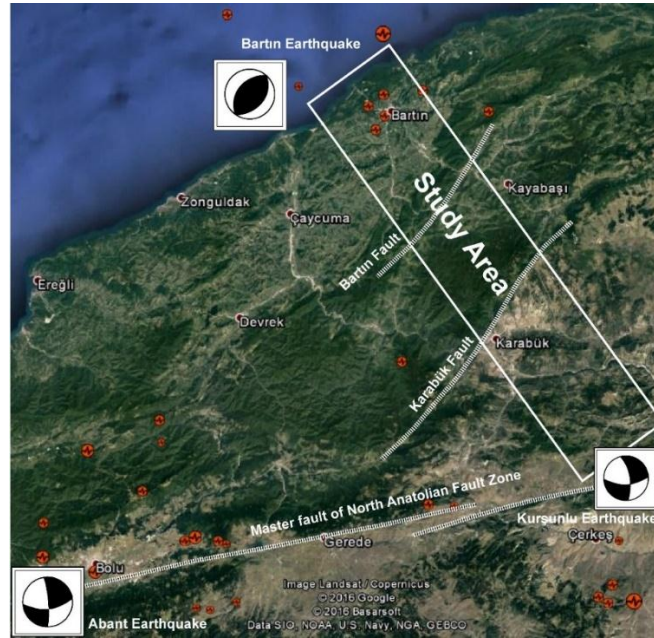


Figure 5.1. The location of the study area respect to some major earthquakes and the seismicity of the region (Google image). The Bartın earthquake giving a solution of reverse faulting where earthquakes on NAF gives dextral strike slip faulting.

To understand the post-Paleogene deformation in the Bartın to Ovacık area, research area was divided into four domains according to their (i) lithological differences, and (ii) trend of bedding planes and folds where domain boundaries are controlled by continuous long scale faults (Figure 5.2).

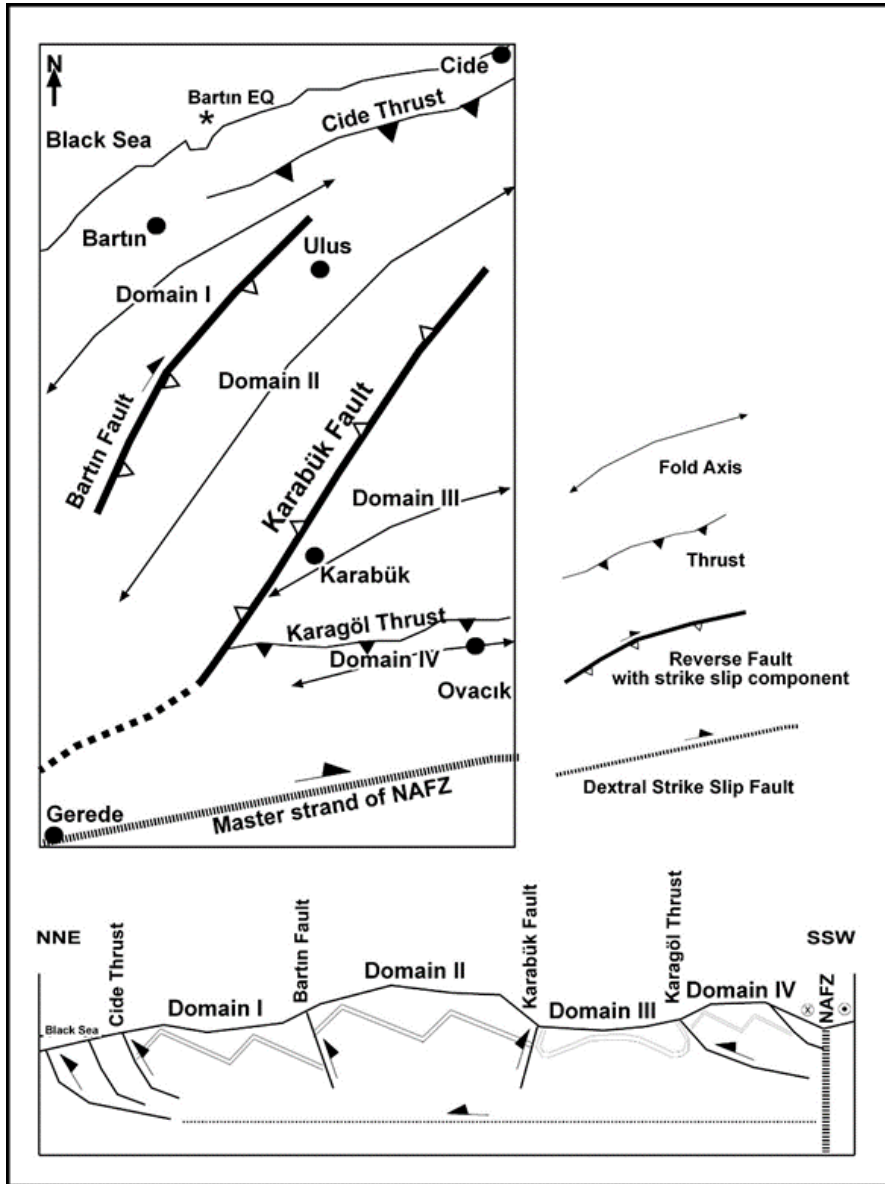


Figure 5.2. Tectonic Model proposed for the evolution of the tectonic structures in Bartın-Ulus-Karabük-Ovacık Region.

The domains are northern (Bartın) domain (I), central (Ulus) domain (II), southeastern (Karabük-Safranbolu) domain (III) and southern (Ovacık) domain (IV) (Figure 5.2). The boundary of the domain (I) and Domain (II) is controlled by NE-trending Bartın Fault. The boundary between domain (II) and (III), by NE-trending Karabük Fault. The boundary between domain (III) and (IV), by E-W-trending Karagöl Fault.

Lithologically (Figure 1.3), northern domain (I) is characterized by Paleozoic sequences, Permo-Triassic red beds, Jurassic-Cretaceous carbonates, Upper Cretaceous pelagic units, basaltic lava, and Paleocene-Eocene sequences with an unconformity in between. The central domain (II) is composed of dominantly Barremian-Cenomanian Ulus Formation and cross-cutting granitic intrusions. The southeastern domain (III) comprises Paleocene-Eocene sequences with unconformably overlying the Jurassic-Cretaceous carbonates. The southern domain is composed of Paleocene-Eocene sequences and Barremian-Cenomanian Ulus Formation, that unconformably overlie the Cretaceous ophiolitic Mélange in the the south.

The statistical analysis on the attitude of bedding planes supports the above-mentioned domain classification. The northern domain has a general bedding strike orientation of  $050^{\circ}\text{N}$  with various folds. The central domain has general trend of  $055^{\circ}\text{N}$  with various faults and folds. The southeastern domain has general trend of  $085^{\circ}\text{N}$ . In southeastern domain, along the margins of the domain (III) the beds gain high angles and place to place with overturned attitude. However, to the center of the domain, beds gain  $05^{\circ}$  to  $10^{\circ}$  dip amounts. Moreover, with respect to other domains, this domain is less folded with wide spectrum of strikes of beds. Furthermore, the southern domain has general trend of  $080^{\circ}\text{N}$  with various folds. It is very clear that there are almost  $30^{\circ}$  angular separations between the domains (I) to (II) and domains (III) to (IV). When the deformational intensity of the domains is compared, the central domain is intensely folded and faulted than other domains.

Based on, the stereographic analysis of folds, each domain has different reflections. Domain (I) folds are NE-trending asymmetrical, indicating a south to north vergence. Domain (II) folds are NE-trending symmetrical structures. However, field surveys support a north vergence with asymmetrical folds. Domain (III) there is uniform distribution of strikes. Almost E-W-trending overturned syncline (Sonya Syncline) parallel to the Karagöl Fault, folds depicts a northward vergence. Domain (IV) folds are almost E-W-trending asymmetrical folds indicating a south to northward vergence. Addition to above, in Domain IV, two rock packages are overthrust onto Domain III sequences having statistically the same fold orientations (Figure 5.2). The Domain IV is divided into Barremian- Cenomanian sequences and Paleogene sequences and statistically analysis separately carried out (Figure 5. 3). The results are; for Barremian-Cenomanian sequences the strike of the beds are  $075^{\circ}\text{N}$  and for Paleogene sequences it is  $085^{\circ}\text{N}$  having an angular difference of  $10^{\circ}$  (Figure 5.3).

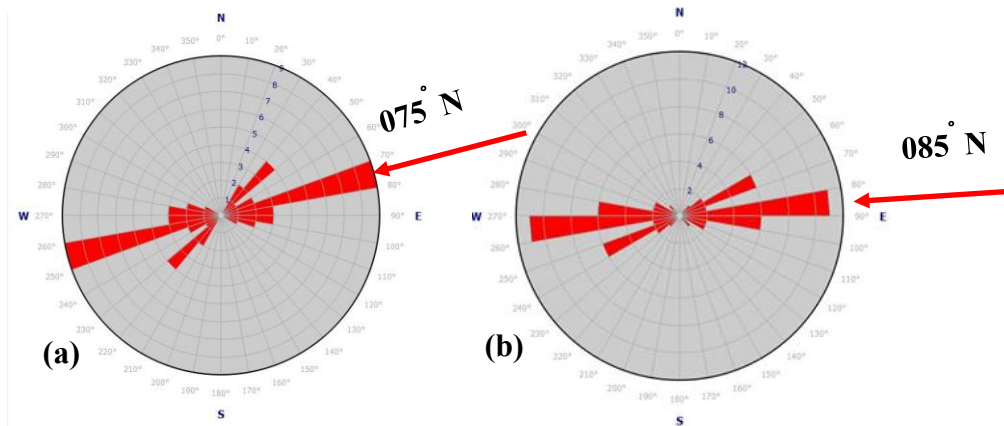


Figure 5.3. Major strike orientations in Barremian-Cenomanian sequences (a) and Upper Paleocene-Lower-Middle Eocene sequences (b) in Domain IV.

It is very clear that there is an angular difference between northern domains (Domain I and II) and southern domains (Domain III and IV) of  $30^{\circ}$ . Domain I and II are probably deformed together manifested with having the same folding attitude. However, Domain I and Domain III having the same age sequences have an angular

difference of almost  $30^{\circ}$ . Moreover, within Domain IV, there is angular difference between Barremian-Cenomanian sequences and Upper Paleocene-Lower-Middle Eocene sequences of  $10^{\circ}$ . When totally analyzed, these angular relations may propose a post-Middle Eocene counter or clockwise rotation of  $20^{\circ}$ . Else, northern domains are experiencing clockwise, whereas the southern domains are counter-clockwise.



## CHAPTER 6

### CONCLUSION

The post-Paleogene deformation studies show that,

- There is a strike of bed orientation difference between the Domains I-II with Domains III-IV of  $30^{\circ}$ . And within Domain IV, there is angular difference between Barremian-Cenomanian sequences and Upper Paleocene-Lower-Middle Eocene sequences of  $10^{\circ}$ . When totally analyzed, these angular relations may propose a post-Middle Eocene counter or clockwise rotation of  $20^{\circ}$ . Or northern domains are experiencing clockwise, whereas the southern domains are counter-clockwise rotations.
- There is a south to north vergence based on the asymmetry of folds and attitude of reverse faults for the period of post-Paleogene-pre Plio-Quaternary.
- The fault-slip data analysis points out that NE-trending Bartın Fault is a strike-slip fault with reverse components developed under an approximately NE-SW compression.
- The fault-slip data analysis points out that NE-trending Karabük Fault is a reverse fault with minor strike-slip component developed under an approximately NW-SE compression.
- There are faults confined to varies lithologies which are (i) post-Late Santonian-early Campanian normal fault with strike-slip component developed under almost E-W extension, (ii) post-Early-Middle Eocene strike-



slip faults developed under NE-SW compression during Plio-Quaternary, (iii) post-Early-Middle Eocene normal faults developed under NNW-SSE extension.

- There are well-developed faults during post-Barremian-Cenomanian. These are (i) strike-slip faults with reverse components developed under almost E-W compression, (ii) reverse fault developed under NE-SW compression. The normal faults are cross-cut by reverse and strike-slip faults manifesting that compression post-dates the extension during post-Barremian-Cenomanian time.
- Ulus domain (central domain) once the site of deposition during Barremian-Cenomanian is an uplifted terrain during the deposition of Paleogene sequences forming an inversion of a basin. The domain has reverse to strike-slip faulted margins causing uplift of the central domain during Paleogene where no deposition took place during Paleocene and Eocene period.

## REFERENCES

- Akbaş, B., Altun, I. E. and Aksay, A., 2002. 1/100000 Ölçekli Türkiye Jeoloji Haritaları. Zonguldak E-28 Paftası. MTA Jeoloji Etüdları Daires (*in Turkish*).
- Akman, Ü., 1992. Amasra-Arıt arasındaki jeolojisi. Doktora Tezi, Ankara Üniversitesi Fen Bilimleri Enstitüsü, 209 p. (*in Turkish*).
- Akman, Ü., 2002. Batı Karadeniz Bölgesinde Bartın-Arı-Kurucaşile dolaylarında yüzeyleyen kayaların stratigrafik tanımlamaları. Türkiye Stratigrafik Komitesi Çalıştayı, Batı Karadeniz Bölgesi'nin Lithostratigrafi Adlamaları, Özler, MTA Genel Müdürlüğü, 17-18 Ocak 2002, Ankara, 10 p. (*in Turkish*).
- Akyol, Z., Arpat, E., Erdoğan, B., Göğeri, E., Güner, Y., Şentürk, L., Tütüncü, K. and Uysal, Ş., 1974. 1/50000 ölçekli Türkiye Jeoloji Haritası Serisi, Zonguldak E29 a, E29 b, E29 c, E29 d, Kastamonu E30 a, E30 d. MTA Yayınları, Ankara (*in Turkish*).
- Aleksandrowski, P., 1985. Graphical determination of principal stress directions for slickenside lineation population: An attempt to modify Arthaud's method. Journal of Structural Geology, vol. 7, pp.: 73-82 .
- Alptekin, Ö., Nabelek, J. L. And Toksöz, M. N., 1986. Source mechanism of the Bartın earthquake of September 3, 1986 in north-western Turkey: Evidence for active thrust faulting at the southern Black Sea margin. Tectonophysics, 122, pp: 73-88.
- Alişan, C. and Derman, A.S., 1995. The first palynological age, sedimentological and stratigraphic data for Çakraz Group (Triassic), Western Black Sea. In Geology of the Black Sea Region, (eds. A. Erler, T. Ercan, E. Bingöl and S. Örcen), pp.: 93-98.
- Allmendinger, R.W. and Jordan, T.E., 1989. Geological map of Hewfoundland Mountains, northwest of Utah. U.S. Geological Survey, 1:31, pp.:680.

Altınlı, İ. E., 1951. Ilıksu civarının jeolojisi (Zonguldak vilayeti). İstanbul Üniversitesi Fen Fakültesi Mecmuası, Seri B, Cilt XVI, Sayı 4, pp.: 301-303 (*in Turkish*).

Anderson, E.M., 1951. The Dynamics of Faulting and Dyke Formation with Application to Britain, vol.2, 206 pp., Oliver and Body, Edinburgh.

Angelier, J., 1979. Determination of the mean principal directions of stress for a given fault population. Tectonophysics, vol. 56, pp.:17-26.

Angelier, J., 1984. Tectonic analysis of fault-slip data sets. Journal of Geophysical Research, vol. 89, pp.: 5835-5848.

Angelier, J., 1989. From orientation to magnitudes in paleostress determinations using fault-slip data. Journal of Structural Geology, vol. 3, pp.:51-65.

Angelier, J., 1994. Fault-slip analysis and paleostress reconstruction (Chapter 4), in Continental Deformation, P.L. Hancock, e., Pergamon Press, Oxford, pp.:53-100.

Arni, P., 1931. Zur Stratigraphie und Tektonik der Kreideschichtungen östlich Ereğli an der Schwarzmeerküste. Eclogae geol. Helvetiae, vol. 25, pp.: 305-345 (*in German*).

Aydın, M., Şahintürk, Ö., Serdar, H.S., Özçelik, Y., Akarsu, I., Üngör, A., Çokuğraş, R. and Özçelik, Y., 1986. Ballıdağ-Çangaldağ (Kastamonu) arasındaki bölgenin jeolojisi. Türkiye Jeoloji Kurumu Bülteni, vol. 30/2, pp.: 1-16 (*in Turkish*).

Aydın, M., Serdar, H.S., Şahintürk, Ö., Yazman, M., Çokuğraş, R., Demir, O. and Özçelik, Y., 1987. Çangaldağ (Sakarya)-Sünnicedağı(Bolu) Yöresinin jeolojisi. Türkiye Jeoloji Kurumu Bülteni, vol. 30/1, pp.: 1-14 (*in Turkish*).

Aydın, M., Şahintürk, Ö., and Şaraoğlu, F., 2001.Orta Pontidler'in Neotektoniği ve Hidrokarbon Arama Alanlarına Olan Etkileri Projesi Jeoloji Raporu. TPAO Rapor No: 4243 (*in Turkish*).

Barka, A. A., 1992. The North Anatolian fault zone. Annales Tectonicae, VI suppl.

Blumenthal, M., 1948. Un aperçu de la geologie des chaînes nord-anatoliennes entre l'Ova de Bolu et le Kızılırmak inferieur. MTA Yayınları, vol. B-13, 265 p.(*in French*).

Bott, M.P.H., 1959. The mechanics of oblique-slip faulting. Geological Magazine, 96, pp.: 109-117.

Bulut, M., Özdemir, M., Altıparmak, S. and Bozkurt, H. E., 1982. Bartın Amasra Taşkömürü Havzası Jeolojisi, Cilt-1 ve Cilt-2. MTA Rapor No: 7201(*in Turkish*).

Carey, E. and Brunier, B., 1974. Analyse theorique et numerique d'un modele mecanique elementary applique a l'etude d'une population failles. Comptes Rendus Hebdomadaires de L'Academie des Science France, Serie D. 279, pp.: 891-894 (*in French*).

Cerit, O., 1990. Bolu masifinin jeolojik ve tektonik incelenmesi. Doktora Tezi, Hacettepe Üniversitesi Fen Bilimleri Enstitüsü, 217 p. (*in Turkish*).

Ciancaleoni, L., 2005. Deformation processes during the last stage of the continental collision: the brittle-ductile fault systems in the Bergell and Insubric areas (Eastern Central Alps, Switzerland- Italy). Ph.D Thesis, Universite De Neuchatel.

Derman, A.S., 1990. Batı Karadeniz bölgesinin Geç Jura ve Erken Kretase'deki jeolojik evrimi. Türkiye 8. Petrol Kongresi Bildiriler, pp.: 314-321 (*in Turkish*).

Derman, A.S. and Özçelik, Y., 1993. Batı Karadeniz Bölgesi'ndeki Paleozoik birimlerin stratigrafisi, sedimantolojik özellikleri ve yörenin muhtemel paleocoğrafik evrimi. A. Suat Erk Jeoloji Sempozyumu, bildiri, Ankara Üniversitesi Fen Fakültesi Jeoloji Müh. Bölümü, 2-5 Eylül 1991, Ankara, pp: 11-20 (*in Turkish*).

Derman, A.S. and Sayılı, A., 1995. İnaltı formation: a key unit for regional geology. Geology of the Black Sea Region, (eds. A. Erler, T. Ercan, E. Bingöl and S. Örçen), pp.: 104-108.

Deveciler, E., 1986. Alaplı-Bartın-Cide (Batı Karadeniz) Jeoloji Raporu. MTA Rapor No: 7938 (*in Turkish*).

- Doblas, M., 1998. Slickensides kinematic indicators. Tectonophysics, vol. 295, pp.:187.
- Erten, H. and Özcan F., 1997. Karabük-Safranbolu-Eflani-Araç Çevresinin Tersiyer Jeolojisi ve Kömür Olanakları Raporu. MTA Rapor No: 10296 (*in Turkish*).
- Etchecopar, A., Vasseur, G. and Daignieres, M., 1981. An inversion problem in microtectonics for the determination of stress tensor from fault striation analysis. Journal of Structural Geology, vol. 3, pp.:51-65.
- Fleuty, M.J., 1974. Slickensides and slickenlines. Geological Magazine, vol. 112, pp.: 319-322.
- Fratschner, W. Th., 1952. Kurucaşile-Eflani-Cide bölgesindeki saha etüdü hakkında ilk not. MTA Rapor No: 2061(*in Turkish*).
- Gayle, R.B., 1959. Sinop Yöresi ile ilgili Çalışma. Perol İşleri Arşiv No: 17 (*in Turkish*).
- Gedik, A. and Korkmaz, S., 1984. Sinop Havzasının jeolojisi ve petrol olanakları. Jeoloji Mühendisliği, vol. 19, pp.: 53-80 (*in Turkish*).
- Göktunalı, K., 1957. Zonguldak Vilayetine Bağlı Ulus Kazasının Cenup Bölgesine Ait Jeolojik Rapor. MTA Rapor No: 2534 (*in Turkish*).
- Görür, N., 1988. Timing of opening of the Black Sea basin. Tectonophysics, v. 147, pp. 247-262 .
- Gümüş, Ö., 1966. II. Bölge Ulus Sahalarının Jeolojisi Hakkında Rapor I. TPAO Rapor No:450 (*in Turkish*).
- Gümüş, Ö., 1967. II. Bölge Ulus Sahalarının Jeolojisi Hakkında Rapor II. TPAO Rapor No:465 (*in Turkish*).
- Güven, A., 1977. Stratigraphy and Sedimentology of Eocene Formations Karabük Area Turkey. Ph. D. Thesis, University of Wales. TPAO Rapor No: 4756.
- Işıker, K., Altınar, D., Batı, Z., Tunay, G., Ekmekçi, E., Tüysüz, O., Aksay, A., Yiğitbaş E., Akay, E., Özkan, Y.Z., Çatma, A., Ekmekçi, E., Yurtsever, Ş., Özbay,

and A. and Gökmenoğlu, O. (Turkish Stratigraphic Committee,), 2004. Batı Karadeniz Bölgesi Lithostratigrafi Birimleri. MTA Genel Müdürlüğü. TPAO Rapor No: 5170 (*in Turkish*).

Kaya, O., Dizer, A., Tansel, I. and Meriç, E., 1982/1983. Ereğli (Zonguldak) alanının Kretase stratigrafisi. MTA Dergisi, vol. 99/100, pp.: 19-33 (*in Turkish*).

Kerey, I. E., Kelling, G. and Wagner, R.H., 1986. An outline stratigraphy and palaeobotanical records from the Middle Carboniferous rocks of Northwestern Turkey. Ann. Soc. Geol. Nord, CV, pp.: 203-216.

Kerey, I.E., 1982. Stratigraphical and sedimentological studies of Upper Carboniferous rocks in Northwestern Turkey. Ph. D. Thesis Keele University.

Ketin, İ., 1953. Zonguldak Vilayetine Bağlı Ovacuma – Eflani Bölgesinin 1/25000 Mikyaslı Jeolojik Lövesine Ait Memuar . MTA Rapor No: 2054 (*in Turkish*).

Ketin, İ., 1966. Anadolu'nun tektonik birlikleri (Tectonic Units of Anatolian Asian Minor). MTA Yayını, vol. 66, pp.: 20-34 (*in Turkish*).

Ketin, İ. and Gümüş, A., 1963. Sinop-Ayancık güneyinde üçüncü bölgeye dahil sahalara jeolojisi hakkında rapor (2.Kısım: Jura-Kretase formasyonlarının etüdü). TPAO Rapor No: 288 (*in Turkish*).

Koçyiğit, A., 1987. Karabük-Safranbolu Tersiyer havzası kuzey kenarının stratigrafisi ve niteliği. Bulletin of the Geological Society of Turkey, vol.30, pp.: 61-69 (*in Turkish*).

Krantz, R.W., 1988. Multiple fault sets and three dimensional strain: Theory and application. Journal of Structural Geology, vol. 10, pp.:225-237.

Nabeel, K.A-A., 2006. A Mathematical Technique for Analyzing Folds with the Computer Program "FOLDPI". Iraqi Jour. Earth Sci., vol. 6, No. 2, pp.: 53-74.

Okay, A. and Tüysüz, O., 1999. Tethyan sutures of northern Turkey. Geological Society of London, v. 156, pp: 475-515.

Özçelik, Ü. and Çaptuğ, A., 1990. Amasra doğusu-Cide arasında kalan alanda yapılan saha gözlemleri ve revizyon çalışmaları. TPAO Rapor No: 2789 (*in Turkish*).

Pascal, C., Angelier, J., Seland, R.T. and Lepvrier, C., 2002. A simplified model of stress-slip relationship: application to the Froy Field, northern North Sea. *Tectonophysics*, 357(1-4), pp.: 103-118.

Ramsay, J.G., 1967. *Folding and Faulting of Rocks*. McGraw-Hill, New York, 568.

Ramsay, J.G. and Huber, M.I., 1987. *The Techniques of Modern Structural Geology*, vol. 2, *Folds and Faultures*. Academic Press, London.

Rutherford, M., Banks, C., Hirst, J.P.P. and Robinson, A. G., 1992. The Mesozoic biostratigraphy of the Pontides. BP Exploration Report. TPAO Rapor No: 3116

Saner, S., Taner, I., Aksoy, Z., Siyako, M. and Bürkan, K.A., 1979. Karabük-Safranbolu Bölgesinin Jeolojisi. TPAO Rapor No: 1322 (*in Turkish*).

Saner, S., Taner, I., Saner, S., Taner, I., Aksoy, Z., Siyako, M. and Bürkan, K.A., 1980. Safranbolu havzasının jeolojik yapısı ve Tersiyer paleocoğrafyası. Türkiye Beşinci Petrol Kongresi, Bildiriler, 111-122 (*in Turkish*).

Saner, S., Siyako, M., Aksoy, Z., Bürkan, K. A. and Demir, O., 1981. Zonguldak Dolayının Jeolojisi ve Hidrokarbon Olanakları: TPAO Rapor No:1596 (*in Turkish*).

Schimmrich, S.H., 1991. Evaluation of computational methods of paleostress analysis using fault-slip data. *Geology These and Dissertations*, 80 p.

Stephen, M.R., Duebendorfer, E.M. and Schiefelbein, I.M., 2007. *Structural Analysis & Synthesis: A Laboratory Course in Structural Geology*. vol. 3. pp.: 61-67.

Sunal, G. and Tüysüz, O., 2002. Palaeostress Analysis of Tertiary Post-Collisional Structures in The Western Pontides, Northern Turkey *Geol. Mag.*, 139(3), pp.343-359.

Şahintürk, Ö. and Özçelik, Y., 1983. Zonguldak-Bartın-Amasra-Kurucaşile-Cide dolaylarının jeolojisi ve petrol olanakları. TPAO Rapor No: 1816 (*in Turkish*).



Şen, Ş., 2001. Karabük-Safranbolu Havzasının Sedimanter Analizi ve Bölgedeki Diğer Çökel Havzalarla İlişkisi. Doktora Tezi, İstanbul Üniversitesi Fen Bilimleri Enstitüsü. TPAO Rapor No: 4254 (*in Turkish*).

Şengör, A.M.C. and Yılmaz, Y., 1981. Tethyan evolution of Turkey. A plate tectonic approach. Tectonophysics, vol. 75, pp.: 181-241.

Şengör, A.M.C., Yılmaz, Y. and Sungurlu, O., 1984. Tectonics of the Mediterranean Cimmerides: Nature and evolution of the western termination Paleotethys. In: J. E. Dixon and A. H. F. Robertson (eds.), The Geological Evolution of the Eastern Mediterranean. Geological Society of London Special publication 17, pp.: 77-122

Şengör, A.M.C., Tüysüz, O., İmren, C., Sakıncı, Eyidoğan, H., Görür, N., Le Pichon, X. and Rangin, C., 2005. The North Anatolian Fault: A new look. Annu. Rev. Earth Planet, vol. 33, pp: 37-112.

Şengün, M., 1993. Geologic evolution of Anatolian segment of the Tethyan belt. Bulletin of the Geological Society of Turkey, vol.36/2, pp.: 81-98.

Temel, R.Ö., Gargili, D., Ceylan, M. and Kırçuval, A., 2015. Bartın-Cide Arasının Hidrokarbon Potansiyelinin Değerlendirilmesi. TPAO Rapor No:5541 (*in Turkish*).

Timur, E., 2002. Üst Paleosen-Alt Eosen Kışlaköy Formasyonu, Karabük-Safranbolu Tersiyer Havzası Güney Kenarı. Türkiye Stratigrafi Komitesi 3. Çalıştayı, Orta ve Doğu Karadeniz Bölgesi'nin Lithostratigrafi Adlandırmaları, Özler, MTA Genel Müdürlüğü, 17-18 Ocak 2002, pp.: 12 (*in Turkish*).

Tokay, M., 1952. Karadeniz Ereğlisi-Alaplı-Kızıltepe-Alacağzı Bölgesinin Jeolojisi. MTA Dergisi, vol. 42/43, pp.: 35-78 (*in Turkish*).

Tokay, M., 1954. Filyos Çayı Ağzı-Amasra-Bartın-Kozcağzı-Çaycuma Bölgesinin Jeolojisi. MTA Dergisi, 46/47, 58-74 (*in Turkish*).

Tokay, M., Ordemir, İ., Doyuran, V., Koçyiğit, A. and Lünel, T., 1986. Karabük Yerleşim Alanı Jeolojik Etüdü. ODTÜ Proje No: 86-03-09-01-02 (*in Turkish*).

Tüysüz, O., Kirici, S. and Sunal, G. 1997. Cide-Kurucaşile Dolayının Jeolojisi. TPAO Rapor No: 3736 (*in Turkish*).

Ustaömer P.A., 1996. Bolu-Yedigöller granitik kayaçlarının petrojenezi ve metajenezi. Doktora Tezi, İstanbul Üniversitesi Fen Bilimleri Enstitüsü, pp.: 196 (*in Turkish*).

Wallace, R.E., 1951. Geometry of shearing stress and relation to faulting. Journal of Geology, vol. 69, pp.:118-130.

Will, T.M. and Powell, R., 1991. A robust approach to the calculation of paleostress fields from fault plane data. Journal of Geophysical Research 99, 20203-20223.

Yergök, A.F., Akman, Ü., İplikçi, E., Karabalık, N.N., Keskin, I., Mengi, H., Umut, M., Armağan, F., Erdoğan, K., Kaymakçı, H., and Çetinkaya, A., 1987. Batı Karadeniz Bölgesi'nin jeolojisi (I). MTA Rapor No: 8273 (*in Turkish*).

Yılmaz, Y. and Tüysüz, O., 1984. Kastamonu-Boyabat-Vezirköprü-Tosya arasındaki bölgenin jeolojisi (İlgaz-Kargı masifinin etüdü). MTA Rapor No: 7883 (*in Turkish*).

Yılmaz, Y., Tüysüz O., Yiğitbaş, E., Genç, Ş. C. and Şengör, A.M.C., 1997. Geology and tectonic evolution of the Pontides, in A.G. Robinson, ed., Regional and petroleum geology of the Black sea and surrounding region: AAPG Memoir 68, pp: 183-226.

Yiğitbaş, E. and Elmas, A., 1997. Bolu-Eskipazar-Devrek-Çaycuma dolayının jeolojisi. TPAO Report No: 37 (*in Turkish*).

## APPENDICES

### APPENDIX A

#### BED MEASUREMENTS

Table A.1. Bed measurements of Domain I

DOMAIN I BEDS			
Formation	Strike(°)	Dip Direction(°)	Dip Amount(°)
Kusuri Formation	N38E	128	19
Kusuri Formation	N80E	170	34
Kusuri Formation	N67E	157	21
Kusuri Formation	N56E	146	25
Kusuri Formation	N62E	152	20
Kusuri Formation	N58E	148	38
Kusuri Formation	N68E	338	59
Kusuri Formation	N54E	324	50
Kusuri Formation	N45E	315	36
Kusuri Formation	N65E	155	35
Kusuri Formation	N60E	150	30
Kusuri Formation	N48E	138	38
Kusuri Formation	N45E	135	46
Kusuri Formation	N77E	347	35
Kusuri Formation	N65E	335	32
Kusuri Formation	N45E	315	41
Kusuri Formation	N85E	175	30
Kusuri Formation	EW	180	25
Kusuri Formation	N42E	132	38
Kusuri Formation	N50E	140	25
Kusuri Formation	N77E	167	13
Kusuri Formation	N57E	147	8
Kusuri Formation	N42E	312	42

Table A.1. Continued

<b>DOMAIN I BEDS</b>			
<b>Formation</b>	<b>Strike(°)</b>	<b>Dip Direction(°)</b>	<b>Dip Amount(°)</b>
Kusuri Formation	N28E	118	30
Kusuri Formation	N22E	292	40
Kusuri Formation	N38E	308	34
Kusuri Formation	N44E	314	40
Kusuri Formation	N30E	300	45
Kusuri Formation	N40E	130	53
Kusuri Formation	N50E	320	35
Kusuri Formation	N70E	160	14
Kusuri Formation	N20E	110	15
Kusuri Formation	N40E	310	26
Kusuri Formation	N38E	308	15
Kusuri Formation	N43E	133	21
Kusuri Formation	N45E	315	23
Kusuri Formation	N56E	146	11
Kusuri Formation	N19E	289	50
Kusuri Formation	N20E	290	18
Kusuri Formation	N15E	285	10
Kusuri Formation	N45E	135	15
Kusuri Formation	N44E	314	37
Kusuri Formation	N39E	309	47
Kusuri Formation	N45E	315	38
Kusuri Formation	N52E	322	44
Kusuri Formation	N55E	325	25
Kusuri Formation	N45E	315	50
Kusuri Formation	N40E	310	40
Kusuri Formation	N37E	307	55
Kusuri Formation	N63E	333	50
Kusuri Formation	N58E	317	28
Kusuri Formation	N57E	327	26
Kusuri Formation	N62E	332	25
Kusuri Formation	N50E	320	38
Kusuri Formation	N35E	305	43
Kusuri Formation	N56E	326	38
Kusuri Formation	N48E	318	42
Kusuri Formation	N41E	311	47
Kusuri Formation	N40E	310	41
Kusuri Formation	N56E	326	45
Kusuri Formation	N45E	135	20
Kusuri Formation	N38E	308	39

Table A.1. Continued

<b>DOMAIN I BEDS</b>			
<b>Formation</b>	<b>Strike(°)</b>	<b>Dip Direction(°)</b>	<b>Dip Amount(°)</b>
Kusuri Formation	N28E	298	27
Akveren Formation	N47E	137	10
Akveren Formation	N63E	153	17
Akveren Formation	N63E	153	30
Akveren Formation	N69E	159	20
Akveren Formation	EW	180	16
Akveren Formation	N71E	161	18
Akveren Formation	N60E	141	21
Akveren Formation	N45E	315	28
Akveren Formation	N50E	320	40
Akveren Formation	N37E	307	50
Akveren Formation	N37E	307	30
Akveren Formation	N55E	325	29
Akveren Formation	N62E	332	35
Akveren Formation	N49E	319	35
Akveren Formation	N40E	310	60
Ulus Formation	N35E	305	40
Ulus Formation	N37E	307	46
Ulus Formation	N20E	290	39
Ulus Formation	N85E	175	40
Ulus Formation	N80E	170	40
Ulus Formation	N75E	165	43
Ulus Formation	N41E	311	38
Ulus Formation	N57E	327	43
Yemişliçay Formation	N46E	136	10
Yemişliçay Formation	N74E	344	60

Table A.2. Bed measurements of Domain II

<b>DOMAIN II BEDS</b>			
<b>Formation</b>	<b>Strike(°)</b>	<b>Dip Direction(°)</b>	<b>Dip Amount(°)</b>
Ulus Formation	N57E	327	43
Ulus Formation	EW	0	65
Ulus Formation	N81E	351	79
Ulus Formation	N58E	148	43
Ulus Formation	N50E	140	52
Ulus Formation	N40E	130	40
Ulus Formation	N35E	125	35
Ulus Formation	N41E	131	30
Ulus Formation	N37E	127	45
Ulus Formation	N65E	155	53
Ulus Formation	N85E	355	40
Ulus Formation	N68E	158	30
Ulus Formation	N75E	165	39
Ulus Formation	N50E	320	17
Ulus Formation	N70E	340	26
Ulus Formation	N15E	285	49
Ulus Formation	N36E	306	37
Ulus Formation	N50E	320	43
Ulus Formation	N34E	124	50
Ulus Formation	N40E	130	57
Ulus Formation	N30E	300	55
Ulus Formation	N49E	319	37
Ulus Formation	N58E	328	40
Ulus Formation	N57E	147	30
Ulus Formation	N65E	155	50
Ulus Formation	N70E	340	60
Ulus Formation	N73E	343	35
Ulus Formation	N75E	345	55
Ulus Formation	N58E	148	25
Ulus Formation	N69E	159	25
Ulus Formation	N50E	140	47
Ulus Formation	N70E	160	35
Ulus Formation	N69E	159	20
Ulus Formation	N50E	140	45
Ulus Formation	N35E	125	55
Ulus Formation	N77E	167	30
Ulus Formation	N60E	150	70
Ulus Formation	N22E	112	40

Table A.2. Continued

<b>DOMAIN II BEDS</b>			
<b>Formation</b>	<b>Strike(°)</b>	<b>Dip Direction(°)</b>	<b>Dip Amount(°)</b>
Ulus Formation	N24E	114	23
Ulus Formation	N32E	122	31
Ulus Formation	N65E	155	50
Ulus Formation	N19E	109	43
Ulus Formation	N52E	322	43
Ulus Formation	N45E	315	55
Ulus Formation	N35E	305	30
Ulus Formation	N30E	300	40
Ulus Formation	N19E	289	48
Ulus Formation	N30E	300	36
Ulus Formation	N30E	120	50
Ulus Formation	N57E	147	26
Ulus Formation	N50E	140	30
Ulus Formation	N57E	147	38
Ulus Formation	N51E	141	42
Ulus Formation	N56E	146	49
Ulus Formation	N60E	150	40
Ulus Formation	N44E	314	46
Ulus Formation	N40E	310	41
Ulus Formation	N65E	335	34
Ulus Formation	N34E	304	35
Ulus Formation	N23E	293	26
Ulus Formation	N30E	120	26
Ulus Formation	N30E	120	21
Ulus Formation	N28E	298	30
Ulus Formation	N50E	320	43
Ulus Formation	N56E	326	42
Ulus Formation	N30E	300	20
Ulus Formation	N53E	323	30
Ulus Formation	N37E	127	50
Ulus Formation	N80E	170	45
Ulus Formation	N50E	140	46
Ulus Formation	N63E	153	45
Ulus Formation	N57E	147	55
Ulus Formation	N42E	132	35
Ulus Formation	N65E	335	55
Ulus Formation	N65E	335	45
Ulus Formation	N88E	358	28



Table A.2. Continued

<b>DOMAIN II BEDS</b>			
<b>Formation</b>	<b>Strike(°)</b>	<b>Dip Direction(°)</b>	<b>Dip Amount(°)</b>
Ulus Formation	N75E	345	36
Ulus Formation	N30E	120	45
Ulus Formation	N69E	159	20
Ulus Formation	N65E	335	46
Ulus Formation	N26E	296	38
Ulus Formation	N15E	285	28
Ulus Formation	N75E	345	30
Ulus Formation	N70E	340	38
Ulus Formation	N45E	315	41
Ulus Formation	N72E	342	40
Ulus Formation	N53E	323	25
Ulus Formation	N55E	325	30
Ulus Formation	N50E	320	50
Ulus Formation	N78E	348	45
Ulus Formation	N65E	335	20
Ulus Formation	N60E	330	42
Ulus Formation	N43E	313	25
Ulus Formation	N15E	285	21
Ulus Formation	N35E	305	25
Ulus Formation	N25E	295	47
Ulus Formation	N35E	305	25
Ulus Formation	N63E	153	25
Ulus Formation	N61E	151	22
Ulus Formation	N67E	157	29
Ulus Formation	N70E	160	45
Ulus Formation	N40E	130	32
Ulus Formation	N35E	125	24
Ulus Formation	N57E	147	29
Ulus Formation	N18E	108	34
Ulus Formation	N64E	154	51
Ulus Formation	N45E	135	28
Ulus Formation	N42E	132	43
İnaltı Formation	N30E	120	30
Ulus Formation	N57E	147	55
Ulus Formation	N42E	132	35
Ulus Formation	N65E	335	55
Ulus Formation	N65E	335	45
Ulus Formation	N88E	358	28

Table A.3. Bed measurements of Domain III

<b>DOMAIN III BEDS</b>			
<b>Formation</b>	<b>Strike(°)</b>	<b>Dip Direction(°)</b>	<b>Dip Amount(°)</b>
Safranbolu Formation	N60E	150	4
Safranbolu Formation	N73E	163	4
Safranbolu Formation	N45E	135	36
Safranbolu Formation	N45E	135	27
Safranbolu Formation	N20E	110	38
Safranbolu Formation	N50E	140	17
Safranbolu Formation	N80E	170	12
Safranbolu Formation	N89E	179	3
Safranbolu Formation	N89E	125	5
Safranbolu Formation	N35E	125	6
Safranbolu Formation	N48E	138	76
Safranbolu Formation	N45E	135	70
Safranbolu Formation	N38E	128	74
Safranbolu Formation	N34E	124	81
Safranbolu Formation	N46E	136	60
Safranbolu Formation	N30E	120	55
Safranbolu Formation	N43E	133	47
Safranbolu Formation	N27E	117	80
Safranbolu Formation	N23E	113	49
Safranbolu Formation	N83W	7	27
Safranbolu Formation	N80W	10	24
Safranbolu Formation	N75E	345	31
Safranbolu Formation	N80E	350	37
Safranbolu Formation	N80W	10	60
Safranbolu Formation	N86E	176	75
Safranbolu Formation	EW	180	50
Safranbolu Formation	N33E	303	76
Safranbolu Formation	N45E	315	65
Safranbolu Formation	N37E	307	88
Karabük Formation	N50E	140	14
Karabük Formation	N65E	155	9
Karabük Formation	N30E	120	11
Karabük Formation	N55E	145	5
Karabük Formation	N63E	153	8
Karabük Formation	N57E	147	11
Karabük Formation	N73E	163	6
Karabük Formation	EW	180	3
Karabük Formation	EW	180	13

Table A.3. Continued

<b>DOMAIN III BEDS</b>			
<b>Formation</b>	<b>Strike(°)</b>	<b>Dip Direction(°)</b>	<b>Dip Amount(°)</b>
Karabük Formation	EW	180	9
Karabük Formation	EW	180	2
Karabük Formation	N79E	169	9
Karabük Formation	EW	180	15
Karabük Formation	N75W	195	10
Karabük Formation	N80W	190	12
Karabük Formation	N88W	182	3
Karabük Formation	N82E	172	7
Karabük Formation	N87E	177	4
Karabük Formation	N81E	171	8
Karabük Formation	N77E	167	17
Karabük Formation	N69E	159	12
Karabük Formation	N79W	191	8
Karabük Formation	N81W	189	9
Karabük Formation	N86W	184	6
Karabük Formation	N67E	157	20
Karabük Formation	N37E	127	40
Karabük Formation	N75E	165	12
Karabük Formation	N47E	137	25
Karabük Formation	N55E	145	14
Karabük Formation	N41E	131	9
Karabük Formation	N38E	128	21
Karabük Formation	N33E	123	18
Karabük Formation	N45W	45	26
Karabük Formation	N75W	15	30
Karabük Formation	N54W	36	40
Karabük Formation	N88W	2	5
Karabük Formation	N78W	12	19
Karabük Formation	N80E	350	35
Karabük Formation	N82E	352	34
Karabük Formation	N82E	172	40
Karabük Formation	N85E	175	36
Ulus Formation	N73E	163	40
Ulus Formation	N43E	133	40
Ulus Formation	N35E	125	50
Ulus Formation	N60E	150	21
Ulus Formation	N63E	153	12

Table A.3. Continued

DOMAIN III BEDS			
Formation	Strike(°)	Dip Direction(°)	Dip Amount(°)
Çerçen-Soğamlı-Akçapınar-Yunuslar Formations-Köseler Member	N80E	170	9
	N53E	143	5
	N37E	127	6
	N48E	138	7
	N67E	157	4
	N83E	173	8
	N88E	178	5
	N72E	162	7
	EW	180	10
	N80W	190	9
	N76W	194	9
	N85E	175	12
	EW	180	5
	EW	180	10
	N76E	166	9
	N80E	170	8
	N86E	176	8
	N85E	175	14
	N78E	168	7
	N70E	160	6
	N69E	159	6
	N67E	157	7
	N70E	160	4
	N85W	5	6
	N65W	25	7
	N62W	208	8
	N70E	340	20
	N72E	162	7
	N78E	168	6
	EW	180	9
	EW	180	11
	EW	180	10
	EW	180	13
	EW	180	20
	N82E	172	85
	N72E	342	11
	N87E	357	21
	N75E	345	17

Table A.3. Continued

DOMAIN III BEDS			
Formation	Strike(°)	Dip Direction(°)	Dip Amount(°)
Çerçen-Soğamlı-Akçapınar-Yunuslar Formations- Köseler Member	N78W	168	70
	N44W	134	40
	N73E	163	10
	N78E	168	25
	N80E	170	12
	N78E	168	14
	N65E	155	12
	N77E	167	12
	N87E	177	5
	N80E	170	6
	EW	180	8
	N70W	200	32
	N78W	192	15
	EW	0	80
	N87E	357	67
	N85E	355	70
	N88E	358	65
	N40W	130	24
	N80W	170	60

Table A.4. Bed measurements of Domain IV

<b>DOMAIN IV BEDS</b>			
<b>Formation</b>	<b>Strike(°)</b>	<b>Dip Direction(°)</b>	<b>Dip Amount(°)</b>
Safranbolu Formation	N42E	132	14
Safranbolu Formation	N61E	151	20
Safranbolu Formation	N80W	10	13
Safranbolu Formation	N67E	337	15
Safranbolu Formation	N77E	167	37
Safranbolu Formation	N88W	182	14
Safranbolu Formation	N65W	205	40
Safranbolu Formation	N50W	40	17
Safranbolu Formation	N80W	10	20
Safranbolu Formation	N63E	153	24
Safranbolu Formation	EW	180	30
Safranbolu Formation	N84E	174	76
Safranbolu Formation	N88W	2	44
Safranbolu Formation	EW	0	64
Safranbolu Formation	EW	0	35
Safranbolu Formation	N58E	328	44
Safranbolu Formation	N53E	323	41
Safranbolu Formation	N81E	171	65
Safranbolu Formation	N73E	163	50
Safranbolu Formation	N88E	178	40
Safranbolu Formation	N82E	172	76
Safranbolu Formation	N70W	20	49
Safranbolu Formation	N84E	354	46
Safranbolu Formation	N69E	339	34
Safranbolu Formation	N80E	350	31
Karabük Formation	N81E	171	12
Karabük Formation	N84E	174	15
Karabük Formation	N87W	183	35
Karabük Formation	N84E	174	52
Karabük Formation	N69E	159	45
Karabük Formation	N62E	152	36
Karabük Formation	N80E	170	50
Karabük Formation	N80E	170	60
Ulus Formation	N42E	132	41
Ulus Formation	N85E	175	20
Ulus Formation	N78W	12	27
Ulus Formation	N43E	133	53
Ulus Formation	N36E	126	42

Table A.4. Continued

<b>DOMAIN IV BEDS</b>			
<b>Formation</b>	<b>Strike(°)</b>	<b>Dip Direction(°)</b>	<b>Dip Amount(°)</b>
Ulus Formation	N33E	123	70
Ulus Formation	N40E	130	80
Ulus Formation	EW	0	50
Ulus Formation	N70W	160	53
Ulus Formation	N80E	170	25
Ulus Formation	N63W	207	45
Ulus Formation	N72E	162	51
Ulus Formation	N67E	157	50
Ulus Formation	N76E	166	35
Ulus Formation	N78E	168	45
Ulus Formation	N70E	160	45
Ulus Formation	N50E	140	35
Ulus Formation	N45E	135	66
Ulus Formation	N76E	166	70
Ulus Formation	N61E	151	44
Ulus Formation	N72E	162	43
Ulus Formation	N77W	13	39
Ulus Formation	N88W	2	74
Ulus Formation	N85W	5	74
Ulus Formation	N84E	354	52
Ulus Formation	N70E	340	43
Ulus Formation	N75E	345	35

## APPENDIX B

### FAULT MEASUREMENTS

Table B. Fault measurements

Site Number	Easting	Northing	Strike (°)	Dip Direction (°)	Dip Amount (°)	Rake (°)	Slip Sense
1	36464355	4557371	N47E	137	45		Normal Fault
2	36462379	4556519	N36E	126	53	88SE	Reverse faulting with strike slip component (Karabük Fault)
			N40E	130	54	78SE	
			N20E	110	61	86E	
			N30E	120	61	75SE	
			N45E	135	69	73SE	
3	36463300	4556900	N17E	287	62	74NW	
			N14E	284	24	86NW	
4	36475766	4575747	N14W	256	73		Normal Fault
5	36455879	4598351	N62E	152	84	21SE	Reverse Fault
			N62E	152	84	37SE	
			N62E	152	84	75SE	
			N73E	163	77	43SE	
			N72E	342	85	64SE	
			N72E	178	88	84SE	
			N60E	330	85	59SW	
			N63E	333	86	60SW	
			N66E	336	87	61SW	
			N69E	339	88	62SW	
			N72E	341	89	63SW	
			N69E	339	88	46SW	
6	36456014	4598139	N61W	209	71	40 W	Strike slip fault with reverse component
			N66W	204	82	12W	
			N56W	34	89	17W	
			N49W	41	82	7W	
			N45W	45	72	8W	
			N39W	51	74	9W	
7	36456026	4598128	N17E	117	56		Normal Fault
8	36439580	4610817	N17W	253	22	69W	Normal Fault with strike slip component
			N5W	265	39	82W	
			N48E	318	35	14W	
			N10W	260	17	85NW	



Table B. Continued

Site Number	Easting	Northing	Strike (°)	Dip Direction (°)	Dip Amount (°)	Rake (°)	Slip Sense
9	36449393	4593487	N19E	289	66	19S	Strike slip fault (Bartın Fault)
			N25E	295	58	7S	
			N20E	290	54	11S	
			N21E	291	62	9S	
10	36477558	4558212	N87W	183	89	4E	Strike Slip Fault
			N80W	10	88	27E	
			N84W	186	87	11E	
			N89W	1	82	12W	
11	36490894	4549945	N29E	299	89	89NE	Normal Fault
12	36479644	4555582	N28W	242	57		Normal Fault
			N87E	177	55	87SE	
13	36486754	4551178	N72E	162	44	79SW	Normal Fault
			N72E	162	44	69SW	
			N84W	186	21	66SE	
			N89E	359	37	81NE	
			N85E	175	16	83S	
			N74E	164	44	89SE	
			N76E	360	21	88N	
			N80E	170	13	88SE	
14	36484178	4550743	N60E	330	55		Normal Fault
			N57E	327	61	81NE	
15	36484176	4550752	N70E	340	21		Normal Fault
16	36483762	4549661	N15E	285	66		Normal Fault